Titanium Alloy Powder Production from Waste Metal

A thesis submitted to the Faculty of Engineering and Built Environment, University of Cape Town, in fulfilment of the requirements for the degree of Master of Science of Engineering.

By

Chetan Chhiba

Centre for Materials Engineering

February 2012

ABSTRACT

Titanium and its alloys are among the most important advanced materials in use today due to attractive properties such as high strength to weight ratio and excellent corrosion resistance. However, the cost of titanium production is high, mostly due to the high cost of extraction. This has led to investigations of potentially lower cost methods such as near-net shape powder metallurgy techniques. One approach, which has the potential of producing the lowest cost powder available, involves converting titanium waste machine turnings to powder using the hydride-dehydride (HDH) process. The focus of this project is directed at this approach where a ball milling process is used to simultaneously hydrogenate and crush the titanium turnings into titanium hydride powder.

A horizontal stirred ball mill with a pin stirrer geometry was found to be the ideal type of ball mill to crush the coarse titanium feed. This type of ball mill consists of a stationary mill chamber in which grinding media are agitated by a rotating stirrer with protruding pins. A 1.3 ℓ laboratory scale ball mill capable of operating under a 200 kPa hydrogen pressure was designed and built.

Milling was performed on commercially pure titanium (CP Ti) and Ti-6Al-4V waste machine turnings, using a fixed feed mass of 2 g and ball charge of 65%. The effect of the stirrer design, stirrer speed and milling time on both the hydrogen absorption rate by the feed and the production of titanium hydride powder were investigated. The hydrogen absorption rates at different milling conditions were compared by analysing the change in hydrogen pressure with milling time. Sieve analysis was used to determine the product size distribution and powder yield after milling. In addition, energy-dispersive x-ray spectroscopy (EDS) analysis was used to determine the powder fraction in the contaminated powder yield recovered after milling.

The stirrer design, stirrer speed and milling time were found to have a strong influence on the hydrogen absorption rate and resulting powder yield. For the range of stirrer configurations used, the optimum stirrer design corresponded to the stirrer configuration with the most pins and the shortest pin length. For the range of stirrer pin tip speeds used, i.e. from 0.5 m/s to 2 m/s, the optimum stirrer speed corresponded to the fastest stirrer speed. Compared to the lower stirrer speeds, this optimum speed resulted in a rapid hydrogen absorption period, followed by saturation. Consequently, it produced the highest powder yield for both feeds, after a fixed milling time. At the optimum stirrer speed, the optimum milling time corresponded to the time taken to reach saturation. For both CP Ti and Ti-6Al-4V feeds, the most powder yield and the least amount of contamination is produced at saturation.

ACKNOWLEDGEMENTS

I would like to thank everyone who assisted and supported me throughout the duration of this project, in particular:

- The UCT Research and Innovation Office and the Department of Science and Technology through the Advanced Manufacturing Technology Strategy programme for their financial support.
- My supervisor Professor R.D Knutsen for his supervision and constant guidance throughout this research project.
- Mr Glen Newins, Mr Horst Emrich, Mr Hubert Tomlinson and all the staff of the UCT Mechanical Engineering workshop who helped with the manufacturing and assembly of my testing rig.
- Beverly Glass for always providing a friendly welcome and for always making sure that I received my ordered parts on time.
- Miranda Waldron from the Electron Microscope Unit for assisting me with the EDS analysis.
- Mr Keith Balchin for providing guidance on operating the testing rig safely.
- Penny Park Ross for ensuring that laboratory chemicals and equipment were always available.
- All the students and staff at the Centre for Materials Engineering for their support, assistance and friendship.

I would also like to say a very special thank you to my parents who have supported me throughout my life and studies.

DECLARATION

I, Chetan Chhiba, know the meaning of plagiarism and declare that all the work in this document, save for that which is properly acknowledged, is my own.

Signature: Date:

TABLE OF CONTENTS

Page

LIST OF FIGURES

Page

LIST OF TABLES

Page

1 INTRODUCTION

1.1 Subject of thesis

This thesis concerns the feasibility of hydrogenating and converting titanium scrap into titanium hydride powder simultaneously by ball milling at room temperature and at a low hydrogen pressure.

1.2 Background to thesis

Titanium and its alloys exhibit attractive mechanical properties such as excellent strength-to- weight ratio, stiffness, and elevated temperature strength as well as good corrosion resistance. This makes them the most important advanced materials for a variety of aerospace, marine, industrial and commercial applications [1]. However, the cost of producing titanium is very high because the current process for refining the ore to metal is a multi-step, high temperature batch process [2]. This has led to the development of alternative low cost methods of producing titanium components, mainly though near-net-shape powder metallurgy techniques [3].

One approach to powder production, which has the potential of producing the lowest cost powder available, is the hydride-dehydride (HDH) process [3]. In the HDH process, titanium or titanium alloy pieces (machining turnings, sponge fines or selected scrap) are hydrogenated to form titanium hydride. These titanium hydrides are brittle and can therefore be easily crushed into fine powder. The titanium hydride powder is then dehydrogenated to obtain the corresponding titanium powder [4], [5] . Consequently, titanium hydride is an attractive raw material for the production of titanium or titanium alloy powder metallurgy components.

Presently in the literature there are mainly two ways of preparing titanium hydride powder. In the first method, hydrogenation is performed by exposing titanium or titanium alloy pieces to hydrogen gas at elevated temperature and/or pressures for several hours. This is followed by slow cooling in order to maintain maximum hydrogen content [6]. Thereafter, the resulting hydrides are pulverised in a separate ball milling process. Alternatively, in the second method, titanium hydride powder is prepared by ball milling titanium powder at room temperature under a hydrogen atmosphere [7], [8]. This ball milling method is used to produce a finer powder particle size than the initial titanium powder size. Compared to the first method, this

improved method reduces the number of processes since the titanium is hydrogenated and reduced in size simultaneously in one process.

Furthermore, unlike the first method, the ball milling method uses pure titanium powder as the starting material for producing titanium hydride powder. As a result, the potential exists to use titanium or titanium alloy scrap as the starting raw material. Recently, this has been achieved through a new patented method which claims to manufacture titanium hydride powder from titanium or titanium alloy scrap. This patented method works under the same principal as the ball milling method described above. However, a detailed description of the development of titanium hydride powder during the milling of titanium or titanium alloy scrap has not been reported to date.

1.3 Objectives of thesis

The objectives of the report are therefore to:

- Design and build a laboratory scale hydrogen pressure ball mill capable of hydrogenating titanium scrap and producing titanium hydride powder. The desired size of the powder particles is less than 105 µm (140 mesh).
- Determine the effect of different milling conditions and parameters on the hydrogen absorption rate.
- Optimize milling conditions and parameters, such as milling speed and milling time, to efficiently convert titanium scrap to powder.
- Examine the size of the titanium powder produced by ball milling.

1.4 Scope and limitations

This thesis covers the designing and testing of a laboratory scale ball mill that hydrogenates and reduces the size of titanium scrap in one process. The project is limited to the hydrogenation and milling of titanium scrap in the form of machine turnings. More specifically, the conversion of Ti-6Al-4V machine turnings into powder is of interest. However, experiments were also conducted on commercially pure titanium (CP Ti) machine turnings in order to serve as a benchmark for Ti-6Al-4V. The focus of this project is to determine how the different milling conditions and parameters affect the hydrogen absorption rate and powder production. Hydrogen absorption was assessed by monitoring the change in hydrogen pressure with milling

time. The hydrogen content of the powders was not determined. In addition, the formation of titanium hydride was not confirmed by any analytical techniques.

1.5 Plan of development

The thesis begins with a two part literature review. The first part is a review of titanium and describes the hydrogen embrittlement of titanium. This is followed by the second part which describes the different types of ball mills as well as the milling variables that have an effect on final particle size. After the literature review, conceptual designs of the chosen ball mill are presented and a detailed description is given of the final design. This is then followed by a detailed account of the experimental procedure used. The results of the experiments are then analysed and discussed. Conclusions are then drawn on the basis of these results and finally, recommendations are made for future work.

2 LITERATURE REVIEW: TITANIUM

2.1 Titanium structure and properties

2.1.1 Material introduction

Titanium is the ninth most abundant element in the earth's crust, making up approximately 0.6% by mass. Behind iron, aluminium and magnesium, it is the fourth most abundant metal in the earth's crust. Unfortunately titanium does not occur in a pure state and is usually combined with oxygen and iron. The present mineral sources of titanium are principally rutile (TiO_2) and ilmenite ($FeTiO_3$) [2], [9], [10]. Rutile contains 93-96% titanium dioxide, whereas ilmenite consists of 44-70% titanium dioxide [9]. Suitable titanium dioxide deposits are predominantly found in Australia, South Africa, Canada, Norway, and Ukraine [11].

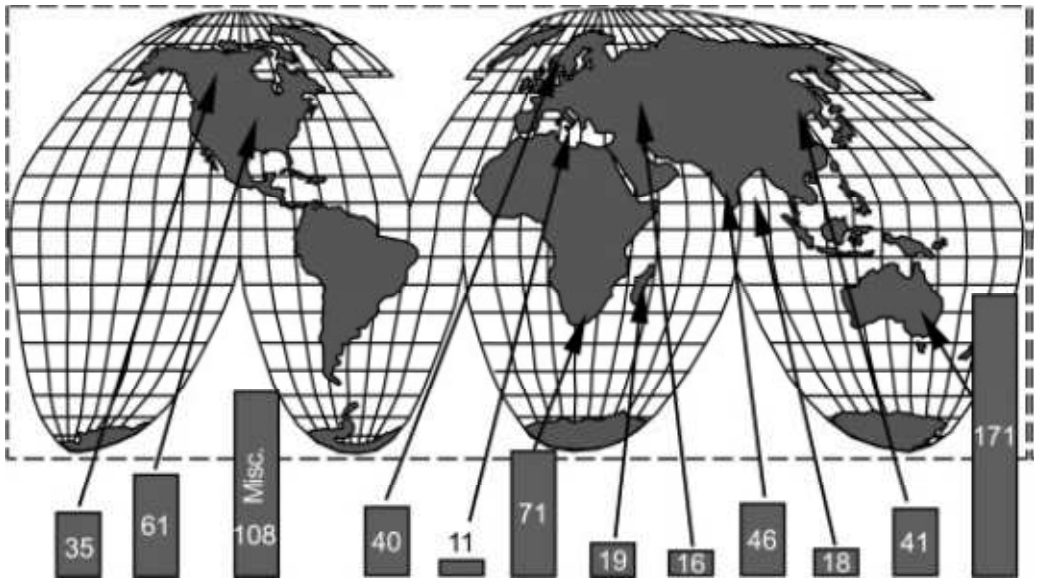

Figure 2.1: Distribution of global titanium oxide deposits (in billions of metric tons, 1999) [11].

Titanium is a widely used engineering material due to its unique set of properties such as low density, high specific strength, high temperature strength and exceptional corrosion resistance [2], [9], [10]. The density of titanium is about 60% that of steel, whereas the elastic modulus is about 55% that of steel. Titanium is non-magnetic and has good heat-transfer properties. Its coefficient of thermal expansion is lower than that of steel and less than half that of aluminium. Titanium also possesses a high degree of immunity against chemical attack by most mineral acids

and chlorides. As a result, it is often chosen over stainless steel in most environments [9].

Commercially pure titanium and some titanium alloys are biocompatible with human tissues and bones. Titanium is used extensively in the production of prosthetic devices such as heart-valve parts and load-bearing leg-bone replacements or splints. In addition, the excellent corrosion resistance and biocompatibility coupled with good strengths make titanium and its alloys useful in chemical and petrochemical applications as well as marine environments [9].

Presently, the highest demand for titanium is from the aerospace industry. It is useful for this industry because of its high strength to weight ratio and high temperature properties. Titanium alloys offer high-strength efficiency and metallurgical stability at elevated temperatures which are necessary for rotating components such as jet-engine blades and gas turbine parts [9].

Figure 2.2: The SR-71 Blackbird was the first all-titanium military airplane. This photo, taken at Dryden Flight Research Centre in 1992, shows the SR-71B taking off with "shock diamonds" in the exhaust [12].

2.1.2 Titanium metallurgy

Crystal structure

Titanium is an allotropic element, i.e. it exists in more than one crystallographic form. At room temperature, pure titanium has a hexagonal closed-packed (hcp) crystal structure which is referred to as "alpha" (α) phase. Above 883ºC, this structure

transforms to a body-centred cubic (bcc) crystal structure, called the “beta” (β) phase. This transformation temperature is known as the β -transus temperature. Due to their different crystal structures, each phase exhibits different properties. Each phase or a combination of both phases can exist at service temperature, through appropriate alloying and/or heat treatment. Depending on the phases present in the microstructure, three classes of titanium alloys exist which are (1) alpha (α), (2) alpha-beta (α + β) and (3) beta (β) [10], [13].

Alloying elements

The addition of alloying elements to titanium results in a wide range of physical and mechanical properties. Alloying elements are usually classified as α or β stabilisers and function to alter the beta-transus temperature. Alpha stabilizers, such as aluminium and interstitials (C, N, O), increase the temperature at which the α phase is stable. Among the α stabilizers, aluminium is the most important alloying element. Alternatively, beta stabilizers, such as vanadium and molybdenum, decrease the temperature at which the β phase is stable. In addition, tin and zirconium are often alloyed in titanium in order to serve as strengthening agents, with nearly no influence on the transformation temperature [10], [13].

2.1.3 Titanium classification

- Unalloyed Ti

Commercially pure (CP), unalloyed titanium is available in four grades. These grades vary according to the amount of interstitial elements (oxygen, nitrogen) and iron content. High purity grades (lower interstitial content) are lower in strength, hardness and transformation temperature than those which have higher interstitial content. More specifically, strength increases with increasing oxygen and iron contents. Due to the variation in the interstitial and impurity levels, unalloyed (CP) grades have yield strengths that vary from 170 MPa to 480 MPa. Generally, unalloyed titanium is used for applications that require excellent corrosion resistance, especially where high strength is not a required property [10], [13].

- Alpha, near-alpha alloys

Alpha alloys, which typically contain aluminium, tin and / or zirconium, are preferred for high temperature and cryogenic applications. Particularly, they have high amounts of aluminium which contributes to oxidation resistance at high temperatures [13].

Compared to other titanium alloys, alpha rich-alloys are more resistant to creep at high temperature. Generally, they also demonstrate the best corrosion resistance properties [10], [13]. However, since they are single-phase alloys, alpha alloys cannot be heat treated to improve their mechanical properties [13].

Near-alpha alloys usually contain small additions of beta stabilizers (e.g.Ti-8Al-1Mo-1V). However, they mainly consist of alpha phase and therefore behave more like alpha alloys than alpha-beta alloys [13].

- Alpha-Beta alloys

Alpha-beta alloys contain one or more alpha stabilisers plus one or more beta stabilisers. Compared to near-alpha alloys, they retain more beta phase after heat treatment. Alpha-beta alloys have excellent combinations of strength and ductility. These alloys can be strengthened from 30 to 50% or more by heat treatment and ageing. Generally, they are much stronger than the alpha or the beta alloys [13].

- Beta alloys

The beta alloys are metastable; in other words they tend to transform to an equilibrium, or balance of structures. These alloys contain considerably more beta stabilisers and less alpha stabilisers than alpha-beta alloys [13]. Compared to alpha and alpha-beta alloys, beta alloys have good formability, high hardenability and excellent forgeability. However, the chief disadvantages of beta alloys are its higher density, lower creep strength and lower tensile ductility when compared to other titanium alloys [10], [13].

Table 2.1: Properties of α, α+β and β Ti alloys [10].

	α	α+β	β
Density	+	+	−
Strength	−	+	++
Ductility	−/+	+	+/−
Fracture toughness	+	−/+	+/−
Creep strength	+	+/−	−
Corrosion behavior	++	+	+/−
Oxidation behavior	++	+/−	−
Weldability	+	+/−	−
Cold formability	− −	−	−/+

2.1.4 Ti-6Al-4V alloy

The most common and widely used titanium alloy is Ti-6Al-4V, which accounts for more than 50% of all titanium in use. Ti-6Al-4V is an alpha-beta alloy containing 6 weight percent aluminium and 4 weight percent vanadium. It is a lightweight alloy that exhibits a good combination of strength and toughness along with exceptional corrosion resistance. Consequently, this alloy is used extensively in the aerospace industry. Due to its unique properties, Ti-6Al-4V has become the standard alloy against which other alloys must be compared when selecting a titanium alloy for a specific application [13].

Table 2.2: Physical and mechanical properties of Ti-6Al-4V [10].

Density	4.43 g / cm^3
Yield Strength	800-1100 MPa
Tensile Strength	900-1200 MPa
Modulus of Elasticity	110-140 GPa
Hardness (Vickers)	300-400
% Elongation	13-16
Fracture Toughness (K_{ic})	33-110 a √m

2.2 Titanium processing

Presently all titanium metal production begins with titanium dioxide (TiO_2) which occurs naturally in the form of a mineral called rutile. Rutile is combined with petroleum coke and chlorinated in a fluid bed reactor at 1000ºC to produce titanium tetrachloride ($TiCl_4$) [2]

$$TiO_2 + 2Cl_2 + C \rightarrow TiCl_4 + CO_2$$

$TiCl_4$ is the starting point for all commercial processes due its high purity and the fact that titanium is separated from oxygen [2]. Introduced at the end of the 1940s, the Kroll process has been the most widely used commercial process for producing titanium sponge. In the Kroll process, magnesium is used to reduce all the $TiCl_4$ at a temperature above 800 ºC according to the reaction [2], [14]:

$$TiCl_4 + 2Mg \rightarrow Ti + 2MgCl_2$$

The magnesium chloride formed by this reaction is periodically tapped off as the reaction proceeds, leaving behind the titanium sponge [2], [14].

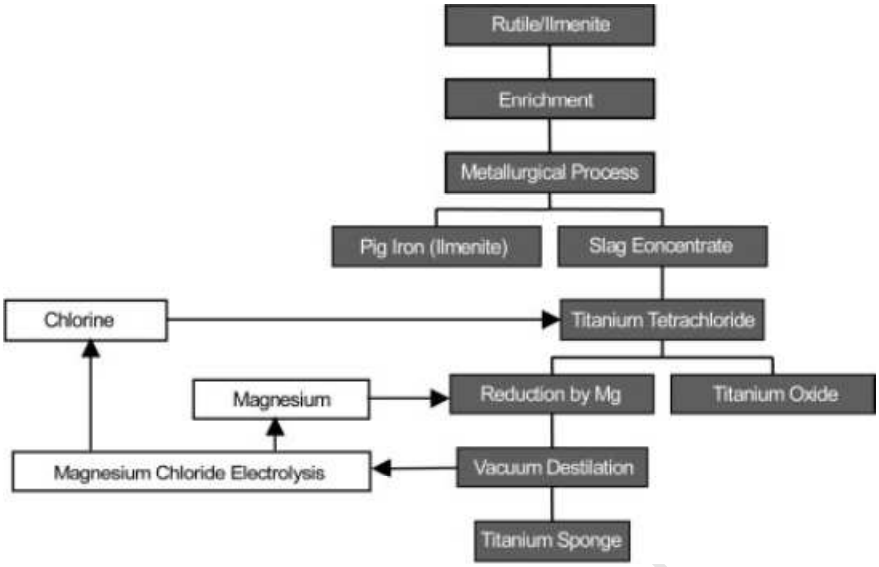

Figure 2.3 Extended Kroll process for titanium sponge production [11].

After the Kroll process, the titanium sponge is melted with reclaimed titanium scrap (revert) and / or alloying elements in a vacuum arc reduction furnace to produce an ingot. In order to remove volatile contaminants (e.g. chlorides) and ensure an acceptable degree of homogeneity, the ingot is remelted once or twice more. The ingot then undergoes primary fabrication, where it is converted into general mill products such as billet, bar, plate, sheet, etc. These mill products can then be used for producing finished parts through secondary fabrication processes [15].

2.2.1 Titanium production drawbacks

Since the introduction of the Kroll process, it has been criticised as expensive, labour intensive and inefficient. The current process for refining the ore to metal is a multi-step, high temperature batch process which consumes a large amount of energy and there are difficulties associated with the removal of $MgCl_2$. However, after more than 60 years and many announced new processes, nothing has replaced it. As a result, titanium remains expensive today due to the high cost of extraction [2], [14].

The cost of titanium production would be less expensive if the metal could be produced by a direct reduction of TiO_2 [14]. The Fray-Farthing-Chen (FFC) Cambridge process has been successful at achieving this. Developed at the University of Cambridge in 1997, the FFC Cambridge process is a novel, simple

electrochemical method that reduces titanium dioxide to titanium powder in one-step. However, despite the numerous apparent benefits, the feasibility of such a reduction reaction has only been demonstrated on a laboratory scale and has not been employed in a commercial-scale facility [16], [17].

2.2.2 Recycling

Due to the large amount of titanium used, there is also a large amount of titanium or titanium alloy scrap produced. Titanium scrap, usually generated during manufacturing processes, is completely recyclable. Presently, titanium scrap is only recycled in a melting process.

Before melting, the scrap must be thoroughly cleaned and carefully sorted by alloy as well as by purity [15]. After adequate cleaning and refining procedures, high quality titanium scrap is re-melted to form ingots and slabs and can thus be put back into circulation again. Titanium scrap is melted by using either vacuum arc reduction or cold hearth melting with electron beam or plasma heating [11].

The strong need for titanium recycling can be realised by looking at the material's production cycle (figure 2.4). On average, only 0.4kg of each 1.3 kg of titanium sponge produced ends up in the finished product. In some cases, due to the complexity of the product manufactured, up to 90% of the input material is being machined away and is available for titanium recycling [11].

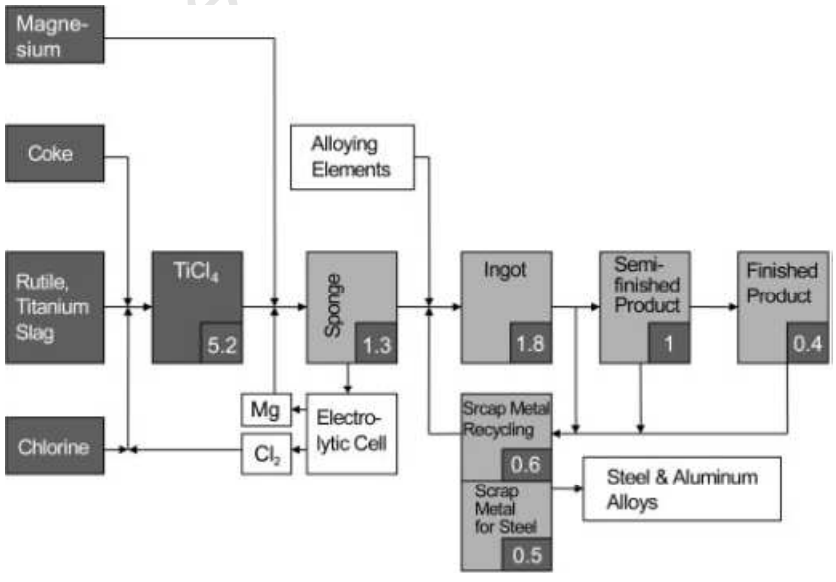

Figure 2.4: Flow chart and mass balance sheet for titanium product fabrication from ore [11].

2.3 Hydrogen embrittlement of titanium

2.3.1 Titanium-hydrogen interaction

As mentioned before, titanium and its alloys are well known for their excellent corrosion resistance. This is due to a very stable, highly adherent and protective oxide film that forms spontaneously on the metal surface when exposed to air and/or moisture [18]. However, if this protective oxide film is destroyed in a hydrogen-containing environment, titanium and its alloys become susceptible to hydrogen damage. Hydrogen damage is caused by brittle hydrides, which form as hydrogen gas diffuses into the material during exposure to either gaseous or cathodic hydrogen [19]. The formation of these hydrides results in severe loss of ductility, i.e. hydrogen embrittlement of titanium and its alloys. In addition, a reduction in the stress-intensity threshold for crack propagation may also occur [1], [19].

Alpha and alpha-beta titanium alloys, when exposed to an external hydrogen environment at room temperature, will degrade primarily through the repeated formation and rupture of the brittle hydride phase. Alternatively, beta titanium alloys do not tend to form hydrides due to their high hydrogen solubility. Consequently, they are less susceptible to hydrogen embrittlement at room temperature and low hydrogen pressures. However, beta alloys have been observed to form brittle hydrides when exposed to very high hydrogen pressures [1].

The exact amount of hydrogen at which a separate hydride phase is formed depends on the composition of the alloy and the previous metallurgical history. In commercially pure, unalloyed titanium, this hydride phase can be found at concentrations as low as 0.5 at. % hydrogen (100 ppm by weight), resulting in measurable embrittlement. However, in the presence of a high residual stress or stress raiser and elevated temperature, hydride formation has been observed at hydrogen levels as low as 30 to 40 ppm (by weight) [19].

2.3.2 Titanium hydride

Although hydrogen has a devastating effect on the mechanical properties of titanium, it can have many positive effects by reacting with titanium to form titanium hydride [20]. The brittleness of titanium hydride provides an economic method for the production of titanium powders. In powder metallurgy applications, these powders can then be used for the cost effective production of near-net shape titanium alloy

components. It has also been shown that finished titanium parts can be manufactured at a significantly lower cost than the conventional route by using a technique based on titanium hydride powder [21] .

Titanium or titanium alloy powders are commonly processed by the well-known hydride-dehydride (HDH) process. In the HDH process, titanium pieces (machining turnings, sponge fines or selected scrap) are hydrided to form titanium hydride. These brittle hydrides are easily crushed to a fine particle size. The powder is then dehydrided by a simple vacuum annealing step in order to obtain the corresponding titanium powder [4], [5] .

Presently, in the literature, titanium hydride powder is prepared via either the conventional method or the recently developed mechanical alloying method. Both methods will be discussed in detail.

Conventional method

The conventional method of preparing titanium hydride powder involves vacuum annealing the titanium or titanium alloy metal at elevated temperatures above 1000℃. This is done to dissolve the protective oxide film on the titanium sample before introducing hydrogen gas. Typically, hydrogen gas is introduced at atmospheric pressure at 400℃ for several hours and the metal is cooled slowly to maximise hydrogen uptake [7]. The amount of hydrogen absorbed is determined by the hydrogen soak and cooling time. Milling of the resulting hydride then takes place at room temperature in a ball mill under an argon atmosphere [5].

Disadvantages of conventional method

It has been established that the conventional method of hydrogenating titanium is difficult. Elevated temperatures and / or pressures for extended periods of time are required for the hydrogen to diffuse into the adherent titanium oxide layer [6]. As a result, a high temperature vacuum / pressure reactor and a process for heating the reaction container are required. Furthermore, a separate process for pulverising the hydrogenated titanium has to be performed. Overall, this method is complicated and leads to poor productivity as well as high manufacturing costs due to high equipment costs [22].

Mechanical alloying method

An alternative and improved method of preparing titanium hydride powder is also available, where titanium hydride is synthesised at room temperature by mechanical alloying. In this method, elemental titanium powder is milled in a ball mill under a hydrogen atmosphere for different periods of time [7], [8], [23]. During milling, the hydrogen pressure decreases indicating absorption of hydrogen by the titanium powder. The resulting hydrides that form have high hydrogen content and about the same thermal stabilities as hydrides produced with the conventional method. In addition these hydrides enhance fracturing and particle size reduction [8]. As a result, the titanium is hydrogenated and reduced in size simultaneously in one process.

Usually, titanium powder with purity greater than 99.9% and particle size of -325 mesh is used as the starting material [6], [7], [23]. However, Chen and Williams [8] have used coarser powder with an average particle size of about 100 mesh. Milling of the titanium powder takes place in a shaker/mixer mill (Spex 8000) with hardened steel vial and balls [6], [7], [23]. After evacuating to 10^{-4} mbar, the vial is charged with above 1 atm (1 bar) of hydrogen gas. If the pressure of the hydrogen gas is lower than 1 bar, a hydrogenation reaction is not performed well. On the other hand if the pressure is too high (above 100 bar), equipment costs start to increase [22]. The hydrogen pressure used in the literature ranges from as low as 2 bar [7] to as high as 11 bar [24].

Determining the amount of hydrogen absorbed

Since the hydrogen pressure drops during milling, fresh hydrogen is loaded periodically into the vial until the titanium is saturated with hydrogen. The total amount of hydrogen absorbed is calculated based on the pressure drop [7]. The change in hydrogen pressure is related to the number of hydrogen atoms absorbed per titanium atom and is represented by the following formula [6]:

$$\frac{H}{Ti} = \frac{2VA\,\Delta P}{Rm} = 4.274 \times 10^{-3}\,\frac{V\Delta P}{m} \qquad (2.1)$$

Where V - volume of the reservoir (cm^3)

A - atomic weight of Ti

ΔP - pressure change in the system (atm)

R - standard volume of gas (cm^3)

m - mass of Ti (g)

The rate of hydrogen absorption can be monitored by the variation in hydrogen pressure. Figure 2.5 below, shows the relationship between the ratio of hydrogen to titanium atoms, H/Ti, and the change in hydrogen pressure with respect to milling time. It is clear that there is little or no hydrogen absorption during the initial milling period. This is followed by a period of rapid hydrogen absorption and saturation for longer times [23], [25]. The reason for this behaviour can be explained by looking at the role of ball milling in promoting hydrogen absorption.

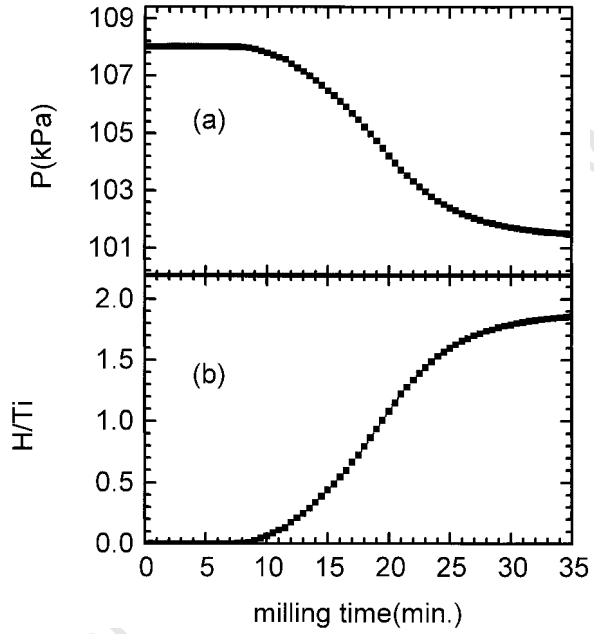

Figure 2.5: Hydrogen pressure (a) and H/Ti ratio (b) as a function of milling time [23].

Role of ball milling in promoting hydrogen absorption

At the start of milling, the period during which little or no hydrogen absorption takes place corresponds to a period where the particle size of the titanium powders are reduced in size and lattice defects are introduced. The smaller particles that are created allow hydrogen absorption to occur rapidly because of the short diffusion distances. Alternatively, lattice defects such as dislocations, provide routes along which hydrogen can diffuse. This is followed by a period where the fine titanium powders begin to rapidly absorb hydrogen and react to form titanium hydride. Due to the embrittlement of titanium by hydride formation, the particle size reduces further upon continuous milling. This results in a large surface area for hydrogen absorption.

After the rapid hydrogen absorption period, the hydrogen pressure decreases to a stable level signifying that the titanium powder is saturated [8], [23–25].

Overall, milling can be viewed as an activation process in hydride formation. In order to summarise, the effectiveness of ball milling in promoting hydrogen absorption results from several factors:

i. Exposing clean titanium surfaces by mechanical removal of oxide films, allowing hydrogen to readily diffuse into the titanium powder [6], [7], [25].

ii. Introducing significant lattices defects which increase the hydrogen diffusion rate into titanium [6], [7], [25].

iii. Reducing the particle size of titanium thereby allowing bulk diffusion to occur rapidly because of the short diffusion distances involved [6], [7], [25].

Modification to the mechanical alloying method

Unlike the conventional method, the mechanical alloying method stated in the literature uses pure titanium powder as the raw material for producing titanium hydride powder. However, a new patented method which claims to manufacture titanium hydride powder from titanium or titanium alloy scrap has recently been invented. This method works under the same principle as the original mechanical alloying method, reported in the literature.

The patented method of manufacturing titanium hydride powder involves charging titanium scrap into a reaction chamber, evacuating the air from the reaction container and supplying hydrogen gas to the reaction container, and performing ball milling. As a result, the titanium scrap is hydrogenated and converted into powder at the same time. Since a separate process for pulverising the titanium hydride does not need to be performed, productivity is improved. Furthermore, manufacturing costs are also reduced since expensive titanium powder or sponge is replaced by titanium scrap as the raw material [22].

3 LITERATURE REVIEW: GRINDING

Grinding is defined as particle size reduction by mechanical means. The primary objective of grinding is to produce powder with a specified particle size distribution (PSD) that is suitable for subsequent processing. Usually, grinding takes place in grinding mills that use mechanical forces to break down solid material into smaller particles. The mill design and mode of operation determines the type of stress, stress intensity and stress frequency distributions exerted to the feed particles. Preventing or minimising contamination and efficient usage of the grinding mill must be considered during grinding. These factors in turn influence the energy utilisation of the mill which is an important factor in industrial scale applications. Examples of grinding mills include media/ball mills, impact mills and fluid-energy mills [26]. The discussion here will be limited to grinding in media mills, specifically ball media mills, since this type of mill has been reported to activate the titanium hydrogenation process [7].

3.1 Grinding principles

3.1.1 Size reduction

The size reduction of feed particles results from the fracture of the particles due to an applied stress. The applied stress has to be larger than the particle strength in order for fracture to occur [26]. Mainly 3 types of size reduction mechanisms occur and are illustrated in figure 3.1. Size reduction by attrition/abrasion forces results in the production of wear debris or particles that are created by the rubbing action between two bodies. Compression applies mechanical energy to compress particles against a surface and fracture them into smaller particles. Impact applies high-energy impacts to fracture the particles [27].

Abrasion tends to give a narrow particle size distribution, impact a broad one and compression an intermediate one. However, in practice, these mechanisms do not occur in isolation, but with one normally dominating. It is believed that compression is more related to crushers, impact to tumbling mills and abrasion to the ultra-fine grinding machines [28].

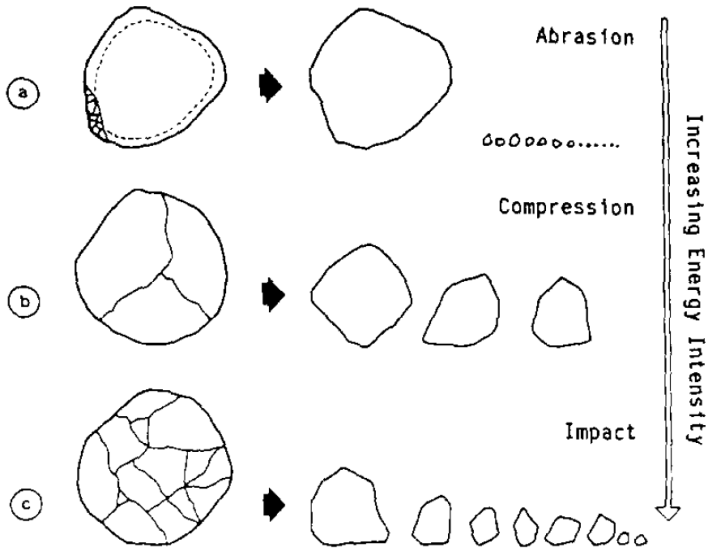

Figure 3.1 : Size reduction mechanisms [28].

3.1.2 Breakage characteristics

The performance of a grinding mill is characterised by the specific rate of breakage and the primary breakage distribution. The specific rate of breakage is defined as the rate , relative to the amount present, at which particles are broken out of a given size class. As a particle size decreases, the strength of the particle increases and the volume stressed decreases with each stress event. Therefore the breakage rate decreases with decreasing particle size. At fixed grinding conditions, the same force is applied to particles of different size, but the applied stress varies. When grinding, smaller particles are subjected to greater stress because of their smaller cross section and are more likely to fracture when stressed. Large particles receive less stress and therefore undergo attrition when stressed. Overall, increasing the particle size causes the breakage rate to initially increase until a maximum is reached. Thereafter, the particles become less likely to fracture at a given stress level [26].

Basically, the breakage distribution is the size distribution obtained when an “average” particle is broken and is independent of the initial size of the particle being broken. Breakage distribution varies with the energy available to the breakage event. In stirred media mills, where there is high-speed impact of the particles, high energy breakage produces very fine fragments [26].

3.1.3 Stress intensity and stress frequency

In grinding mills, stress is applied to the feed particles through the mechanical action of the mill. The rate of breakage depends on the frequency of the applied stress i.e. the number of stress events per unit time and the stress intensity at each stress event. As the stress intensity increases, the probability of breakage at each stress event increases. Overall, at a certain stress intensity, a certain product fineness can be produced only with a certain number of stress events [26].

For a particular mill design, there is an optimum stress intensity that would produce the finest product for a given energy consumption. Below that optimum, particle breakage becomes less efficient since more stress events are required to break a particle. If the stress intensity is higher than optimum, energy utilisation (i.e. newly generated surfaces related to energy input) of each stress event decreases due to increased energy losses [29].

3.2 Media mills

Media mills are the most widely used grinding machines for producing fine powders. These mills contain grinding media which can consist of balls, rods, pebbles, etc. Depending on the action of the mill, the motion of the media involves collisions between each other and with the walls of the mill chamber. As a result, grinding occurs when the feed particles are caught between these collisions [26]. Media mills which use ball shaped grinding media are commonly referred to as ball mills and will be discussed in the next section.

Breakage characteristics for these mills are determined by the frequency of media collisions (stress frequency) and the energy associated with each collision (stress intensity). Collision frequency depends on the motion of the mill and the number of grinding media. The collision energy is also related to the mill motion as well as the mass of the individual media elements [26].

Grinding usually takes place in either batch or continuous mode. In batch grinding, material is ground and then removed for analysis. For continuous grinding, the feed particles are continuously fed into the mill chamber and are removed on the other side. If the particles are oversized for the application, they are returned into the mill chamber for further grinding. This is known as a closed grinding circuit. An open

circuit would involve passing the feed product through a number of grinding stages (sometimes in different mills) until the required product size is met [30].

In batch grinding, breakage rates and breakage distributions for the different particle sizes can be used to predict the product size distribution as a function of milling time. An approximate relationship between milling time and desired product size can be given by the following equation. This equation states that milling time varies roughly with the reciprocal of the desired product size [26].

$$t \approx \frac{x_t}{x_p S_t} \tag{3.1}$$

Where, x_t is a characteristic size of the feed material

x_p is the corresponding size of the product

S_t is the breakage rate for the feed particles

3.3 Types of ball media mills

High energy ball mills are used in two powder processing techniques, mechanical alloying (MA) and mechanical milling (MM). Mechanical alloying can be described as mixing and milling of elemental metal powders (of different metals or alloys/compounds). This process involves material transfer in order to obtain a homogenous alloy. Conversely, mechanical milling only involves milling of pure metals, intermetallics or pre-alloyed powders without any material transfer [31]. Since the objective of this project is to mechanically convert titanium metal into powder, this technique applies.

Different types of high energy ball mills are used to mechanically reduce particle size. These mills differ in their capacity, efficiency of milling, speed of operation and milling kinetics [31]. The following ball media mills are commonly used.

3.3.1 Shaker mills

Shaker/mixer mills are high energy ball mills that accommodate sample sizes ranging from 0.2 - 10 grams. These types of mills are commonly used for laboratory and alloy screening purposes. They consist of a vial, containing the sample and grinding balls, which is secured in a clamp and swung energetically back and forth several times a

minute. This shaking motion is combined with lateral movements of the ends of the vial, so that the vial moves in a “figure 8” motion. As the container is swung, the inertia of the grinding elements causes them to move independently, into each other and against the container wall, grinding the sample. Due to the amplitude and velocity of the clamp’s swing, high ball velocities and hence ball impact forces are created, enough to pulverize tough samples [31].

The shaker mill is also available in a dual clamp version with two clamps for increased throughput. This allows twice as many samples to be ground simultaneously in a given time. Various vial materials are available with a choice of steel, tungsten carbide, agate, zirconia, silicon nitride, alumina, and plastic vials [31].

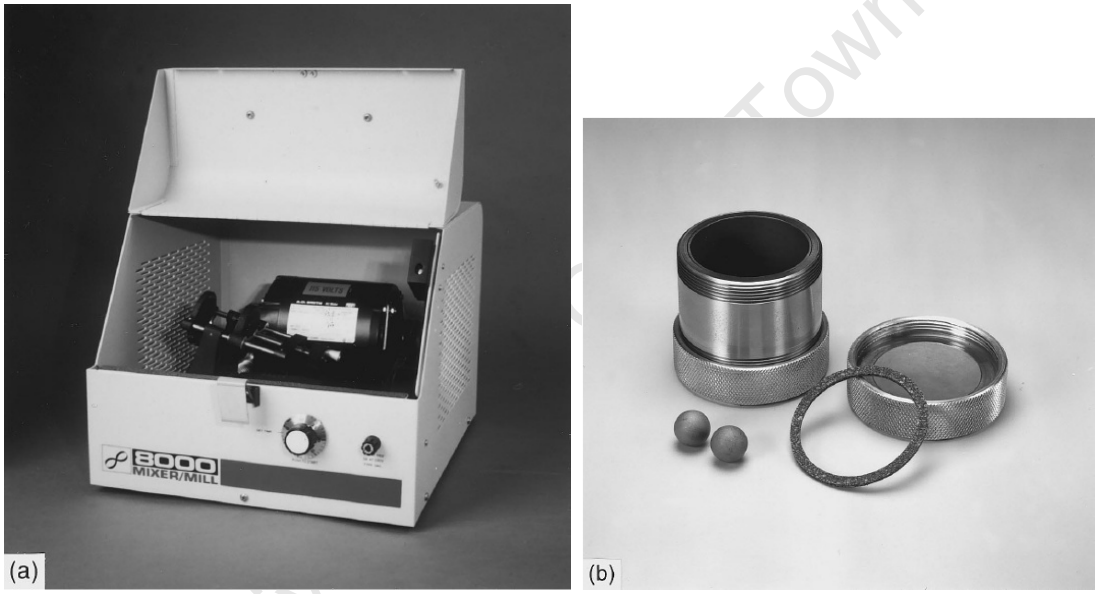

Figure 3.2: (a) SPEX 8000 shaker/mixer mill in the assembled condition. (b) Tungsten carbide vial set consisting of the vial, lid, gasket and balls [30].

3.3.2 Planetary ball mills

The planetary ball mall is a centrifugal mill that owes its name to the planet-like movement of its vials. These vials, consisting of the sample and grinding balls, rotate around their own axis on a counter-rotating support disc. Centrifugal forces created by the vials rotating around their own axes and that from the rotating support disk both work on the contents of the vial. Initially when the mill is started, the centrifugal force of the rotating vial causes the rotating grinding balls to rub against the inside wall, thus crushing the material by abrasion. At a certain critical speed, the stronger centrifugal force of the supporting disc causes the grinding material and balls to

separate from the inner wall of the vial. As a result, the grinding balls cross the vial at high speeds and collide with the grinding material on the opposite wall, reducing the sample material via impact [31].

Planetary ball mills are equipped with either two or four milling stations. Recently, a planetary mill with a variable transmission ratio was also developed. In contrast to the conventional planetary mills, the rotational speed of the vials and the supporting disc can be adjusted completely independently of each other. As a result, it is possible to obtain high impact energy or high abrasion by controlling the movement and trajectories of the grinding balls [31].

Furthermore, the grinding vials and balls are available in different materials such as zirconia, chrome steel, Cr-Ni steel, tungsten carbide and plastic polyamide [31].

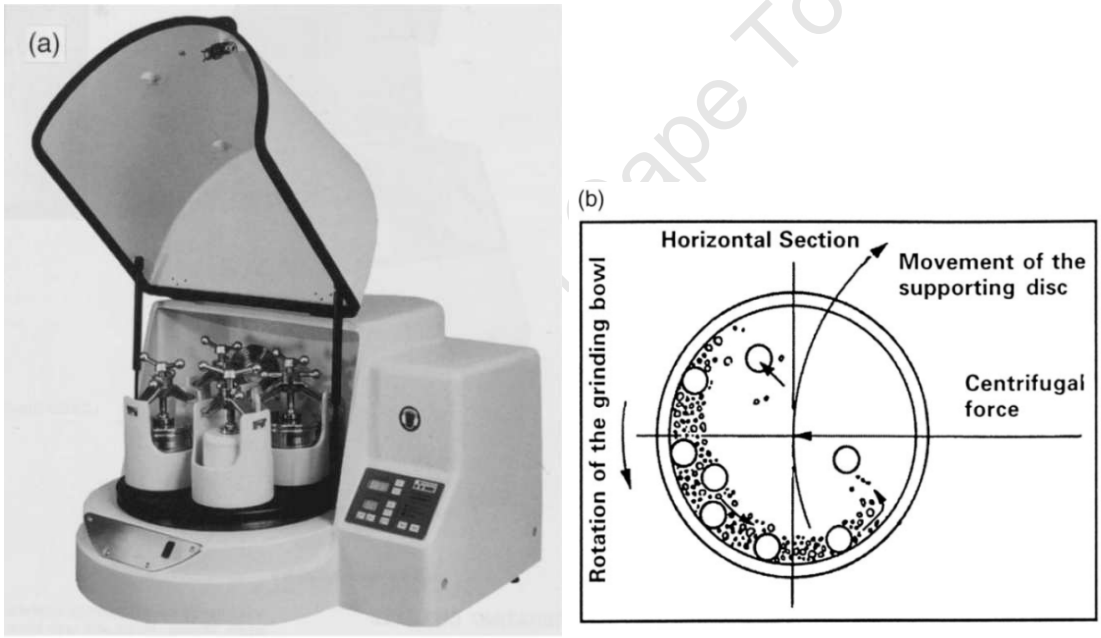

Figure 3.3: (a) Fritsch Pulverisette P-5 four station ball mill. (b) Schematic depicting the ball motion inside the ball mill [31].

3.3.3 Tumbling ball mills

A conventional tumbling ball mill consists of a rotating horizontal drum, partially filled with grinding balls. As the drum rotates, the balls move up the wall of the drum and fall back into the charge below when the force of gravity exceeds friction and centrifugal forces [26], [32]. Thus the grinding energy is supplied by and limited by gravity [26]. Initially, the ball charge gains potential energy that is transferred into kinetic energy as the ball charge falls from the rotating drum. Feed particles are

therefore broken by impact forces when caught in the collisions between balls and between balls and the drum wall [32].

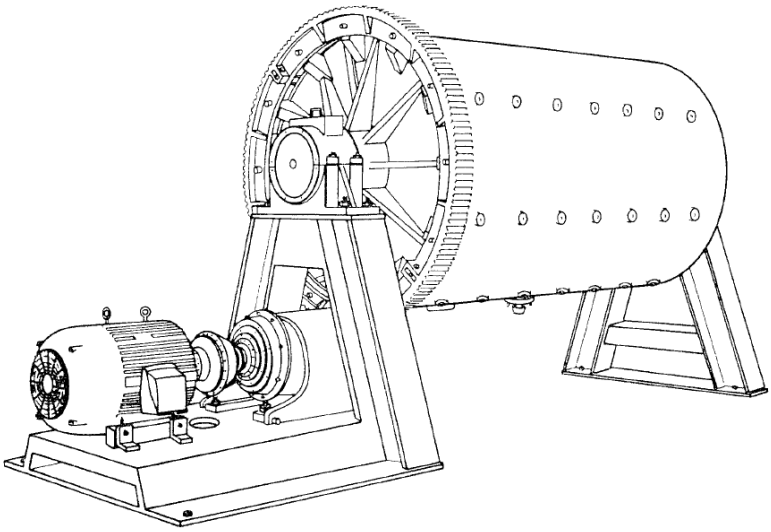

Figure 3.4: Commercial tumbling ball mill [27].

At low rotational speeds, the balls may roll or 'cascade' down the surface of the charge. As the speed increases, the balls start to project off the chamber wall and remain in free flight until falling back down [26], [27]. Therefore, as the speed of the drum increases, the rate of grinding increases. However, the maximum speed of the mill is limited by the critical speed of the mill, where the grinding balls are centrifuged at the mill chamber wall. As a result, the grinding balls cannot exert any impact force and the grinding action stops [31]. Tumbling mills are usually operated at 70-80% of the critical speed which corresponds to the maximum power input. Assuming the slip of the charge against the chamber wall is negligible; the critical rotational speed of the mill is calculated using the following equation [26]:

$$\textit{Critical Speed: } N_c = \frac{60}{\pi}\sqrt{\frac{g}{2(D-d)}} \tag{3.2}$$

Where: N_c *= critical speed (rpm)*

g = gravitational constant

D = mill diameter

d = media diameter

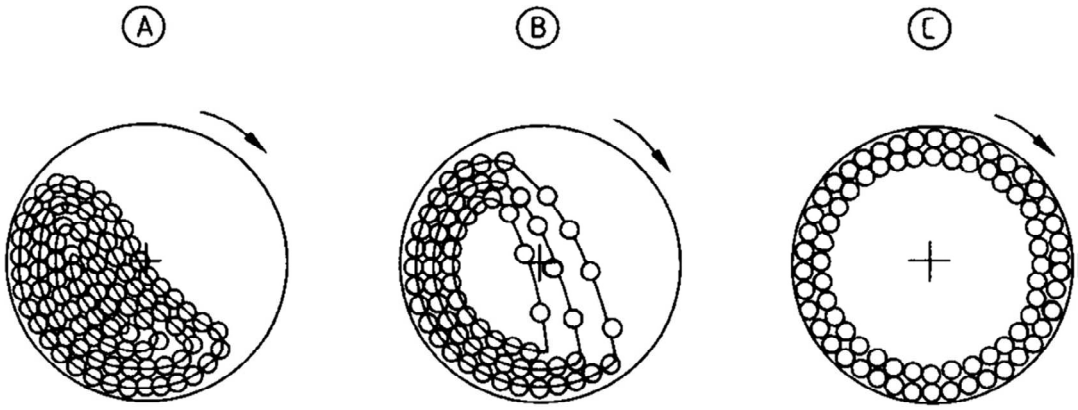

Figure 3.5: Types of motion in a tumbling ball mill: (a) cascading, (b) falling (c) centrifugal [33].

In batch grinding, media filling levels of about 50% of the free mill chamber volume are common. The amount of feed that is loaded into the mill is considered to be optimum when the voids in the media bed are just filled. Too much feed results in "cushioning" of media-media impacts and a loss of energy. However, too little feed will allow too much direct media-media contact and will result in high wear of media. The bulk volume of feed particles should be about 40% of the bulk volume of the media for optimum grinding [26].

3.3.4 Attritor mills (Stirred media/ball mill)

Attritor mills consist of a stationary mill chamber in which grinding media are moved by a rotating shaft (attritor/stirrer) with attached arms or discs. Due to the stirring motion of the grinding media, these types of mills are also referred to as stirred media/ball mills. The power input is used directly for agitating the ball charge to achieve grinding and is not used for rotating or vibrating the mill chamber in addition to the media [30]. As a result, milling is accomplished by impact and attrition forces between media balls, between balls and container walls, and between balls and stirrer [31].

Closed-type stirred media mills are classified according to the mill chamber orientation i.e. either horizontal or vertical and are usually equipped with a water jacket for cooling purposes. Low-speed mills are usually orientated vertically because the grinding action relies, to some extent, on gravity. Alternatively, high speed mills are orientated horizontally, where centrifugal forces dominate over gravity. In high speed horizontal mills, tangential speeds of up to 20 m/s can create centrifugal accelerations of more than 50 times the acceleration due to gravity [26], [34].

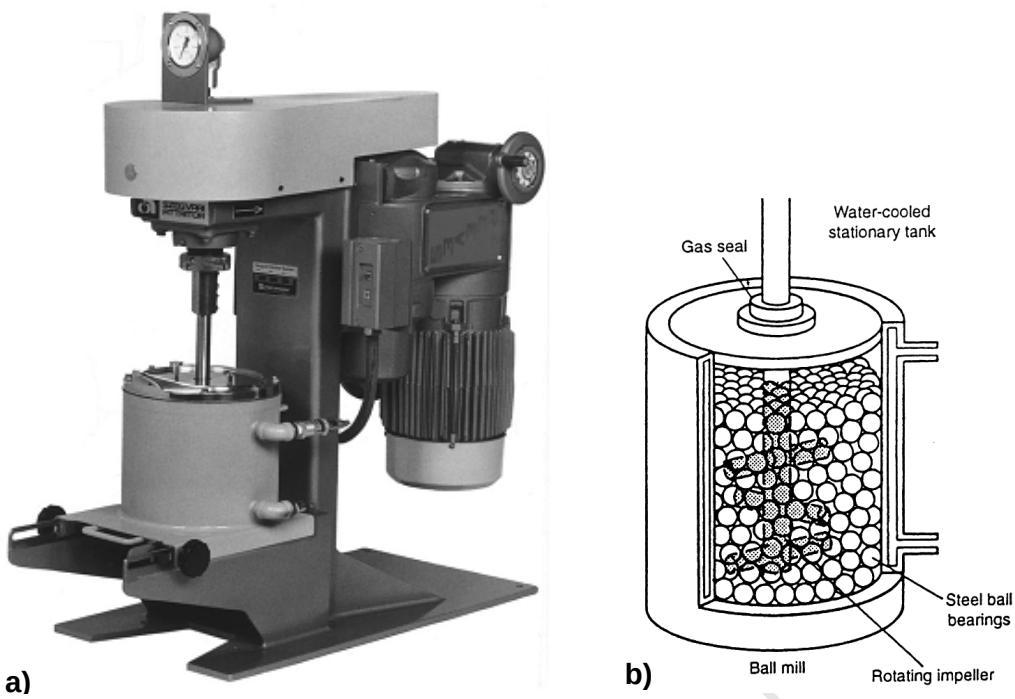

Figure 3.6: (a) Vertical attritor mill (b) section of mill chamber showing the arrangement of rotating arms on the stirrer in the attrition ball mill [31].

Furthermore, the volume capacity of stirred media mills can vary from less than 1ℓ up to more than 1 m^3. Usually, between 70 and 85% of the free mill chamber volume is occupied by the grinding media. The grinding media type and size are chosen depending on the feed material and size [34].

Stirred media mills are available in different designs which vary according to stirrer geometry and chamber design as well as separation device. Separation devices such as screens or a rotating gap are used; which allows the fine product particles through and prevents grinding media from leaving the mill chamber. Three types of stirred media mills can be distinguished [34]:

- Stirred media mill with disc stirrer
- Stirred media mill with pin-counter-pin stirrer
- Stirred media mill with an annular gap geometry

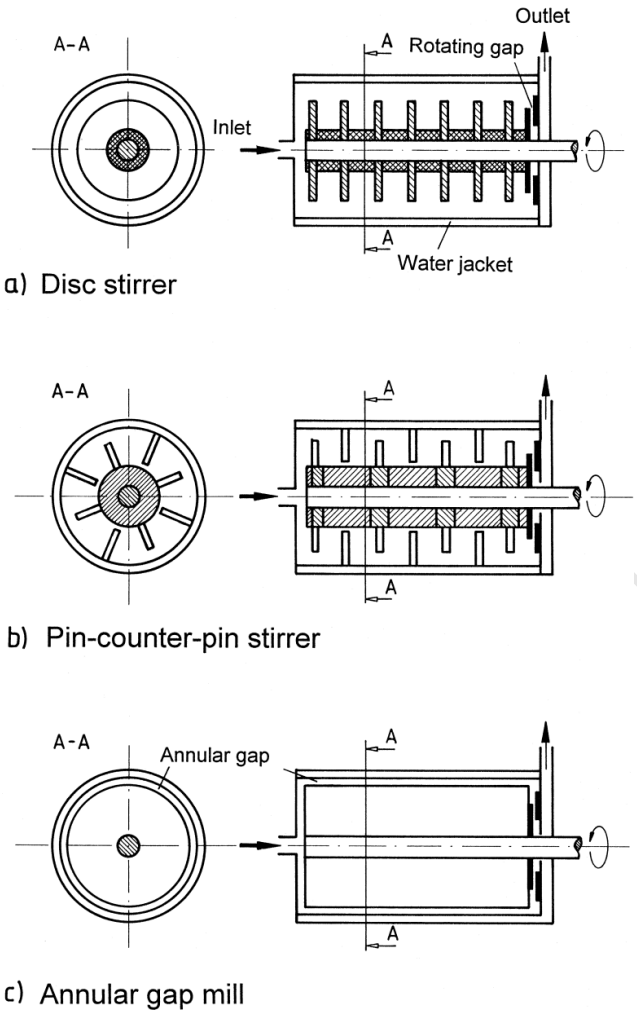

Figure 3.7: Different stirrer and mill chamber geometries [34].

There are mainly two types of stirrer geometry, disc stirrer or pin-counter-pin stirrer. Disc stirrers agitate the grinding media / product mixture mainly by adhesion forces. On the other hand, the pin-counter-pin stirrer transfers energy to the media/product mixture mainly by impact forces. This is due to the stirrer configuration which consists of a rotating pin stirrer and stationary counter pins located on the chamber wall. As a result, the power density at the same circumferential speed is larger in the pin stirrer geometry than in the disc stirrer [34].

The highest power density is found in the annular gap mill. This mill consists of a smooth rotor and mill chamber, such that energy is transferred only by abrasion forces. However, the rotor and/or chamber can also be equipped with pins, producing impact forces in addition to abrasion. This creates an even higher energy density. Furthermore, the width of the annular gap is usually 4 to 10 times the diameter of the grinding media [34].

3.3.5 Comparison between tumbling and stirred ball mill

Due to the operation of tumbling ball mills, they are generally not used in fine grinding applications. The power consumption of tumbling mills is limited by the critical speed of the mill, where the grinding media are centrifuged at the chamber wall, and as a result the power intensity is low [34], [35]. Another disadvantage is that a large part of the mill volume has to be kept empty to allow the mill charge to tumble. In addition, as the grinding media ball size decreases, the size of the inactive zone increases. However, the main reason is the poor energy efficiency experienced when grinding to fine sizes [35].

At product sizes finer than 80% passing 75 µm, the efficiency of tumbling ball mills rapidly decreases and below 30 µm, grinding using tumbling ball mills becomes uneconomical. For tumbling ball mills, the practical limit to product fineness is considered to be 40 - 45 µm [36], [37]. From figure 3.8, it is clear that stirred mills are much more efficient for fine grinding and regrinding than tumbling ball mills. Consequently, with the introduction of stirred mills, fine grinding becomes economical [37].

High speed stirred media mills are increasingly used for fine and ultra-fine grinding applications. They are capable of delivering greater stress intensities and can achieve better energy efficiency than tumbling ball mills in fine and ultra-fine grinding. The stationary mill chamber and rotating stirrer in stirred ball mills provide a more direct and efficient means of transferring energy for particle breakage. Stirred mills also feature a high stirring velocity, aiming to supply sufficient energy input for grinding finer [36].

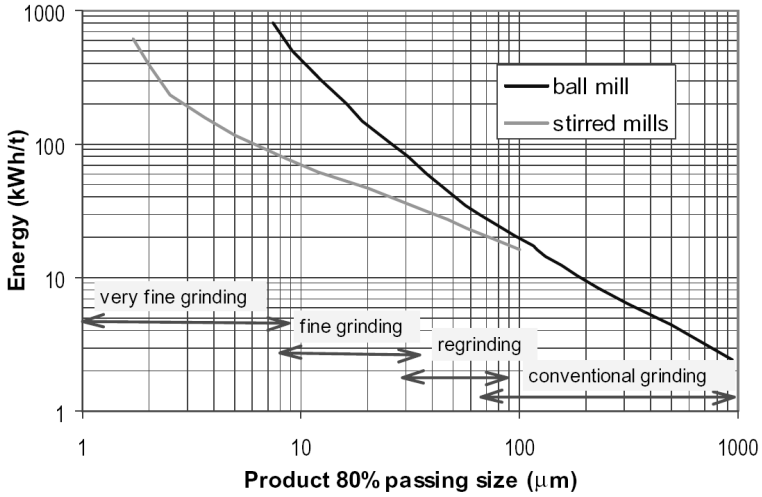

Figure 3.8: Schematic of energy consumption at different grinding stages [37].

Furthermore, the greater performance of stirred media mills over tumbling ball mills in fine grinding can also be extended to coarse grinding applications. F.Shi *et al* [36] investigated the grinding performance of tumbling ball mills and stirred mills for coarse grinding (i.e. using large feed). For stirred mills, they found that using larger and heavier grinding media provided higher kinetic energy, resulting in a combination of impact and attrition breakage modes. This impact breakage mechanism plays a major role for the size reduction of large feed. As a result, the stirred mill took very short milling time (approximately 20 s) to break a feed of 3.35 mm to a product 80% passing size (P_{80}) less than 100 µm. They also found out that on average, 30% energy saving can be expected using the stirred mill over the ball mill for coarse grinding [36].

Overall, stirred ball mills provide the greatest flexibility and can be used in both fine and coarse grinding applications. In addition, milling variables such as grinding media type, size and quantity as well as milling speed and feed rates can easily be modified to meet specific product requirements. This particularly makes the design very versatile and easy to operate [30]. Therefore, a stirred ball mill is the best possible candidate for this study. Since the titanium feed particle in this study are large compared to those used in the literature, a horizontal stirred ball mill should be designed. Compared to low speed vertical stirred ball mills, high speed horizontal mills are capable of producing higher stress intensities which are required for breaking the large titanium feed. A more detailed discussion into horizontal stirred ball mills will follow in section 3.5.

3.4 Milling variables

Mechanical milling involves optimisation of a number of variables to achieve the desired product size. Some of the important parameters that have an effect on final particle size are:

- milling speed
- milling time
- type, size and size distribution of the grinding medium
- ball-to-sample weight ratio
- extent of filling the mill
- milling atmosphere

It is important to note that the interaction between these variables is very strong and therefore the effect of one variable cannot be evaluated without considering the others [31].

3.4.1 Milling speed

Depending on the design of the mill, there are certain limitations to the maximum feasible speed. For example, tumbling ball mills cannot perform efficient grinding above its critical speed since the balls are simply pinned to the mill chamber and do not fall down to exert any impact force. Usually the maximum speed is about 80% of the critical speed so that the balls fall down from the maximum height and produce the maximum collision energy.

Another limitation to high speeds is the resulting rise in temperature within the mill chamber. This may be advantageous in endothermic processes favouring the formation of desired phases. However, in some cases, the rise in temperature may result in the decomposition of metastable phases formed during milling [31].

3.4.2 Milling time

Milling time is the time required to achieve a desired particle size. It varies depending on the type of mill used, the intensity of milling, the ball to sample weight ratio and the temperature of milling. Therefore, optimum milling times are chosen according to the combination of the above mentioned parameters. However, if the feed is milled for times longer than required, the level of contamination increases and undesirable phases may form [31].

3.4.3 Grinding media type

The following factors, some of which are interrelated, are considered when selecting grinding media:

Specific gravity: the density of the media should be higher than the feed material to be ground so that the balls create enough impact force [30].

Initial feed size: media size should be chosen depending on initial feed size. Smaller media cannot easily break up large feed [30].

Final particle size: final feed size is dependent on the grinding media size, i.e. smaller media are more efficient at producing finer particles [30].

Hardness / fracture toughness: harder media are more wear resistant and generate less contamination [30].

Cost: expensive media tend to have better wear properties and therefore last longer [30].

In addition, smaller media provide more contact with the feed than larger media, resulting in a higher collision frequency (stress frequency). However, the stress intensities associated with small media is less due to the small mass of the media. Large size media provide higher stress intensities due to the large weight of the media [26].

Hardened steel, tool steel, hardened chromium steel, tempered steel, stainless steel, tungsten carbide - cobalt and bearing steel are the most common types of materials used for the grinding medium [30], [31].

Table 3.1 : Typical properties for some steel grinding media [38].

Description	Specific Gravity	Hardness (Rockwell C)	Relative cost
Carbon Steel Balls (SAE 1013-case-hardened, SAE 1065—through-hardened)	7.8	60-62	Low
Chromium Steel Balls (SAE 52100)	7.8	62-66	Low to Moderate
Stainless Steel Balls (AISI 440-C)	7.7	55-64	Moderate
Steel Shot, Through-Hardened	7.8	55-60	Low

Partyka and Yan [35] investigated the effect of ball size on the product size distribution in a tumbling ball mill. They proved that smaller media are best suited for fine feeds, while larger media are required for coarse feed. For all the tests, the milling speed and time were kept constant and a ball charge of 20% was used. Figure 3.9 below shows the results for a 55 µm fine feed. All charges are suitable for fine grinding below 45 µm, however the smallest charge is the most efficient since it achieved a fine product while consuming the least amount of energy. On the other hand, with the 1000 um coarse feed test, figure 3.10 shows that the largest charge is most suitable for grinding this feed to fine sizes. It is also shown that small media are inefficient and unsuitable for breaking large feed [35]. Overall, media size should be matched to the size of the feed being ground.

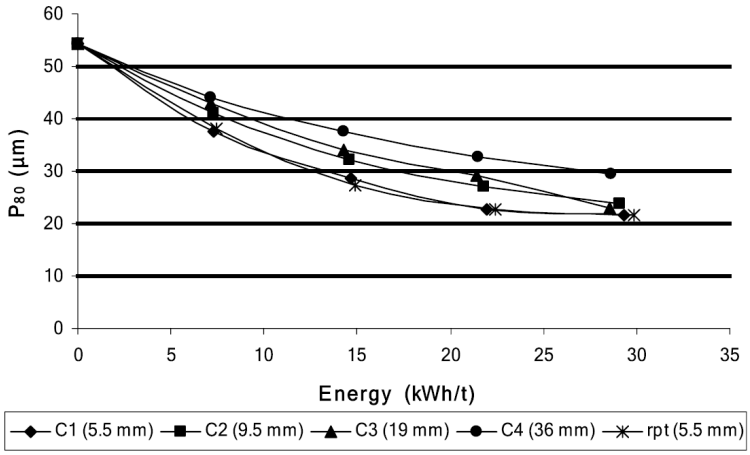

Figure 3.9: 80% passing size of the product versus energy for 55 um feed [35].

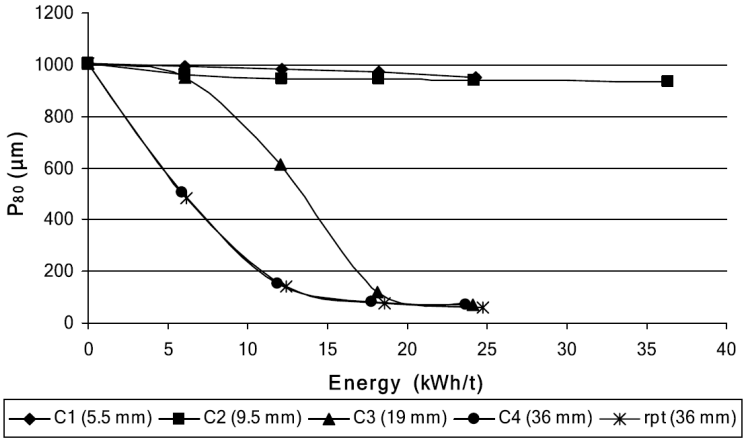

Figure 3.10: 80% passing size of the product versus energy for 1000 um feed [35].

Although only one size of the grinding medium is usually used, the effect of different size balls has been investigated. It has been predicted that the highest collision energy can be obtained if balls with different diameters are used. This is due to the random motion of the different sized balls instead of the well-defined trajectories associated with same size balls [31]. In addition, using different media sizes can also extend the range of particle sizes that can be ground. However, for large reduction ratios, it is usually best to grind in stages. This involves grinding using progressively finer media in different mills or different compartments of a continuous circuit mill [26].

3.4.4 Ball to sample weight ratio

The ratio of the weight of the grinding media balls to the feed sample (BSR) also referred to as charge ratio (CR) is an important variable in the milling process. It

affects the milling time required to achieve a certain size, with higher ratios resulting in shorter milling times. At high BSR, both the stress frequency and intensity increases because of an increase in weight proportion of the balls [31].

Small *et al*. [6] investigated the effects of the BSR on hydrogen absorption rates when milling titanium powder in a Spex shaker mill. Different numbers and sizes of balls were used while the sample mass was kept constant at 1g. In this case, since a sample mass of 1 g was used, the BSR is equal to the weight of the balls. The various ball-to-sample weight ratios are summarised in table 3.2. For each test, the number of hydrogen atoms absorbed per titanium atom was plotted as function of milling time until saturation and is shown in figure 3.11. From figure 3.11, it is clear that high BSR results in rapid hydrogen absorption and therefore faster saturation times [6].

Table 3.2: Ball-to-sample weight ratios [6].

Number of balls	Diameter of balls (mm)	Total ball weight (g)
1	19.0	28.47
2	12.7	17.00
2	11.1	11.35
1	14.3	12.14
1	12.7	8.50
2	9.5	7.11
2	7.9	4.09
1	11.1	5.67
2	6.4	2.17

In all cases the sample mass was 1.0 g.

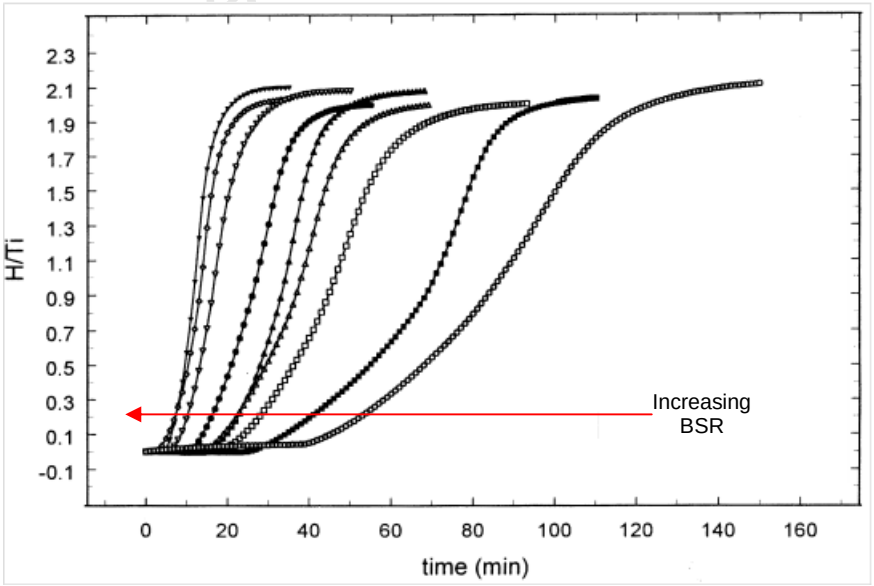

Figure 3.11: Number of hydrogen atoms absorbed per Ti atom as a function of milling time [6].

3.4.5 Extent of filling vial

It is important to ensure that there is enough space for the charge to move around freely in the milling chamber. In horizontal stirred ball mills, the media charge usually occupies 70 to 80% of the free mill chamber volume. In vertical stirred mills, the media charge can be in the 60% range [39]. Tumbling ball mills are commonly filled to about 50% of the mill volume [26].

If the charge is large, then there is inadequate space for the balls to move around and therefore the impact energy is minimal [31]. In addition, hydraulic packing may occur where the media becomes densely packed and non-flowable. Hydraulic packing leads to significant temperature and/or pressure increases and can result in excessive mill chamber and media wear [39]. Alternatively, if the charge is too small, then the production rate is small [31].

3.4.6 Milling atmosphere

Milling normally takes place in chambers that have been either evacuated or filled with an inert gas such as argon or helium. The milling atmosphere is important since it prevents oxidation and/or contamination of the sample. High purity argon is the most common gas used [31]. Different atmospheres have been used during milling for specific purposes. For example, nitrogen atmospheres are used to form metal nitrides and hydrogen atmospheres are used to produce hydrides.

More importantly to this study, a hydrogen atmosphere is required for the hydrogenation of titanium to form titanium hydride.

3.5 High speed horizontal stirred ball mill

In high-speed horizontal (HSH) stirred mills, centrifugal forces are predominant due to high stirrer tip speed and horizontal design that minimizes gravitational forces [26], [29]. The grinding energy is derived from the kinetic energy of the media. Effective transfer of energy from the grinding media to the material being ground occurs at higher speeds. As a result, increasing the stirrer speed increases both the media collision frequency and the impact energy. This leads to higher breakage rates and also extends the range of particle sizes that can be broken [26]. The main breakage modes in HSH mills are attrition combined with impact events, where particles are broken due to the stress acting between the densely packed grinding media. This

stress is proportional to the acting forces and the size of the particles being stressed [29].

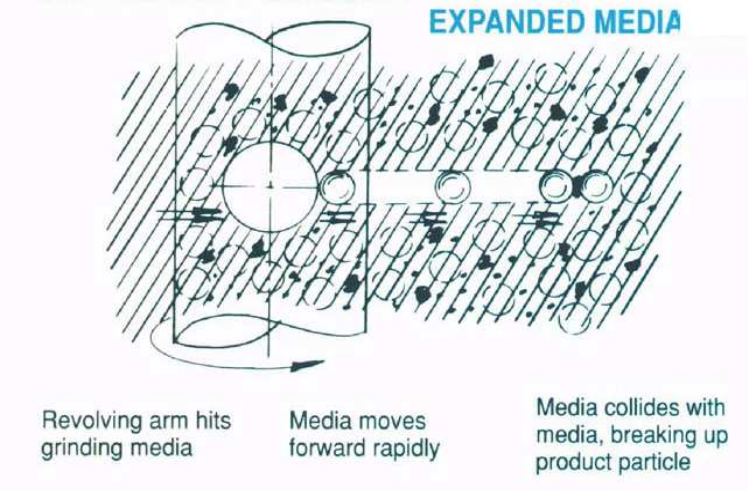

Figure 3.12 : Shows the grinding action of the stirrer inside a stirred ball mill [30].

For HSH mills with disc stirrer design, two zones of high energy density occur. One zone is near the discs where high velocity gradients exist and another zone is located at the mill chamber wall. About 90% of the input energy is dissipated in these zones, although these zones only occupy 10% of the mill chamber volume [40]. Therefore, for optimum grinding, the grinding media have to pass through these zones.

The grinding process in stirred media mills is determined by the stress frequency and stress intensity at each stress event.

3.5.1 Stress intensity

Stress intensity is the most important parameter to determine milling efficiency in HSH mills [29]. The stress intensity is defined differently for the two zones of high energy density. In the zone around the stirrer, the grinding media are accelerated towards the mill chamber wall and thus acquire kinetic energy [41]. Due to the high velocity gradients along the stirrer and near the mill chamber wall, grinding media move at different velocities [42]. As a result, grinding media with higher velocities collide with grinding media with lower velocities and lose a part of their kinetic energy. This kinetic energy can thus be used to grind the feed particles. In contrast, in the zone at the mill chamber wall, particles are stressed between grinding media which are pressed against the chamber wall because of centrifugal acceleration [41]. However, for HSH mills, the stress intensity based on the centrifugal is relatively small compared to that based on the kinetic energy of the grinding media [42].

Therefore, assuming that the elasticity of the feed material is much smaller than that of the grinding media, the stress intensity is approximately proportional to the kinetic energy of the grinding media and is given by:

$$\mathrm{SI} \propto \mathrm{SI}_{\mathrm{GM}} = d_{\mathrm{GM}}^{3}\, \rho_{\mathrm{GM}}\, v_{\mathrm{t}}^{2} \tag{3.3}$$

Where: d_{GM} – diameter of the grinding media

ρ_{GM} – density of the grinding media

v_t – tangential velocity of the grinding media

From equation 3.3 above, it is evident that the stress intensity is fixed during the milling process since the grinding media size, grinding media density and stirrer speed is normally constant.

3.5.2 Number of stress events

The average number of stress events of each particle (*SN*) is determined by the number of media contacts (N_c), by the probability that a particle is caught and sufficiently stressed at a media contact (P_s) as well as by the number of feed particles in the mill (N_p) [43].

$$\mathrm{SN} = \frac{N_{\mathrm{C}}\, P_{\mathrm{S}}}{N_{\mathrm{P}}} \tag{3.4}$$

The number of media contacts can be assumed to be proportional to the rotational speed of the stirrer, to the milling time and to the number of grinding media in the mill chamber. The probability that a particle is caught and sufficiently stressed is proportional to the active volume between two media which in turn is proportional to the grinding media diameter. Therefore, particles have a higher probability of being stressed if large grinding media are used. Furthermore, the number of feed particles is proportional to the overall volume of the feed particles [42].

4 DESIGN OF STIRRED BALL MILL

One of the objectives of this project is to design and build a laboratory scale ball mill capable of hydrogenating titanium waste metal and producing titanium hydride powder. As described in the literature review in section 3.3.5, the horizontal stirred ball mill is the ideal type of ball mill to grind the coarse titanium feed. More specifically, as mentioned in section 3.3.4, the horizontal stirred ball mill with a pin-counter-pin stirrer geometry is found to provide a higher power density than the disc stirrer. The main components of the stirred ball mill are the mill chamber and the stirrer. Each of these components would have to meet specific requirements and are described further below.

4.1 Mill chamber design

4.1.1 Design requirements

In order to hydrogenate the titanium feed, the mill chamber will be filled with hydrogen gas to a pressure of 200 kPa. As a result, the mill chamber has to be designed as a pressure vessel. However, prior to filling with hydrogen gas, the air in the mill chamber will be evacuated until a vacuum of at least 1×10^{-1} mbar is reached. Since hydrogen gas is an extremely flammable gas, this is done to prevent the possibility of an explosion. Therefore, the mill chamber has to be leak tight, preventing hydrogen gas from escaping and air from entering the mill chamber. In addition the mill chamber would also need to have gas inlet ports for argon and hydrogen gas as well as exhaust ports for evacuating the air and venting the mill.

Furthermore, a convenient method for adding the feed and removing the mill contents (i.e. product yield and grinding media) has to be incorporated into the design of the mill chamber. Once the mill chamber is emptied after milling, it is highly unlikely that all the product and grinding media are removed. As a result, having the option of opening the mill chamber would be desirable. This provides the opportunity to ensure that all the mill contents are removed and that the inside of the mill is clean before the next test. In addition, the inside of the mill chamber can also be inspected for any signs of wear.

Since a rise in temperature within the mill is also expected, it would be useful to monitor and control the temperature during milling. Therefore locations for a thermocouple and a cooling system such as a copper cooling coil or water jacket have to be included in the design of the mill chamber.

4.1.2 Conceptual designs

Four mill chamber concepts will be discussed in detail.

Concept 1: Split mill chamber with bearing and seal cartridges

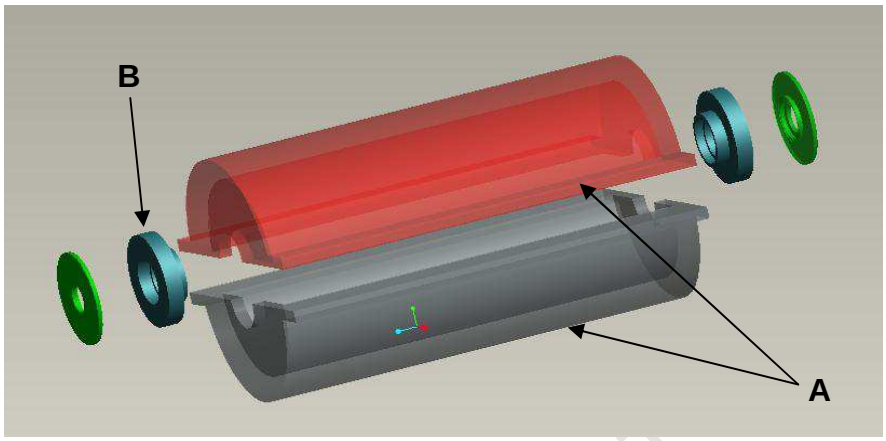

Figure 4.1: Exploded view of mill chamber. A – two symmetrical halves of the mill chamber and B – bearing and seal cartridge.

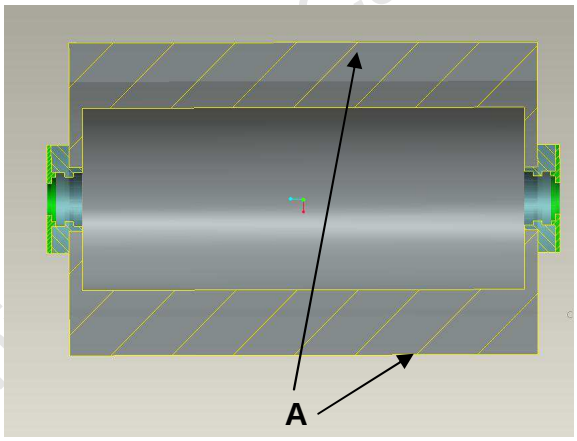

Figure 4.2: Cross-sectional view of mill chamber. A – sealing lips.

Design Description:

This concept consists of a cylindrical mill chamber made up of two symmetrical halves. The two halves are bolted together, with an intermediate gasket, along the sealing lips which are located on the longitudinal sides of the mill chamber. Two concentric holes are machined at the centre of either side of the mill chamber for locating the stirrer shaft bearing and seal cartridges. Once the bearings and shaft seals are placed into cartridges, the cartridges are mounted into these holes. Prior to milling, feed and grinding media have to be added before bolting the top half of the

mill chamber. After every test, the bottom half of the mill chamber has to be removed in order to empty the mill contents.

Concept 2: Mill chamber with removable discharge tray

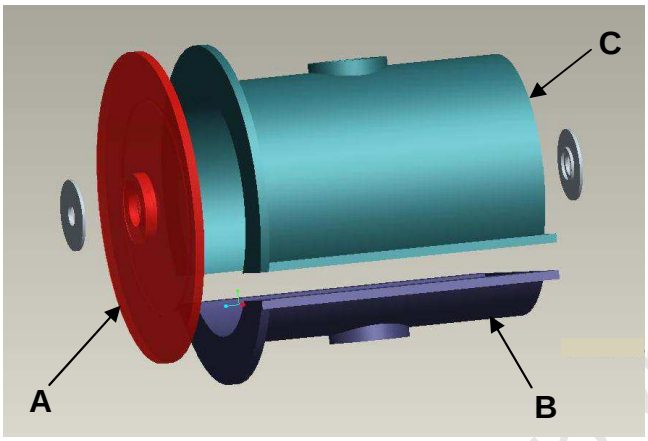

Figure 4.3: Exploded view of mill chamber assembly. A – end flange, B – discharge tray and C – mill chamber (top half).

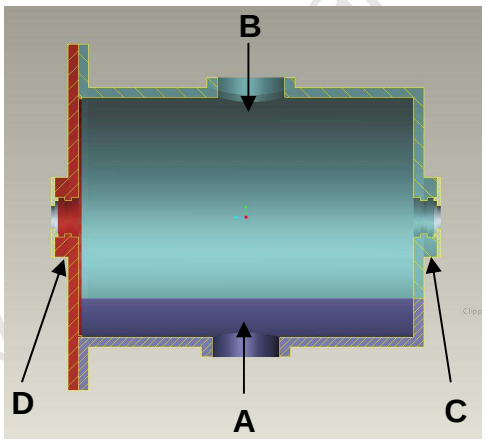

Figure 4.4: Cross-sectional view of mill chamber assembly. A - outlet opening, B - inlet opening, C - bearing shoulder (closed side of mill chamber) and D - bearing shoulder (flange).

Design Description:

This design again consists of a split mill chamber with two halves which together forms a cylindrical chamber. However, it differs from concept 1 in that the mill chamber is split below the stirrer shaft bearing and seal location holes. In addition, an end flange is included in the design which ensures that the two halves are held together. Similar to concept 1, sealing lips are also located along the longitudinal sides of the mill chamber. In order to house the stirrer shaft bearings and seals, both

the closed sides of the top half of the mill chamber as well as the flange are machined to have shoulders. The top half of the mill chamber has an inlet opening through which feed and grinding media can be added and the discharge tray has an outlet opening for removing the mill contents after milling. The option also exists to remove the entire discharge tray for ensuring that all the mill contents are removed between each test.

Concept 3: Rotatable mill chamber with inlet/outlet feed lid

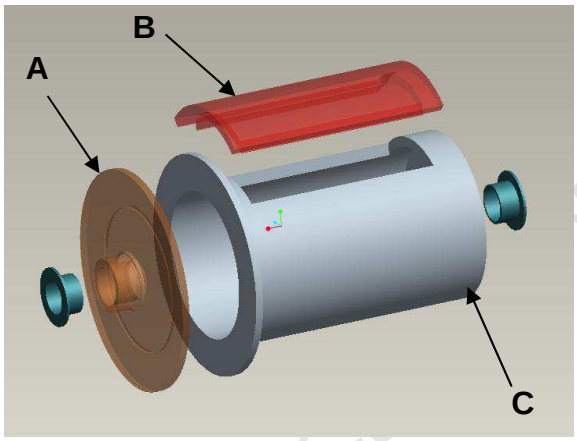

Figure 4.5: Exploded view of mill assembly. A – end flange, B – feed inlet/outlet and C- mill chamber

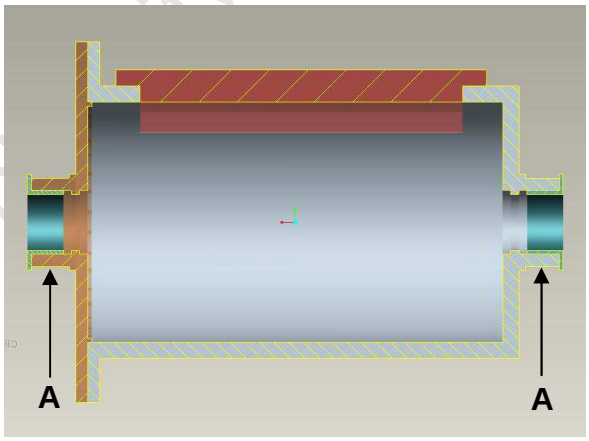

Figure 4.6: Cross-sectional view of mill assembly. A - shoulder supports.

Design Description:

This design consists of a cylindrical mill chamber with a single opening that functions as an inlet for the feed and grinding media as well as an outlet for removing the mill contents after milling. Similar to concept 2, a flange closes the open side of the mill

chamber. Both the closed end of the mill chamber as well as the flange is machined to have shoulders for housing the stirrer shaft seals and bearings. These shoulders also allow a support system with bearings to be mounted, which allow the whole mill chamber to rotate. Therefore the feed opening can be positioned to the top for adding feed and grinding media before milling and positioned to the bottom for removing the mill contents after milling.

Concept 4: Mill chamber designed for a cantilever stirrer shaft

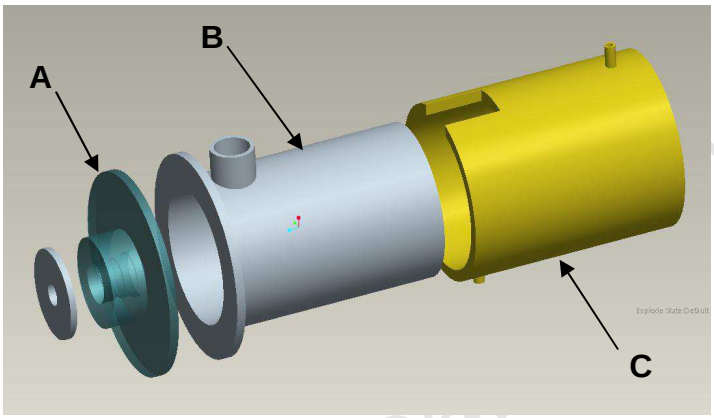

Figure 4.7: Exploded view of mill chamber assembly. A – end flange, B – mill chamber and C – water jacket.

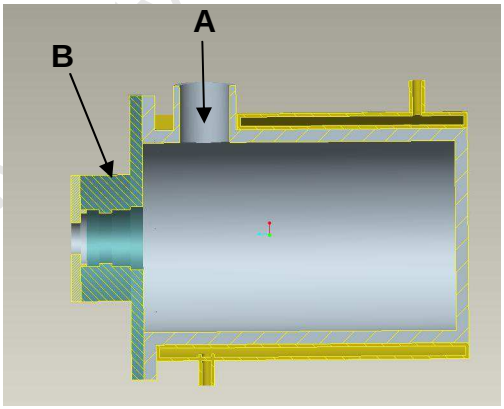

Figure 4.8: Cross-section view of mill assembly. A – feed inlet opening and B – hub flange which houses stirrer shaft bearings and seal.

Design Description:

The design and assembly of this mill chamber is similar to concept 3, except the closed end of the mill chamber does not have a stirrer shaft bearing and seal housing. In addition, the removable lid has been replaced with a feed inlet opening.

The design of the mill chamber also allows a removable water jacket to be placed over the mill chamber for cooling purposes. The hub flange is machined to house the stirrer shaft seal as well as a double bearing arrangement for supporting a cantilevered stirrer shaft. Feed and grinding media are added via the feed inlet and the mill contents are removed by unbolting the mill chamber from the end flange.

4.1.3 Design decision

A list of disadvantages and advantages will be given for each of the mill chamber concept designs. The design which best meets the mill chamber design requirements will be chosen.

Concept 1: Split mill chamber with bearing and seal cartridges

Design Advantages:

- Inspecting and cleaning the inside of the mill chamber is simple because of the split chamber design
- Mill assembly consist of two halves and thus one common sealing surface, thereby minimising the risk of a pressure/vacuum leak.
- Bearing and seal cartridges allows for easy mounting of the bearings and seals

Design Disadvantages:

- For every test, the mill chamber has to be opened for adding the feed and grinding media as well as for removing the mill contents.
- Difficult to ensure that the bearing and seal cartridge holes on either side of the mill chamber is concentric. This could lead to stirrer shaft misalignment problems.
- The gasket between the sealing lips may affect the roundness of the bearing and seal cartridge holes, thereby increasing the risk of a leak.
- Adding a cooling system around the mill chamber is also difficult and will prevent the opening/closing of the mill chamber.

Concept 2: Mill chamber with removable discharge tray

Design Advantages:

- Mill chamber has an inlet and outlet opening for adding and removing feed respectively and therefore requires no disassembly.
- Easy to ensure that the stirrer shaft bearings are aligned.
- The discharge tray can be removed to ensure that all the mill contents are removed after every test. Removal of the discharge tray also allows for periodic inspection of the inside of the mill chamber and enables cleaning of the mill chamber.

Design Disadvantages:

- Mill content may fall out of the discharge tray upon removing it, since one side is open.
- Adding a cooling system is difficult because of the sealing lips and the feed inlet opening. In addition, adding a cooling system will also prevent the removal of the discharge tray.
- Compared to concept 1, the mill chamber assembly is made up of three separate components. As a result, the possibility of a leak is greater.

Concept 3: Rotatable mill chamber with inlet/outlet feed lid

Design Advantages:

- A single opening is used for both adding feed and removing mill contents.
- The mill chamber is rotatable thereby facilitating the adding / removal of feed.
- The size of the feed opening is large enough such that the mill chamber does not have to be disassembled for removing residual mill contents. The inside of the mill chamber can also be cleaned and inspected through this opening.

Design Disadvantages:

- Adding a cooling system will obstruct the feed inlet/outlet opening.

- Similar to concept 2, the mill assembly consist of three parts. Therefore, compared to concept 1, the possibility of a leak is also greater with this design.

Concept 4: Mill chamber designed for a cantilever stirrer shaft

Design Advantage:

- A cooling system can be added without obstructing the feed inlet opening.
- The mill chamber assembly only consists of two parts and therefore the possibility of a leak is less likely to occur when compared to concepts 2 and 3.
- Only one stirrer shaft seal is required at the flange side, since the stirrer shaft is cantilevered.
- The mill chamber can easily be unbolted for cleaning and periodic inspection.

Design Disadvantage:

- The mill chamber has to be unbolted from the flange in order to remove the bulk of the mill contents after every test.

Chosen design

After analysing each conceptual design, the mill chamber discussed in concept 4 is chosen. The list of advantages for concept 4 exceeds those of the other concepts and meets most of the specified mill chamber requirements. However, it has one minor problem where the mill chamber has to be opened after every test in order to remove the bulk of the mill contents. This can be considered time consuming especially if many experiments are conducted. The mill contents can also easily fall out upon opening the mill chamber. Therefore, it would be desirable if the bulk of the mill contents were first emptied through an alternative method, before opening the mill chamber to remove the remaining contents.

4.2 Specific mill chamber design description

A detailed description of the chosen mill chamber design will follow.

4.2.1 Modifications to chosen mill chamber design

Cooling system

Ideally, the water jacket suggested in concept 4 would function best if it fits tightly over the mill chamber in order to increase its contact area. However, manufacturing the water jacket with a tight clearance over the mill chamber would be difficult. Alternatively, it was decided to rather wind copper tubing along a helical groove machined on the outside of the mill chamber. Similar to the water jacket, water flowing through the copper coil would then cool the mill chamber.

Rotatable mill housing

By making the mill chamber rotatable, the feed inlet opening on the mill chamber can also be used as an outlet for emptying the mill contents. In this way, the bulk of the milled contents can first be emptied through the inlet/outlet opening and thereafter the mill chamber can be opened for removing the remaining contents. In order to facilitate rotation of the mill chamber, the mill chamber design was modified such that support stands can be used to slightly elevate the mill chamber above the work bench. These stands would then allow the mill chamber to rotate about the stirrer shaft.

4.2.2 Material selection

Since the feasibility of using a stirred ball mill to activate the hydrogenation process has to be investigated, the mill chamber assembly was made from mild steel. Mild steel is relatively cheap and provides the necessary material properties that are acceptable for a pressure vessel. Since it is a ferrous metal, it has the advantage of being magnetic. Therefore, if it contaminates the non-magnetic titanium product yield, it can easily be separated by using a magnet. In an ideal situation, the inside of the mill chamber is lined with a wear resistant material. Using a wear resistant lining prolongs the life of a mill and most importantly prevents contamination. However, a lining was not used in this study because the main objective is to find the optimum milling parameters. Eventually when the optimum milling parameters are found, a suitable lining can be added.

Furthermore, the support stands were also made from mild steel. In order to facilitate rotation of the mill chamber, phosphor bronze bushes were also pressed into the stands.

4.2.3 Mill chamber dimensions

In order to test the feasibility of using a stirred ball mill, a laboratory scale mill with a 1.3 litre capacity and a length to diameter ratio of 1:1 was designed. As a result, both the inner diameter and the length of the mill chamber were calculated to be 120 mm, using the following formula:

$$V = (\pi d^2 h) /4 \tag{4.1}$$

Where: V - volume of the chamber (i.e. 1.3 ℓ)

d - inner diameter of the mill chamber

h - length of the mill chamber

In terms of finding the minimum wall thickness to safely hold 200 kPa of hydrogen gas, the following formula was used:

$$P_{all} \times s.f = \frac{\sigma_y}{2R_2^2}\left(R_2^2 - R_1^2\right) \tag{4.2}$$

Where: P_{all} - allowable working pressure (i.e. 0.2 MPa)

s.f - safety factor

σ_y - yield strength of mild steel (≈ 200 MPa)

R_1 - inner radius of the mill chamber (i.e. 60 mm)

R_2 - outer radius of the mill chamber

For a safety factor of 4, the corresponding minimum wall thickness was calculated to be less than 1 mm. This is due to the high yield strength of the mild steel relative to the low operating pressure of the mill. Clearly this wall thickness is impractical and difficult to manufacture. Consequently, a larger wall thickness is required. In order to account for the wear of the inner wall and to allow the helical groove to be machined on the outer wall, a conservative wall thickness of 6 mm was chosen. Since the hub flange forms part of the mill chamber assembly, it is also designed to have the same wall thickness.

Furthermore, when a cylinder is subjected to internal pressure, a three-dimensional complex stress system is created within the structure. Since the mill chamber is manufactured from a ductile material, the maximum shear stress theory is used as the yield criterion. According to this theory, failure of the mill chamber is avoided by ensuring that the maximum shear stress in the chamber wall is less than (or equal to) the maximum shear stress at yield in a tension-test specimen of the same material.

In the case of a cylinder, the maximum shear stress is at the inside radius and is given by the following equation:

$$\tau_{max} = \frac{\sigma_H - \sigma_R}{2}; \qquad \sigma_H > \sigma_R \tag{4.3}$$

Where: τ_{max} *- maximum shear stress*

σ_H *- hoop stress*

σ_R *- radial stress*

Based on the selected dimensions, the hoop and radial stresses were calculated for the mill chamber as follows:

1. Maximum hoop stress (which occurs at the inside radius, R_1):

$$(\sigma_H)_{max} = P_{all}\left(\frac{R_2^2 + R_1^2}{R_2^2 - R_1^2}\right) \tag{4.4}$$

   Based on the above equation, the maximum hoop stress was found to be 2.1 MPa.

2. Maximum radial stress (σ_R) is simply equal to the internal pressure of 0.2 MPa (compressive).

In order to prevent cylinder failure: $\tau_{max} = \frac{\sigma_H - \sigma_R}{2} \leq \frac{\sigma_y}{2}$

$$\therefore \sigma_H - \sigma_R \leq \sigma_y \tag{4.5}$$

By substituting the maximum hoop and radial stresses into equation 4.5, the difference between the two stresses was calculated to be 2.3 MPa. Since this difference is significantly lower than the yield strength of mild steel, the condition in equation 4.5 is satisfied and thus it is safe to assume that the mill will operate safely at 200 kPa without failing. Therefore, the dimensions for the mill chamber are acceptable. Detailed calculations for the mill chamber and a complete set of machine drawings for the mill chamber assembly are included in the Appendix.

4.2.4 Design features

The final design of the mill chamber is made up of a thin-walled cylinder with one end closed and the other end open. The open end of the cylinder has a welded flat face flange, with an o-ring groove. Once the o-ring is placed in position, the mill chamber is sealed and bolted closed with a separate hub flange. The hub flange houses the stirrer bearings and therefore supports the stirrer shaft. In addition, the face of the hub flange has a raised ring machined into it which mates with the inner diameter of the mill chamber. This raised ring is important because it ensures that the mill chamber and stirrer remain concentric.

A support shoulder was also added to the closed-end side of the mill chamber in order to allow a support stand to be located on this shoulder. This support stand, together with another stand on the existing shoulder of the hub flange, ensures that the stirrer shaft of the mill assembly is concentric with the drive motor shaft. These stands also elevate the mill chamber above the work bench and therefore facilitate with the rotation of the mill chamber. The rotation of the mill chamber is important because it assists with adding feed and grinding media as well as removing the mill contents. It was decided to have only one neck-flanged opening on the mill chamber which serves as both an inlet and outlet for the feed and grinding media. By making the mill chamber rotatable, this allows the flanged opening to be positioned to the top for adding feed and positioned to the bottom for removing the mill contents. In addition, this flanged opening is threaded so that a threaded plug with an o-ring can be used to seal the opening.

For cooling purposes, a copper tube was wound around a helical groove on the outside of the mill chamber. This groove was machined around the mill chamber in order to increase the contact area of the copper coil. Alternatively, in terms of monitoring the temperature inside the mill chamber, the threaded plug which seals the feed inlet/outlet was adapted to include a type K thermocouple. A compression fitting was used on the plug to keep the thermocouple securely in place.

Furthermore, another neck-flanged opening on the closed-end side of the mill chamber serves as a gas inlet/outlet. Before milling, air in the mill chamber is evacuated through this opening and it also serves as an entry point for hydrogen and argon gas. After milling, this opening also allows residual gas to flow out of the mill chamber and into a fume cupboard.

Figures 4.9 and 4.10, below, illustrate the various design features of the mill chamber after manufacturing and assembly.

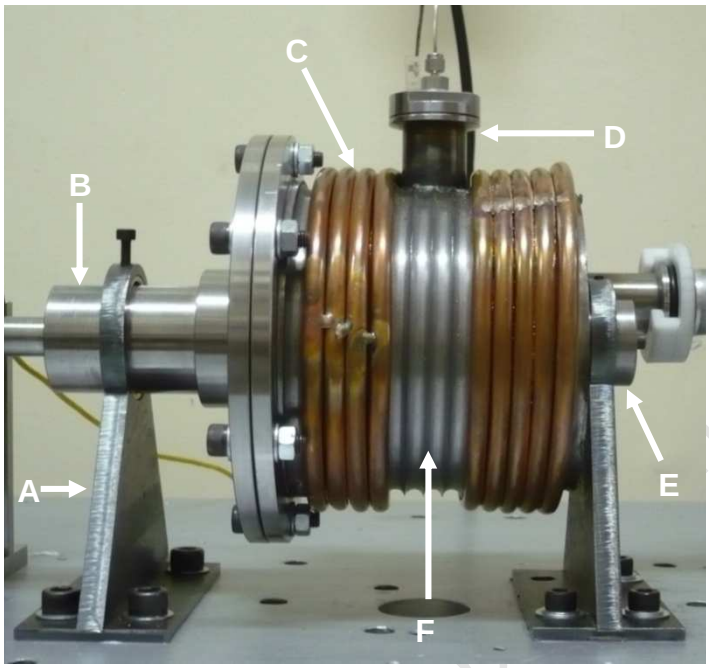

Figure 4.9: Front view of mill chamber assembly. A – hub support stand, B – hub flange, C – copper cooling coil, D – feed inlet/outlet neck-flange, E – support shoulder and F – mill chamber with helical groove.

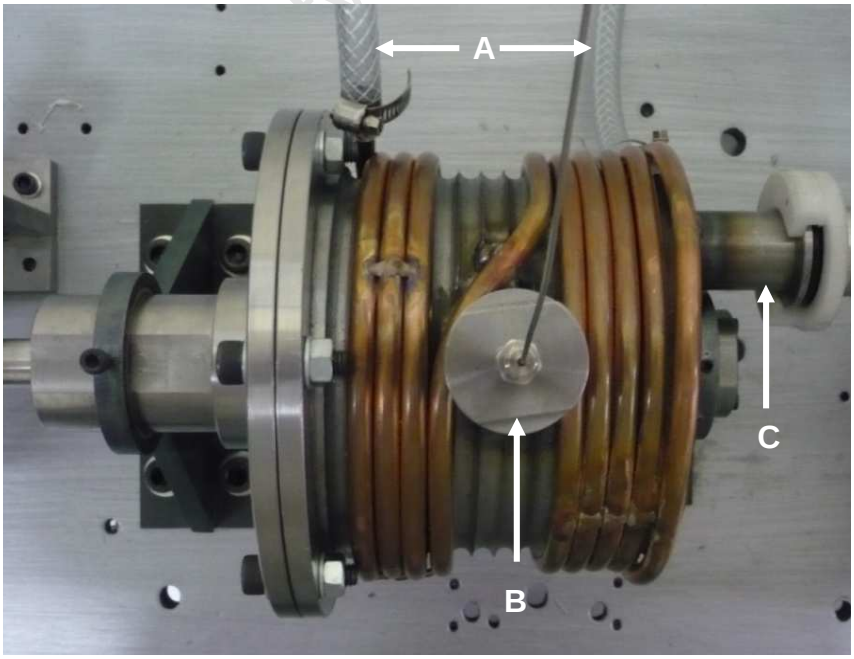

Figure 4.10 : Top view of mill chamber assembly. A – water inlet and exit points, B – threaded plug with thermocouple attachment and C – gas inlet/outlet neck-flange.

4.3 Stirrer design

4.3.1 Design requirements

The stirrer is a key component in the stirred ball mill as it is responsible for projecting the grinding media into the more active regions. It has to be designed in order to facilitate feed circulation and eliminate any dead zones in the mill. For the pin-counter-pin stirrer, dead zones are usually present at the bottom of the mill, between two stirrer pins and the chamber wall. Therefore the stirrer design is important and its efficiency to eliminate dead zones is influenced by the pin length and the number of pins along the stirrer. The pin length determines the gap between the pin tip and mill chamber wall, while the number of pins determines the distance between successive pins along the stirrer. However, to find the optimum stirrer design, these parameters have to be chosen experimentally. Therefore, the design of the stirrer has to be versatile, allowing different sets of pin lengths and number of pins to be used.

Note, for this study, stationary counter pins which are located on the mill chamber wall were not included in the design of the stirrer. Since the pin length and number of pins will be changed frequently, removing and replacing these pins would be difficult. Therefore, simply a pin stirrer was designed and not a pin-counter-pin stirrer.

4.3.2 Conceptual designs

Two stirrer concepts will be discussed in detail.

Concept 1: Stirrer with pressed pins

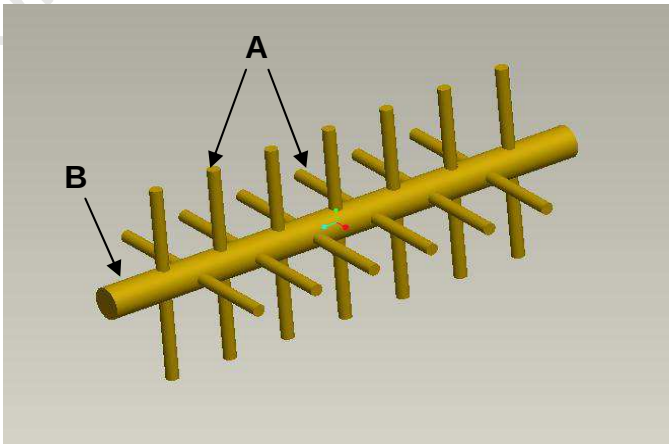

Figure 4.11: Stirrer shaft with pressed pins. A – pins and B – stirrer shaft.

Design Description:

A fixed number of pins with a certain length and diameter are pressed into the stirrer shaft. Holes are machined along the stirrer shaft such that the pins are orientated 90º to one another and located at a fixed distance apart. As the stirrer shaft rotates, the pins come into contact with grinding media and force them outwards towards the chamber wall as a result of centrifugal forces.

Concept 2: Stirrer consisting of pin-collar sub-assemblies

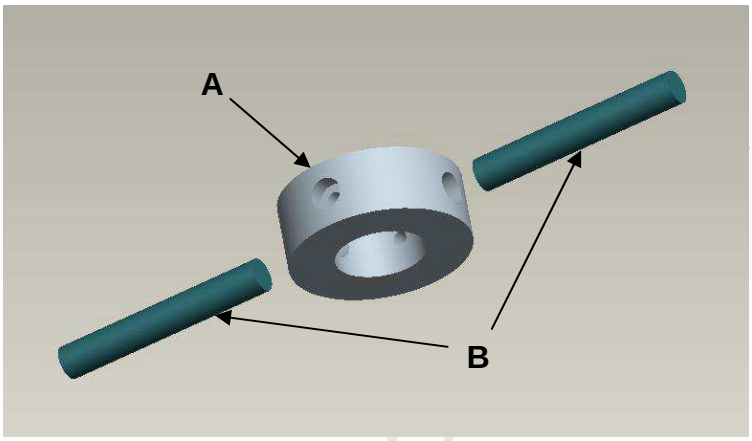

Figure 4.12: Exploded view of pin-collar sub-assembly. A - collar and B - pair of pins.

Design Description:

This stirrer assembly consists of a stirrer shaft with a set of removable pin-collar subassemblies. Each pin-collar sub-assembly consist of a pair of pins pressed into a collar. Pins with different lengths can be pressed into the collars. Threaded holes are also machined into the collar, so that set screws can be used to lock the collar to the stirrer shaft. Once the collars are slid over the stirrer shaft, their orientation can be adjusted. In addition, appropriately sized spacer collars can be used between pin-collar sub-assemblies in order to keep them at a fixed distance apart.

4.3.3 Design decision

Similar to how the mill chamber design was chosen, a list of disadvantages and advantages will also be presented for the two stirrer design concepts. The design which best meets the stirrer design requirements will be chosen.

Concept 1: Stirrer with pressed pins

Design Advantages:

- Pins are placed at 90° to each other thereby increasing the chance of contact with the grinding media.
- Pins are easily removed and can be replaced with pins that have the same or different pin length.

Design Disadvantages:

- Along the stirrer shaft, holes for the pins are machined at a fixed distance apart. As a result, a whole new stirrer shaft has to be manufactured for different pin-to-pin spacing.
- If the number of pins along the stirrer shaft is increased, a new stirrer shaft has to also be manufactured.

Concept 2: Stirrer consisting of pin-collar sub-assemblies

Design Advantages:

- Pins are easily removed from the collars and can be replaced with pins that have the same or different length.
- Pin-collar subassemblies allow both the distance between pins along the stirrer shaft and the angle between each pin to be varied.
- The number of pins along the stirrer can easily be adjusted by either adding or removing pin-collar sub-assemblies.

Chosen design

Based on its advantages and flexibility, concept 2 is chosen. This concept allows the pin length and the number of pins along the stirrer to be varied without having to manufacture a new stirrer.

4.4 Specific stirrer design description

A detailed description of the chosen stirrer design will follow.

4.4.1 Material selection

Based on the function of the stirrer assembly, it constantly experiences both impact and shearing stresses from the grinding media. The stirrer is also located in the active grinding region of the mill. As a result, a material which offers good wear and corrosion resistance is required. Stainless steel AISI 304 was selected as a suitable material for the stirrer assembly, since it meets both of these requirements. The selected diameter of the stirrer shaft and pins are standard sizes and therefore require minimum machining. Consequently, these components were manufactured from stainless steel AISI 304. However, the pin-collars and spacer collars require more intricate machining as will be described later in section 4.4.4. Due to the difficulty of machining austenitic stainless steel, Böhler M300 was selected as an alternative material for manufacturing both types of collars. This martensitic stainless steel has similar mechanical properties and chromium content as stainless steel. The mechanical properties of Böhler M300 are listed in table 4.1, below.

Table 4.1: Mechanical properties of M300 at a hardened and tempered condition [44].

Mechanical Properties	
Brinell Hardness	270-330
Ultimate Tensile Strength	900 - 1100 MPa
Yield Strength @ 0.2% strain	650 MPa

4.4.2 Stirrer dimensions

The section of the stirrer shaft that protrudes inside the mill chamber has a nominal diameter of 20 mm and a length of 120 mm. Each pin-collar subassembly has a pair of 8 mm diameter pins pressed into 40 mm x 20 mm x 12 mm collars. Since the optimum pin length has to be investigated, two sets of pins were manufactured. The length of each set of pins was chosen according to how many grinding media can pass between the pin tip and chamber wall. For a two grinding media spacing between the pin tip and mill chamber wall, a set of 30 mm pins were manufactured. Alternatively, a set of 26 mm pins were manufactured in order to give a three grinding media spacing.

In addition, the optimum number of pins along the stirrer has to be investigated. Since each pin-collar sub-assembly consists of a pair of pins, the number of pin-collars determines the total number of pins on the stirrer assembly. The number of pin-collars used along the stirrer shaft was chosen according to how many grinding media can pass between each successive pin. For a two grinding media spacing between each consecutive pin, 6 pin-collars are required along the stirrer shaft; resulting in a stirrer with 12 pins. However, for a three grinding media spacing, 5 pin-collars with a total of 10 pins are required. Based upon the required grinding media spacing between each pin, suitable spacer collars are placed in between each pin-collar. The thickness and the amount of spacer collars required are shown in table 4.2. Note that the end spacers are placed between each side of the chamber wall and the pin-collar. Furthermore, a complete set of machine drawings for the stirrer assembly are included in the Appendix.

Table 4.2 : Spacer collar requirements for each configuration

	6 pin-collar configuration	**5 pin-collar configuration**
spacer collars	5 x 6 mm	4 x 9 mm
end spacer collars	2 x 8 mm	2 x 11 mm

4.4.3 Design features

The final design of the stirrer assembly consists of a stirrer shaft and a set of removable pin-collar sub-assemblies. Each pin-collar sub-assembly consists of a collar with a pair of pins that are 180° apart. These pins are pressed into the collar and can easily be removed so that different sets of pin lengths can be used. In addition, since these pin-collars are not permanently fixed to the stirrer shaft, the number of pin-collars on the shaft can easily be varied. More importantly, the total number of pins along the stirrer shaft can be varied. Overall, the pin length and the number of pins can easily be changed, giving rise to different stirrer configurations. Appropriately sized spacer collars were also designed to keep these pin-collar sub-assemblies evenly spaced along the stirrer shaft.

In order to find the optimum stirrer design, the mill chamber will be opened frequently in order to change the stirrer configuration. As a result, a cantilevered stirrer shaft was designed which protrudes from the hub flange into the mill chamber. In order to support the stirrer assembly, a double bearing arrangement was designed and

located in the hub flange. Since the stirrer is only supported by the hub flange of the mill assembly, the mill chamber can easily be removed.

Furthermore, four flat sides, each at 90º to one another, were machined along the section of the stirrer shaft which protrudes in the mill chamber. Similarly, the inner diameters of the pin-collars also have matching flat sides machined into them. This was done to prevent any relative rotational motion between the pin-collars and stirrer shaft. These flat sides also allow each pin-collar sub-assembly to be orientated at 90° to one another. In addition, the pin-collars have two set screws which secure the collars axially along the stirrer shaft. As a result, both the set screws and the flats enable the transfer of torque from the stirrer shaft to the pin-collar sub-assemblies.

Figure 4.13 : Shows a pair of stirrer pins pressed into a collar.

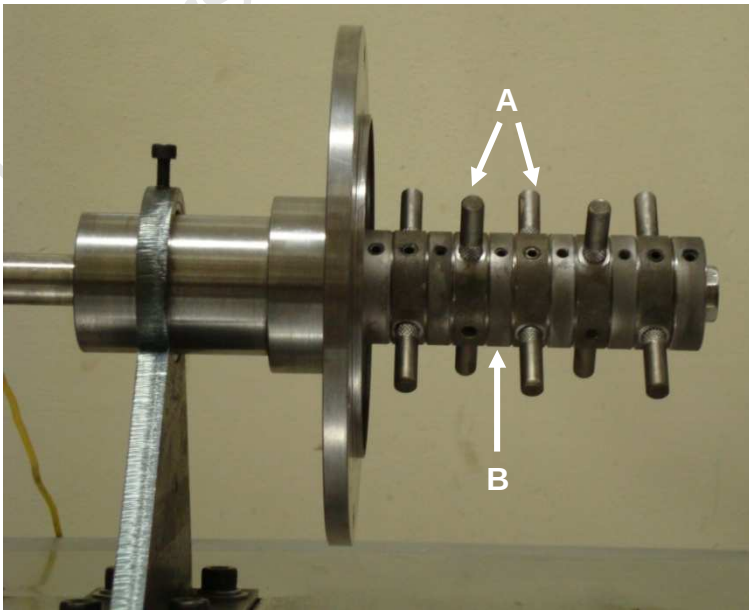

Figure 4.14 : Shows cantilevered stirrer assembly. A – pin-collar subassemblies set at 90º to each other and B – spacer collar.

4.5 Drive motor and control

As mentioned before, hydrogen gas is classified as an extremely flammable gas. Since the mill chamber will be pressurized with hydrogen gas, it is imperative that there are no sources of ignition around the mill. However, a potentially hazardous area would be around the drive motor. If there is a hydrogen leak, the resulting explosive atmosphere around an ordinary “sparking” electric motor could cause an explosion or fire. As a result, a flameproof motor with an explosion protected (Ex d) enclosure had to be acquired. These motors are designed to operate in environments that continuously, periodically or intermittently contain flammable gases. In addition, the motor enclosure is designed to perform two functions. Firstly, the enclosure prevents an internal explosion from igniting the surrounding atmosphere. Secondly, it prevents the external exposed surfaces from exceeding the auto-ignition temperature of the flammable gas.

The smallest available motor was found to be a 3-phase, 0.75 kW motor with a rated speed of 930 rpm. Since only a 1.3 litre laboratory scale mill was designed, this motor provides more than enough power and speed. For the purpose of transmitting power from the drive motor shaft to the stirrer shaft, a flexible jaw coupling was used at the ends of both shafts.

Furthermore, in order to vary the speed of the motor, an existing variable speed drive was connected to the flameproof motor. An existing LCD preset counter and rotational speed sensor was also connected. As a result, the speed of the motor can be measured and the motor can be programmed to run for a predetermined amount of cycles.

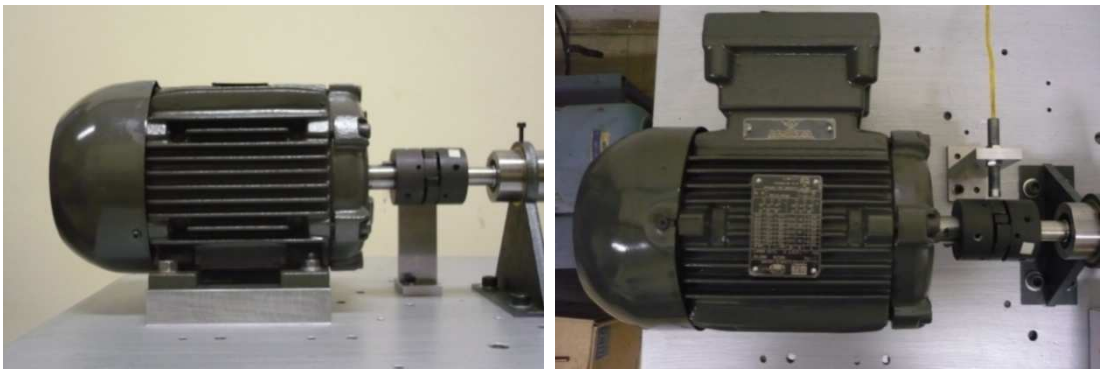

Figure 4.15: Shows the front and top view of the flameproof motor.

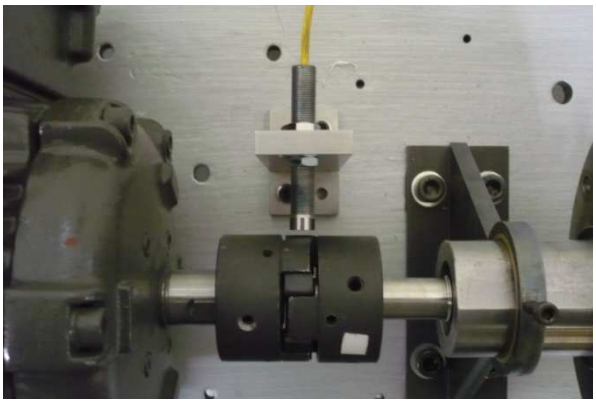

Figure 4.16 : Shows the flexible jaw coupling and the rotational speed sensor.

4.6 Piping and instrumentation

4.6.1 Pipeline design

A single pipeline was designed to deliver gas to the mill chamber and remove residual gas after milling. Air in the mill chamber is also evacuated through this line. The pipeline consists of individual flanged pipe fittings which are listed in table 4.3. Together, these fittings create a pipeline assembly that starts at the neck-flanged opening, located at the closed-end side of the mill chamber, and ends with the attachment of the vacuum pump hose.

Table 4.3 : Various flanged pipe fittings used in the pipeline assembly

Diameter Nominal (DN) mm	Type of Fitting	Material
25	2 x 90° mitered elbows	Aluminium
25	1 x equal tee	Aluminium
25	1 x gas manifold	Aluminium
--	1 x flange-to-fitting adapter	Aluminium

The elbow and T-pipe fittings were already available and therefore did not require any design. However, a gas manifold pipe fitting with flanged ends had to be designed and manufactured. This allows the gas and vent lines to be connected to the main pipeline. In addition, an adapter that converts a tapered thread fitting into a flange was designed and manufactured for the pressure gauge.

In order to provide a seal, an o-ring supported by a centring ring is placed between each pipe fitting. Since the pipe fittings would be subjected to both positive pressure and vacuum, suitable threaded clamping collars were designed and manufactured from acetal plastic. These clamping collars are designed to draw the two pipe fittings together in order to compress the o-ring and thereby result in a seal.

The machine drawings for the gas manifold fitting, pressure gauge adapter fitting, centring ring and clamp collars are presented in the Appendix.

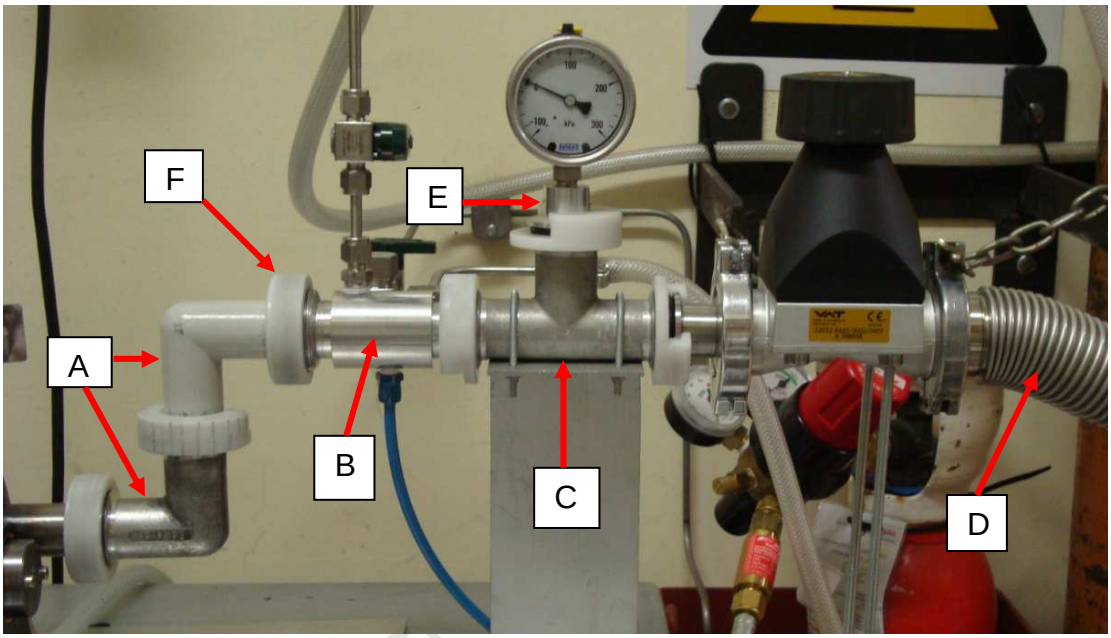

Figure 4.17: Shows pipeline assembly. A - 90º elbow fittings, B – gas manifold fitting, C – equal tee fitting, D – vacuum hose, E – pressure gauge adapter and F – clamping collar.

4.6.2 Valves

Before hydrogen gas is introduced, the air in the mill chamber will first be evacuated using a vacuum pump. Thereafter, the mill chamber will be purged with argon gas and then evacuated once again. Consequently, along with a hydrogen gas line, an argon gas line was also connected to the gas manifold. However, in order to control the flow of each gas into the mill chamber, a quarter-turn plug valve was installed between each gas line and the gas manifold. A vent valve, which removes the residual gas from the mill chamber after milling, was also installed into the gas manifold. In addition, since the vacuum hose is connected to the same pipeline as the gas manifold, a diaphragm vacuum valve was installed in order to isolate the vacuum system from the gas system.

As a safety precaution, the end of the hydrogen line which connects to the gas manifold was fitted with a lift check valve. Its purpose is to prevent unintended reverse flow from the mill chamber pipeline into the hydrogen line. This may occur if there is a leak in the hydrogen line and the line pressure drops below that of the mill chamber. Alternatively, on the other end of the hydrogen line, a hydrogen flashback arrestor was also fitted to the hydrogen regulator. A flashback is a flame travelling, at supersonic speed, in the opposite direction to normal gas flow. If a flashback occurs, the flashback arrestor features a flame arrestor which has a very high thermal conductivity that quickly removes the heat from the flame, thereby extinguishing it. In the event of sustained, multiple flashbacks, it also features a temperature-activated cut-off valve that permanently cuts off the gas supply.

Figure 4.18: Vacuum diaphragm valve.

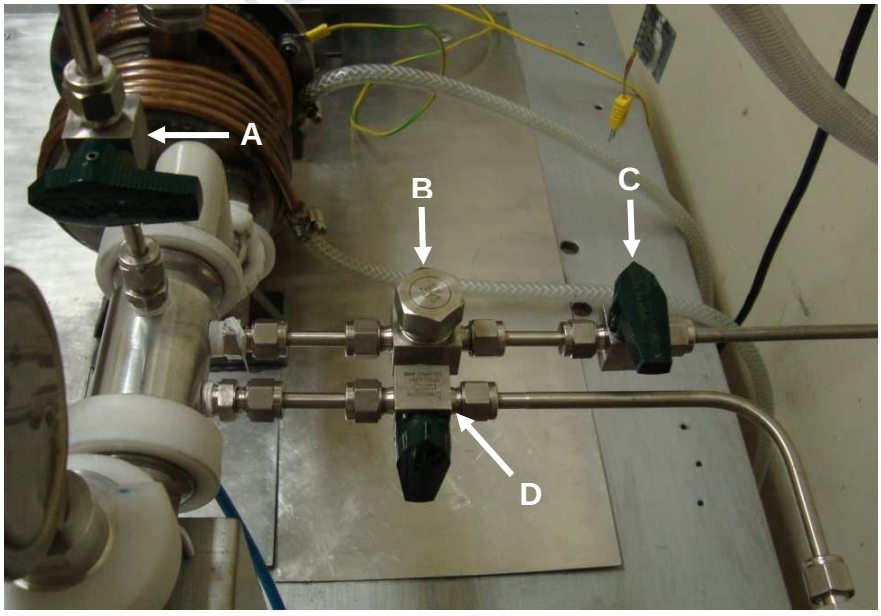

Figure 4.19: Shows the valves fitted to the gas manifold. A – vent valve, B – lift check valve, C – hydrogen control valve and D – argon control valve.

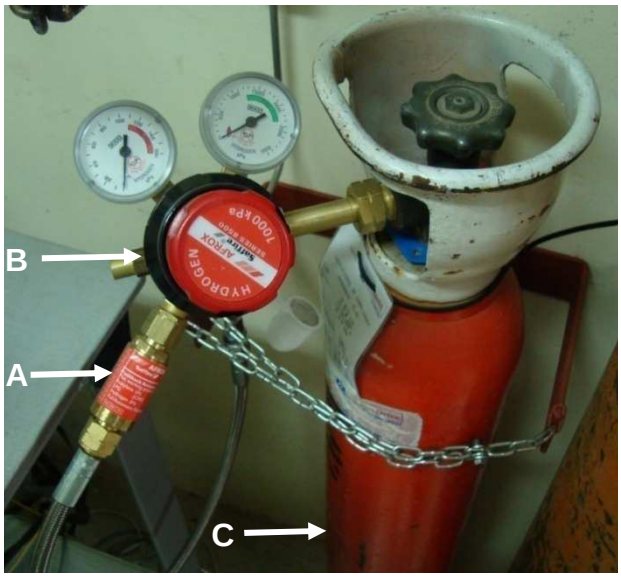

Figure 4.20: Shows the pure hydrogen cylinder (C), fitted with a multi-stage hydrogen regulator (B) and flashback arrestor (A).

4.6.3 Gauges

A bourdon tube pressure gauge was acquired and installed in the main pipeline between the gas manifold and vacuum diaphragm valve. The selected pressure gauge has a range from -100 to 300 kPa and measures in 20 kPa increments. Its main function is to simply provide a rough estimate of the gauge pressure in the mill chamber. However, during milling, small changes in the hydrogen pressure are expected. As a result, a digital manometer was installed in order to provide a more accurate reading of the mill pressure. It has a range of 200 kPa and measures in 0.1 kPa increments.

Figure 4.21: Bourdon tube pressure gauge.

Furthermore, in order to measure the vacuum in the mill chamber, a vacuum gauge is required. However, since the vacuum system has a vacuum gauge with digital display, it was not necessary to install one in the main pipeline.

4.7 Miscellaneous parts

4.7.1 Bearings

Single row, deep groove ball bearings with contact seals on both sides had been selected to support the stirrer assembly. These bearings are simple in design, suitable for high speeds and require little maintenance. More importantly, these bearings accommodate axial loads in both directions, in addition to radial loads.

4.7.2 Pressure seal

In order to seal the stirrer shaft, a radial shaft seal was required. However, during milling, the seal will be exposed to pressure from the mill chamber. As a result, a pressure shaft seal that is capable of operating across a pressure differential was required. When this type of shaft seal is subjected to pressure, the lip of the seal is pressed harder against its counterface, resulting in a seal. A pressure shaft seal capable of withstanding a pressure differential of 0.63 MPa was acquired. Along with the bearings, this seal was also housed in the hub flange.

4.8 Categorisation and conformity assessment of mill

Before the stirred ball mill can be operated, the hazard level of the pressure equipment (i.e. the mill chamber and the piping) has to be determined. According to the South African National Standard (SANS) 347 [45], the pressure equipment can be classified into one of five hazard categories:

- Sound Engineering Practice (category 0)
- Category I
- Category II
- Category III
- Category IV

The category into which the pressure equipment falls into will determine whether or not an independent conformity assessment or verification is required before operation. The category depends on the:

1. Type of pressure equipment, for example pressure vessels, piping [45].
2. The state of the intended fluid contents i.e. gas or liquid [45].
3. The fluid group of the intended contents – group 1 = dangerous or group 2 = not dangerous [45].

Fluid group 1 consist of fluids that are explosive, flammable, toxic, corrosive, oxidising and saturated or superheated steam. On the other hand, fluid group 2 consists of fluids other than those found in group 1 [45]. In this project, the mill chamber and piping will be pressurised with hydrogen gas. Since hydrogen gas is extremely flammable, fluid group 1 applies.

Table 4.4 below, extracted from SANS 347 [45], can now be used to find the relevant figures for determining the applicable hazard category for the mill chamber (pressure vessel) and piping. These figures consist of graphs where design pressure (PS) in kPa is plotted against the volume (V) in litres for pressure vessels and against nominal size (DN) in mm for piping.

Table 4.4: Pressure equipment classifications and relevant figures [45]. Relevant classifications and figure for the mill chamber and piping are highlighted in red and green respectively.

1	2	3	4	5	6	7	8	9	10
Equipment type	**Pressure Vessels[a]**				**Steam generator**	**Piping[b]**			
State of contents	**Gas**		**Liquid[c]**			**Gas**		**Liquid[c]**	
Fluid group[d]	1	2	1	2		1	2	1	2
Refer to figure (in SANS 347)	1	2	3	4	5	6	7	8	9
For two-phase flow, the equipment should be categorized to the higher risk.									

[a] For transportable gas containers and transportable vessels for dangerous gases see figure 10 (see also SANS 10019).

[b] Design and construction requirements for piping shall be as given in annex B.

[c] No pockets of gas may form above the liquid in the equipment, including steam.

[d] Fluid group 1 = dangerous; fluid group 2 = not dangerous (see 4.3.1).

4.8.1 Determining the hazard category for mill chamber

For a pressure vessel containing a dangerous gas, table 4.4 shows that the relevant figure in SANS 347 is figure 1. Since the mill chamber can be treated as a pressure vessel, the graph in this figure is used to determine the hazard category for the mill chamber. Figure 1 from SANS 347 is shown below in figure 4.22. For a design pressure of 200 kPa and a volume of 1.3 ℓ, figure 4.22 shows that the mill chamber falls into the sound engineering practice (SEP) category. This category does not require the mill chamber to undergo any conformity assessment. However, it requires the mill chamber to be designed and manufactured in accordance with sound engineering practice in order to ensure safe use.

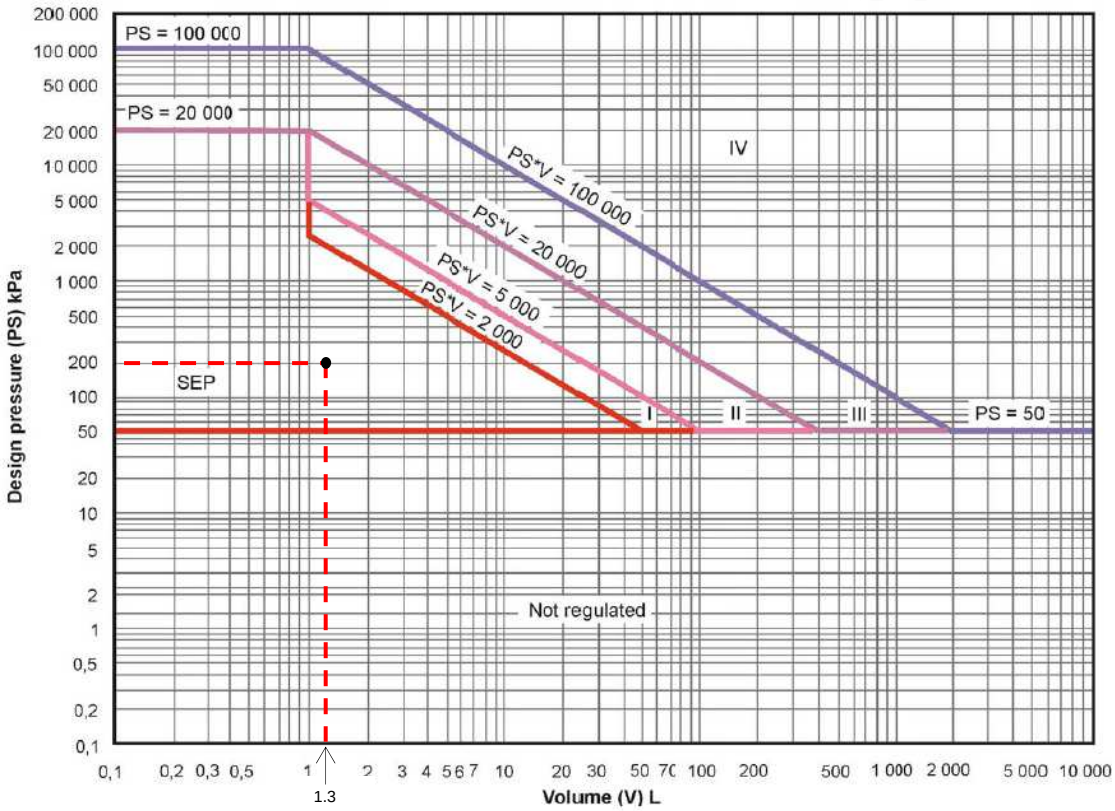

Figure 4.22: Graph for vessels – Dangerous gas [45].

4.8.2 Determining the hazard category the piping

For piping containing a dangerous gas, table 4.4 shows that the relevant figure in SANS 347 is figure 6. The graph in this figure is shown below in figure 4.23 and is used to determine the hazard category for the piping. For a design pressure of 200 kPa and a nominal diameter of 25 mm, figure 4.23 shows that the piping falls on the borderline of the SEP category. Similar to the mill chamber, the piping does not require any conformity assessment.

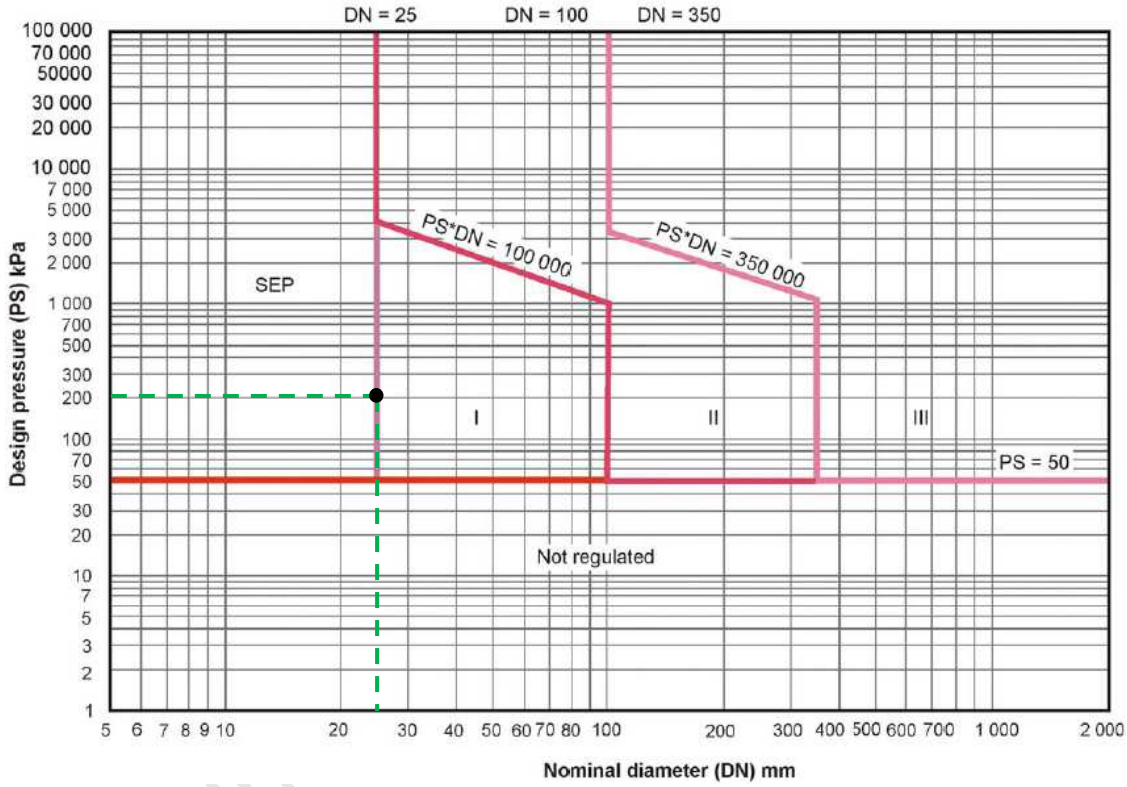

Figure 4.23: Graph for piping - Dangerous gas [45].

5 EXPERIMENTAL PROCEDURE

5.1 Materials

5.1.1 Titanium turnings (feed)

The titanium scrap turnings used in this study were commercially pure titanium (CP Ti) Grade 2 and Ti-6Al-4V. Tables 5.1 and 5.2 show the elemental composition for CP Ti and Ti-6Al-4V respectively.

Table 5.1: Composition of CP Ti Grade 2 [44].

Element	C	Fe	H	N	O	Ti
Weight %	0.1 max.	0.3 max.	0.015 max.	0.03 max.	0.25 max.	99.2

Table 5.2: Composition of Ti-6Al-4V [44].

Element	Al	Fe	O	Ti	V
Weight %	6	0.25 max.	0.2 max.	90	4

The scrap turnings had a width of 3±1 mm and a thickness of 0.25±0.05 mm. These scrap turnings were produced using a lathe under dry cutting conditions i.e. no cutting fluid was used. Cutting fluids are usually oil-based and therefore not easily removed. They may form a thin film on the surface of the titanium and thereby prevent the hydrogen from diffusing during milling.

Figure 5.1: Shows the physical appearance of the turnings, A - CP Ti and B - Ti-6Al-4V.

5.1.2 Grinding media

Stainless steel AISI 316 balls with a diameter of 4 mm were used as grinding media. Tables 5.3 and 5.4 show the elemental composition and mechanical properties, respectively.

Table 5.3: Composition of grinding media [46]

Element	C	Mn	Si	P	S	Ni	Cr	Mo	Fe
Weight %	0.08 max.	2.00 max.	1.00 max.	0.045 max.	0.03 max.	10-14	16-18	2-3	balance

Table 5.4: Mechanical properties of grinding media [47].

Density	8027 kg / m^3
Yield Strength	310 MPa
Tensile Strength	620.5 MPa
Modulus of Elasticity	193 GPa
Hardness (Rockwell B)	75 - 95

Since there is insufficient literature regarding the optimum grinding media size for coarse feed, the feasibility of using these balls was investigated. Compared to larger balls, these balls are expected to provide more grinding contacts per revolution, resulting in faster grinding of the feed. In addition, smaller voids are created by these balls, thereby limiting the size of the final product.

Figure 5.2: Shows the 4 mm grinding media.

5.2 Feed and grinding media preparation

5.2.1 Feed

Prior to milling, both feeds were first weighed into 2 g samples using a *Mettler AC 100* microbalance scale. Thereafter, both feeds were ultrasonically cleaned in acetone for 5 minutes and allowed to dry.

5.2.2 Grinding media

A ball charge of 65% of the free mill chamber volume was used for all the experiments. Prior to milling, batches of grinding media were placed in a meshed basket and then ultrasonically cleaned in a beaker of acetone for 5 minutes. The meshed basket served as a strainer in order to easily separate the grinding media from the acetone solution. Once separated, each batch of grinding media was allowed to dry.

5.3 Testing procedure

All milling tests performed in this project were carried out on the stirred ball mill rig (figure 5.3), which was described in Chapter 4. For all the experiments, the following procedure was followed. Once the desired stirrer design had been configured, the mill chamber was bolted closed and the main pipeline attached to the mill. Thereafter, the feed and grinding media were inserted through the inlet/outlet opening at the top of the mill chamber and then sealed closed with the threaded plug. A vacuum pump removed the air by pumping the mill chamber down to a vacuum of 1×10^{-1} mbar. After removing the air, the mill chamber was purged with argon gas and then pumped down once again to the same vacuum. Next, the mill chamber was filled with 99.99% pure hydrogen gas to a pressure of 200 kPa. Before milling commenced, the digital manometer was used to monitor the hydrogen pressure in the mill chamber. Any significant pressure drop would indicate a leak in the mill system. In addition, a *Dräger X-AM 5000* portable hydrogen leak detector was also placed near the mill system. If no leaks were found, milling was performed at the desired stirrer speed and milling time. During milling, the change in the hydrogen pressure and the temperature within the mill chamber was monitored and recorded, every 10 minutes. After milling, the residual gas in the mill chamber was vented into a fume cupboard. Following this, the mill chamber was purged with argon gas, before

removing the product and grinding media. A more detailed operating procedure can be found in the Appendix.

Figure 5.3: Stirred ball mill rig with vacuum pump system highlighted in red.

5.4 Preliminary experiments

5.4.1 Temperature calibration

The temperature reading from the thermocouple located in the feed inlet/outlet plug measures the overall temperature of the mill environment. However, during milling, the local temperature induced by grinding media impacts is expected to be higher. Therefore, the measured temperature from the thermocouple is not a true representation of the actual temperature near the grinding media. In effect, during milling, there is a temperature gradient between the tip of the thermocouple and the grinding media.

In order to correlate the measured temperature with the actual temperature, trial tests were performed by milling CP Ti feed under an argon atmosphere. Trial tests were not performed under a hydrogen milling environment because of the reactive nature of this gas. Instead, argon gas was found to be a more suitable milling atmosphere for these experiments because of its inert nature. By treating the argon gas as an

ideal gas, the ideal-gas equation of state (Boyle's Law) can be used to obtain the actual or predicted temperature at a given milling time. For a fixed mass, the ideal gas equation can be simplified such that the properties at two different states are related to each other by the following equation:

$$\frac{P_1V_1}{T_1} = \frac{P_2V_2}{T_2} \tag{5.1}$$

Where: $P_{1,2}$ *- pressure in kPa*

$V_{1,2}$ *– volume in* m^3

$T_{1,2}$ *– temperature in kelvin*

Since the volume of the mill chamber remains constant during milling, equation 5.1 can be further simplified:

$$\frac{P_1}{T_1} = \frac{P_2}{T_2} \tag{5.2}$$

Prior to milling, it is safe to assume that there is no temperature gradient between the tip of the thermocouple and the grinding media. In other words, the temperature near the grinding media and thermocouple are both at room temperature. Using equation 5.2, with T_1 and P_1 being room temperature and initial filling pressure respectively, the predicted temperature (T_2) at a given milling time can be calculated based on the corresponding recorded pressure (P_2).

Four trial tests were performed, each at a different stirrer pin tip speed. The ball charge and milling time were both kept constant. The milling parameters are summarised in table 5.5 below. The testing procedure described in section 5.3 was followed except the mill chamber was filled with argon gas to a pressure of 200 kPa. During milling, the thermocouple temperature and the argon pressure were recorded every 10 minutes.

Table 5.5: Milling parameters for all four trial tests.

Trial test	**1**	**2**	**3**	**4**
Pin tip speed (m/s)	0.5	1	1.5	2
Milling time	2.5 hours			
Ball charge	65%			

Using equation 5.2, the predicted temperature (T_2) was calculated at each 10 minute interval, for all four stirrer pin tip speeds. For each pin tip speed, the relationship between the measured thermocouple temperature and the corresponding predicted temperature is shown in figure 5.4. From figure 5.4, it is clear there is a linear relationship between the two temperatures for all four stirrer pin tip speeds.

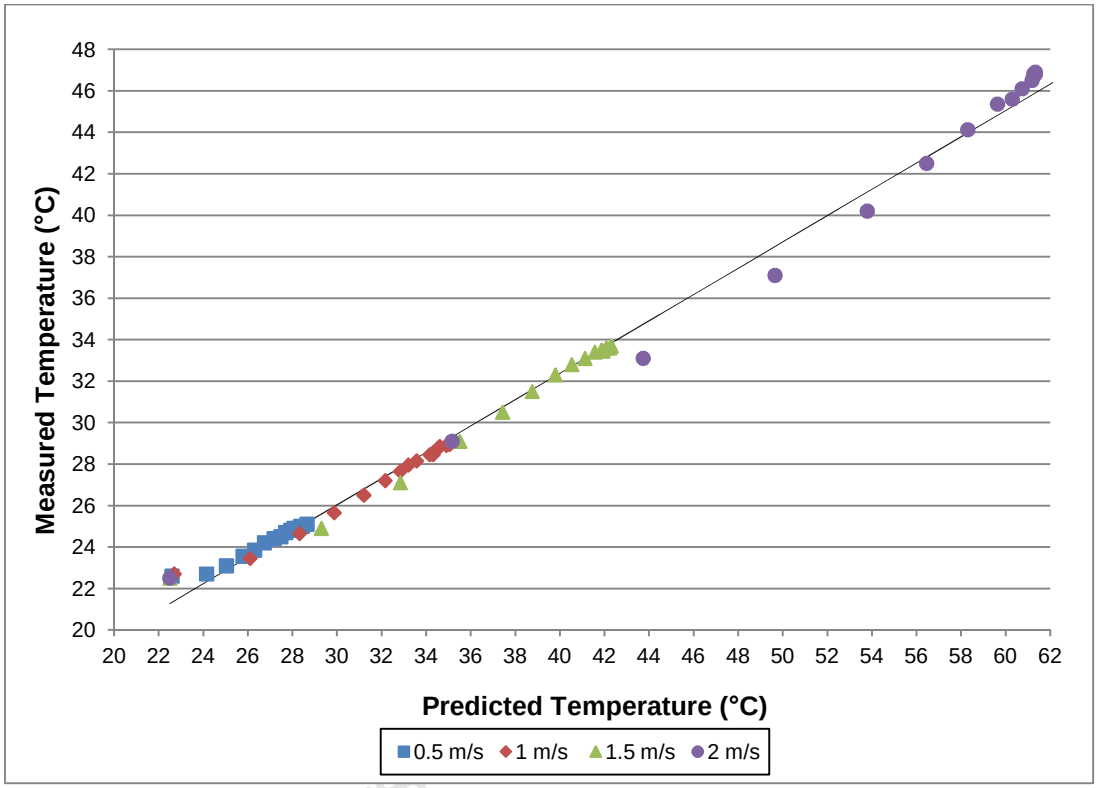

Figure 5.4: Temperature calibration graph showing the linear relationship between the measured and predicted temperature

Figure 5.4 can now be used to determine the correct temperature from the measured temperature, when milling takes place under an argon atmosphere. However, the actual experiments performed in this study use a hydrogen milling environment. Notwithstanding the fact that hydrogen has a different thermal conductivity to argon, the relative slow rate of change of temperature over the duration of the test implies that thermal conductivity will not have a notable influence on the temperature measurement. Therefore, figure 5.4 can also be used to determine the correct temperature from the measured temperature when milling takes place under a hydrogen atmosphere.

5.4.2 Determining whether hydrogen diffuses into the milling chamber and/or grinding media

During milling, a drop in the hydrogen pressure represents absorption of hydrogen by the titanium feed. However, assuming there is no hydrogen leak, a drop in pressure may also be a result of hydrogen gas diffusing into either the grinding media or the mill chamber. Consequently, in order to determine whether or not this really occurs, trial tests were performed with only grinding media and therefore no feed.

Once again, four trial tests were performed, each at a different pin tip speed. The ball charge and milling time were both kept constant. The same milling parameters listed in table 5.5 were used, except a milling time of 1 hour was used. The testing procedure described in section 5.3 was followed except no feed was added.

By using the relationship exhibited in figure 5.4, the measured thermocouple temperature at each 10 minute interval was used to determine the corresponding corrected temperature for each stirrer pin tip speed. Using equation 5.2, with T_1 and P_1 being room temperature and initial hydrogen filling pressure respectively, the corrected temperature (T_2) at each interval was used to calculate the corresponding pressure (P_2). This calculated pressure (based on the corrected temperature) together with the recorded gauge pressure and corrected temperature, at each interval, are plotted for each stirrer pin tip speed in figures 5.5 to 5.8

Since the calculated pressure is determined from equation 5.2, its value is based on the assumption that the hydrogen gas in the chamber remains constant. From figures 5.5 to 5.8, for all four trial tests, it is clear that the recorded gauge pressure follows a similar trend to the calculated pressure. As a result, this proves that the mass of hydrogen gas remains the same in the mill chamber when milling with no feed and that the hydrogen gas does not diffuse into either the grinding media or mill chamber. Therefore, if a drop in the hydrogen pressure occurs (provided there are no hydrogen leaks) when milling titanium feed, it is safe to assume that only the feed absorbs hydrogen.

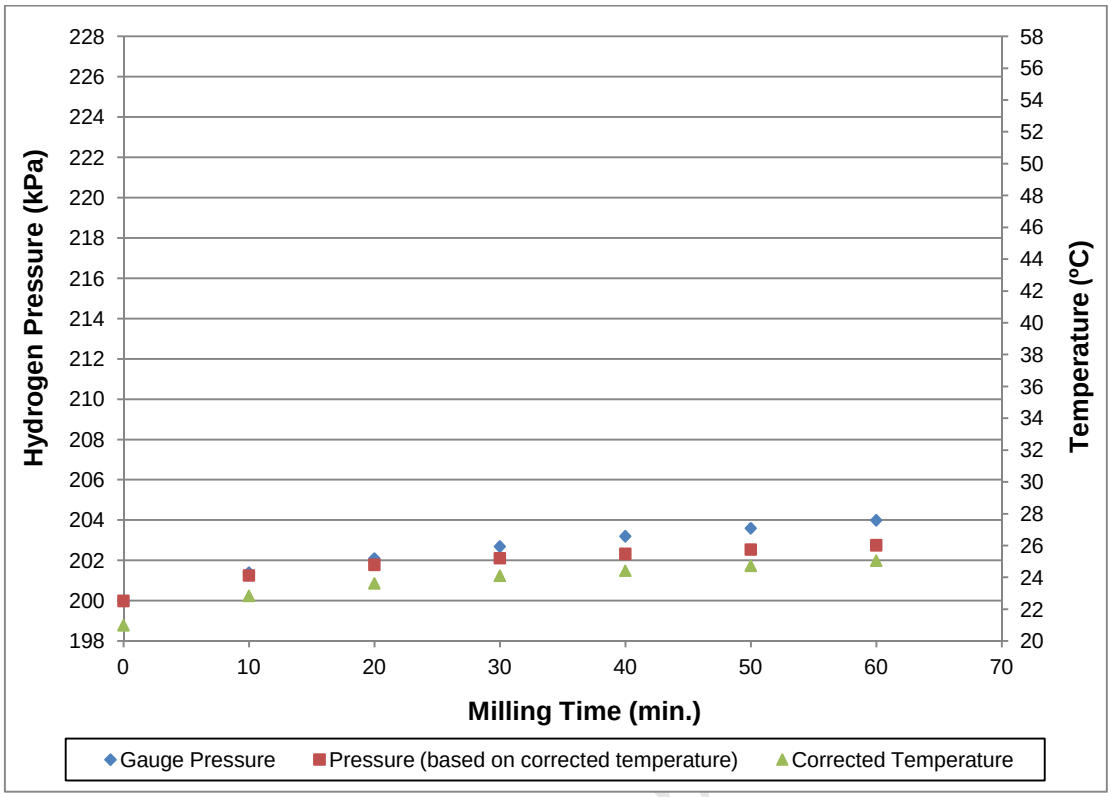

Figure 5.5: Hydrogen pressure and temperature variation when milling at a stirrer pin tip speed of 0.5 m/s for 1 hr and using no feed.

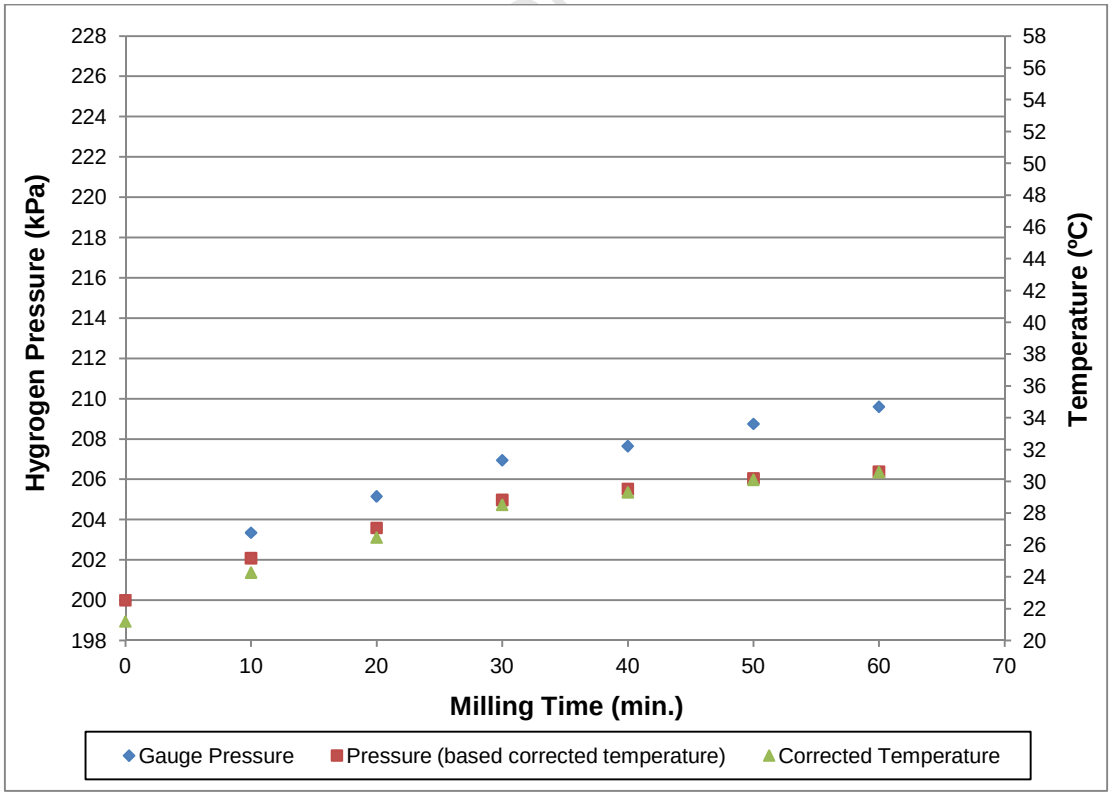

Figure 5.6: Hydrogen pressure and temperature variation when milling at a stirrer pin tip speed of 1 m/s for 1 hr and using no feed.

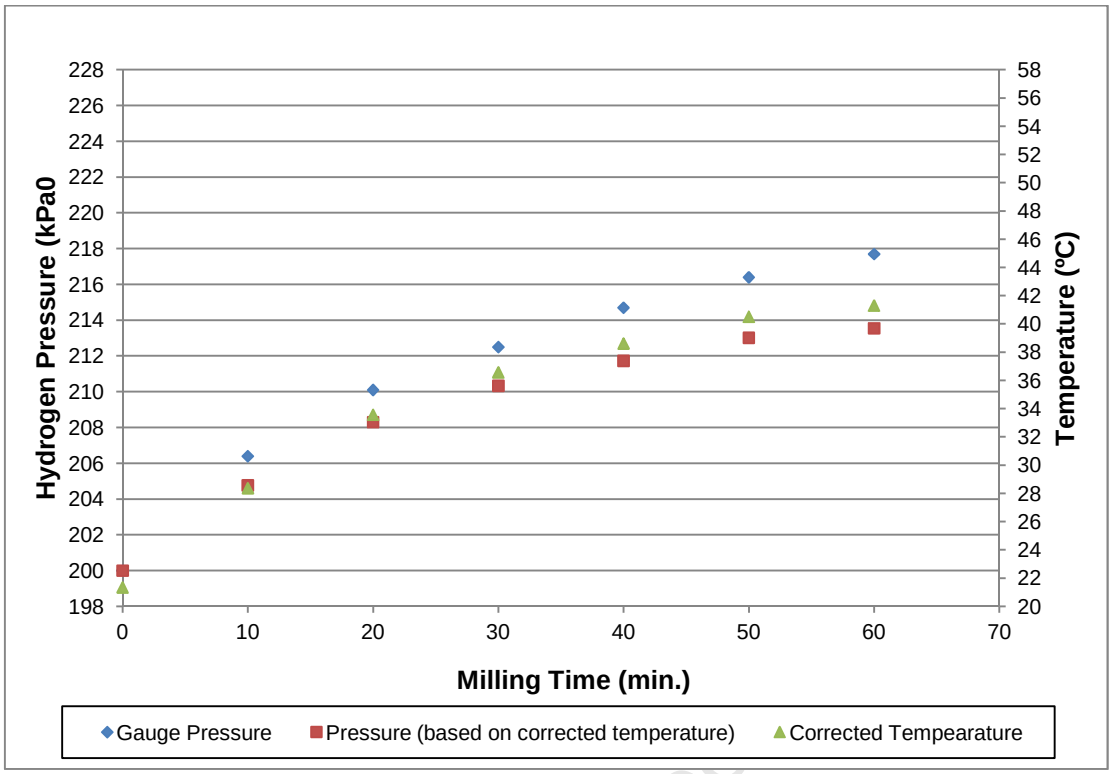

Figure 5.7: Hydrogen pressure and temperature variation when milling at a stirrer pin tip speed of 1.5 m/s for 1 hr and using no feed.

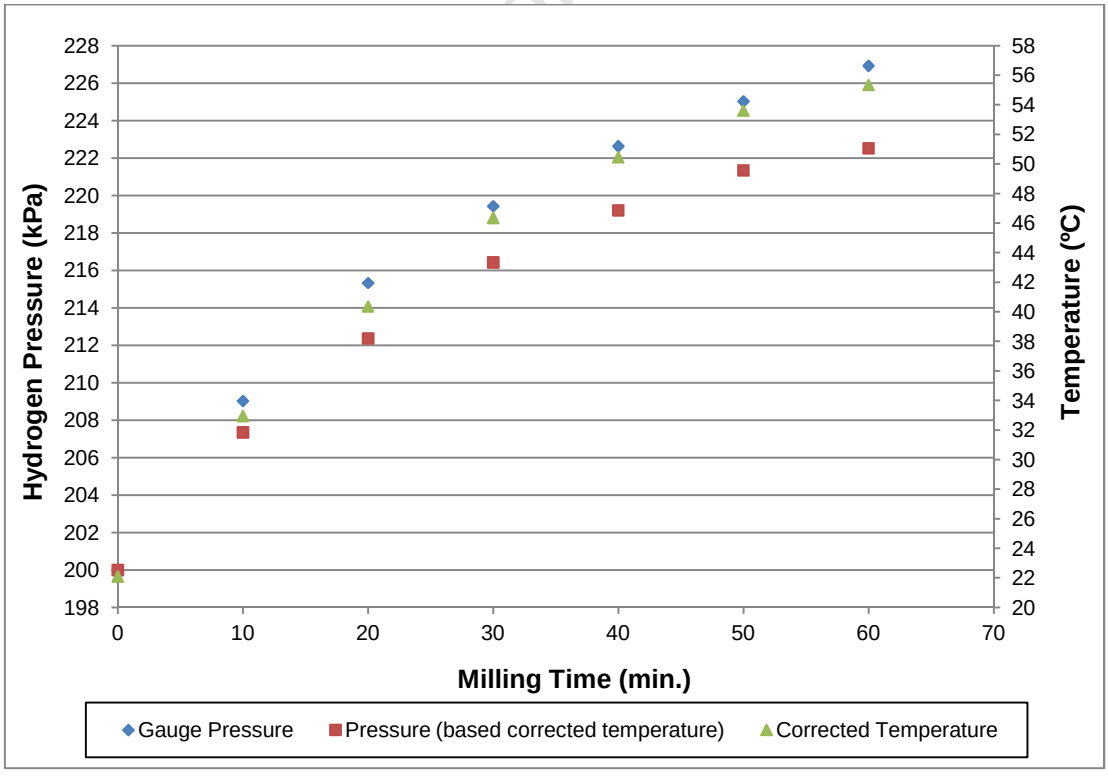

Figure 5.8: Hydrogen pressure and temperature variation when milling at a stirrer pin tip speed of 2 m/s for 1 hr and using no feed.

5.5 Experiments to determine optimum milling parameters

In order to determine which milling parameters affect the hydrogen absorption rate and the resulting product size distribution, the following milling parameters were selected for investigation:

- Stirrer Design
- Stirrer Speed
- Milling Time

A set of experiments were designed to find the optimum milling parameters that efficiently converted both CP Ti and Ti-6Al-4V feeds to powder. The testing procedure described in section 5.3 was followed for all the experiments. For all the tests, 2 g of both feed types and a ball charge of 65% of the free mill chamber volume were used. Furthermore, the mill chamber was only filled once with hydrogen gas, prior to milling. Although the hydrogen pressure dropped during milling, fresh hydrogen gas was not loaded. This was done to compare how the hydrogen pressure varies with milling time for each milling parameter.

In addition, two different types of graphs were plotted after each experiment. One graph illustrates the variation of hydrogen pressure and temperature with milling time. The other graph is a bar chart which shows the product size distribution. Since each test was repeated at least three times in order to show repeatability, the average data points were plotted on both graphs. The maximum and minimum value of each data point was plotted as error bars.

5.5.1 Optimising the stirrer design

Initially tests were conducted to determine the best pin stirrer that facilitates feed circulation and breakage. As mentioned before, both the pin length and the number of pins on the stirrer play an important role. Consequently, based upon 4 mm grinding media, two sets of pins and pin-collars were investigated. This gave rise to four different stirrer configurations as described in table 5.6 below.

Table 5.6: Various stirrer configurations and the corresponding grinding media spacings.

	Number of pin-collars	Pin length	Pin-to-pin gap i.t.o. grinding media	Pin tip-to-chamber wall gap i.t.o. grinding media
1	6 pin-collars (12 pins)	26 mm	2	3
2		30 mm	2	2
3	5 pin-collars (10 pins)	26 mm	3	3
4		30 mm	3	2

For each stirrer configuration, milling of CP Ti was performed at a fixed pin tip velocity of 1.5 m/s for 2.5 hours. In order to maintain the same tangential velocity, the 26 mm pin length stirrers ran at 326±2 rpm, while the 30 mm pin length stirrers ran at 300±2 rpm. After milling, the resulting product size distribution and hydrogen pressure variation for each stirrer configuration was then analysed in order to find the optimum stirrer design.

Furthermore, for this investigation, these experiments were not repeated for the Ti-6Al-4V feed. In terms of finding the optimum stirrer design, it is assumed that the Ti-6Al-4V feed will provide a similar conclusion as the CP Ti feed.

5.5.2 Effect of the stirrer speed

In order to determine the effect of stirrer speed on the hydrogen absorption rate by the feed and the resulting product size distribution, four different pin tip speeds were tested. A pin tip velocity of 0.5 m/s, 1 m/s, 1.5 m/s and 2 m/s were selected for investigation. Initially, CP Ti was milled at each of these stirrer pin tip speeds for 2.5 hours using the optimum stirrer design found in the previous section. From this range of pin tip speeds, the optimum stirrer speed was chosen according to the one that resulted in the fastest hydrogen absorption rate and produced the most powder yield.

For the same range of stirrer pin tip speeds tested on CP Ti, it is assumed that the Ti-6Al-4V feed will follow a similar trend and therefore have the same optimum pin tip speed as CP Ti. As a result, milling of Ti-6Al-4V was only performed at this optimum pin tip speed for the same milling time of 2.5 hours. The resulting hydrogen absorption rate and the product size distribution were then compared to the corresponding results for CP Ti results.

5.5.3 Effect of milling time

Once the optimum stirrer speed was found, the corresponding optimum milling time had to be investigated. Since the level of contamination increases with milling time, the milling time that results in the best combination of minimum contamination and maximum powder production had to be selected. By analysing the variation of hydrogen pressure with milling time, for CP Ti at the optimum stirrer speed, three milling times were investigated. At the optimum speed, tests were conducted for 1 hour and 1.5 hour, and the corresponding product size distributions were then compared to that of the 2.5 hour test. In addition, the amount of contamination produced at each milling time, as a percentage of the total feed mass, was also compared.

Similarly to CP Ti, in order to find the optimum milling time, three milling times were also investigated for Ti-6Al-4V at the optimum speed. Consequently, 1.5 hour and 2 hour tests were conducted, and the corresponding product size distributions were compared to that of the 2.5 hour test. Similarly to CP Ti, the amount of contamination produced at each milling time, as a percentage of the total feed mass, was also compared for the alloy.

5.6 Product separation

After milling and venting the chamber of hydrogen, the main pipeline was disconnected from the mill chamber and the threaded inlet/outlet plug was removed from the top of the mill chamber. The mill chamber was then rotated by 180º so that the inlet/outlet opening is now positioned at the bottom. This allows the product yield and grinding media to be emptied into a collection tray. Since it is highly unlikely that all the product yield and grinding media are removed, the mill chamber was also unbolted and emptied into the tray as well.

5.6.1 Sieve separation process

In order to separate the product yield from the grinding media, a 2800 µm mesh sieve and receiver were used. The mill contents were placed on a clean sieve with the receiver attached. By shaking the receiver and sieve in the horizontal plane, the grinding media being larger than this mesh size would remain at the top and only the product yield would pass through into the receiver.

5.6.2 Filtration separation process

The sieve separation process is ineffective at removing the fine powder which coats the grinding media. In an attempt to remove this coating, the grinding media was ultrasonically cleaned in an acetone solution. After all the grinding media was cleaned, the acetone solution was poured through filter paper in order to collect the fine powder. In addition, the stirrer assembly and the inside of the mill chamber were also coated with powder. As a result, ethanol was used to rinse the excess powder off these surfaces and the resulting ethanol-powder solution was collected. Similar, to the acetone solution, the ethanol solution was also poured through filter paper. Furthermore, it should be noted that this method does not completely remove all the powder from the various contact surfaces. An adherent layer of powder still remains on the grinding media, stirrer and inner wall of the mill chamber and thus there remains unrecovered powder. As a result, the total powder yield after milling is lower than expected.

5.6.3 Magnetic separation process

After milling, noticeable wear tracks were found along the inner wall of the mill chamber. On the other hand, by visual inspection, minimum wear was found on the stirrer pins and grinding media. Therefore, the main source of contamination is expected from the inner wall of the mill chamber. Since the mill chamber is made from mild steel, the contaminant particles can be extracted from the product yield by using a magnet.

The magnetic separation process was done after the sieve and filtration separation process. Magnetic (contaminate) particles were easily removed from the product yield which was recovered through the sieve separation process. However, the magnet was ineffective at separating the fine contaminant particles from the powder which was recovered through the filtration separation process. The potential amount of titanium powder available in this contaminated powder blend is discussed further in section 5.7.2.

5.7 Product analysis

5.7.1 Sieving analysis

The product size distribution was examined by sieve analysis. More specifically, a hand sieving method was used. In hand sieving, product particles are passed through a set of sieves of decreasing mesh size, one sieve at a time. The range of stainless steel laboratory sieves used for all the experiments are listed in table 5.7.

Table 5.7: Sieve sizes used for product size analysis

Sieve size (µm)
2000
1180
710
500
250
106

The hand sieving procedure involves placing the product on a clean, dry sieve with the receiver attached. While holding both sieve and receiver, the passage of the product through the sieve is aided by a back-and- forth rotational motion in the horizontal plane. The product that remains above the sieve is weighed and set aside, while the product that passes through is analysed further by using the next sieve size and same sieving procedure.

The size distribution of the product yield recovered from the sieve separation process was analysed after the magnetic separation process. In order to illustrate the product size distribution for each test, the sieved data was summarised in the form of a bar chart. Figure 5.9 shows a fictitious product size distribution bar chart. The bar chart shows the product yield, as a percentage of the total feed mass, which passes through a certain sieve size, but remains above the next sieve. Note the first label on the x- axis represents the product yield with a particle size greater than 2000 µm. Since the initial feed does not pass through a 2000 µm sieve, this may indicate the amount of feed that does not break into smaller fragments. Furthermore, also note that the last label represents the magnetically separated amount of powder with a particle size equal to or less than 106 µm. Therefore it does not consist of any magnetic contaminants.

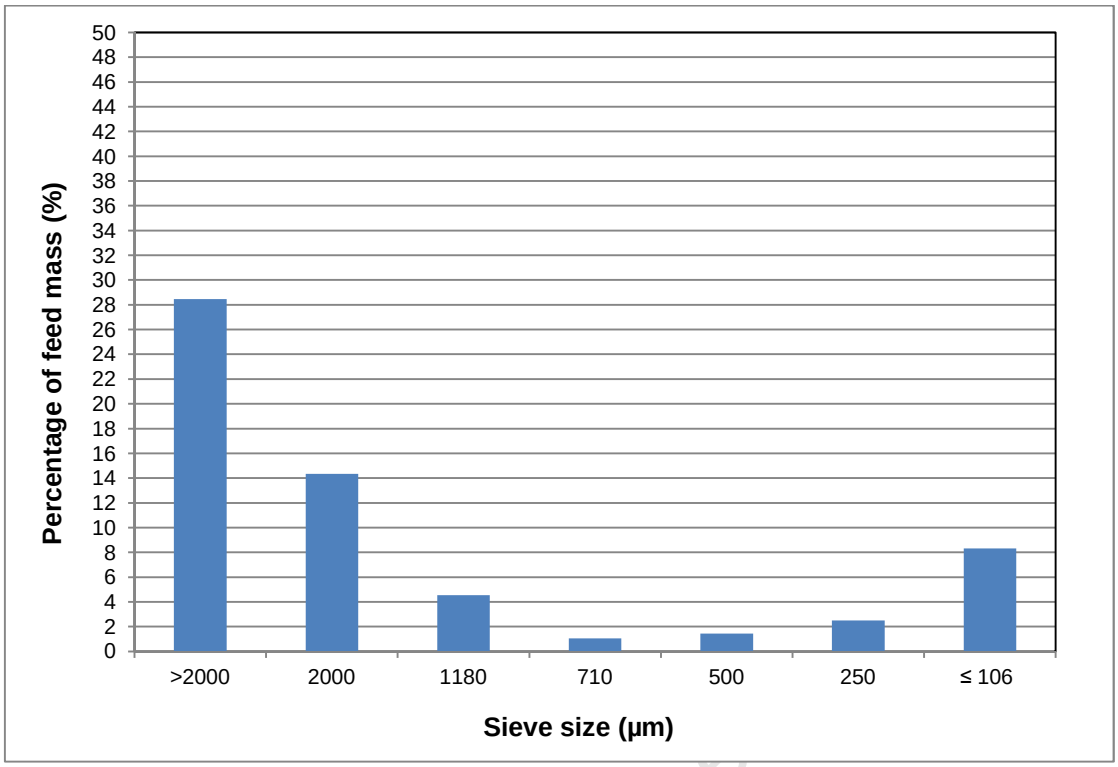

Figure 5.9: Example of a product size distribution bar chart generated after sieving analysis.

In addition, the size of the contaminated powder particles recovered from the filtration separation process was also analysed. In all cases, the contaminated powder passed through a 106 µm sieve.

5.7.2 Composition analysis of contaminated powder

The elemental composition of the contaminated powder was carried out using energy-dispersive x-ray spectroscopy (EDS). The powder was analysed using the *FEI Nova NanoSEM 230* scanning electron microscope equipped with an EDS system. This technique was used to determine the potential amount of titanium powder trapped in the contaminated powder blend. Similarly, the level of contamination was also established through this technique.

Note that this technique was successful at determining the titanium powder fraction of the contaminated powder blend produced after milling CP Ti. However, the Ti-6Al-4V powder fraction could not be accurately determined through this technique. This is possibly due to peak overlap errors for titanium, vanadium and the other transition elements found in the contaminated powder blend as well as the high background scatter for aluminium. Therefore, for the alloy, only the amount of

contamination in the contaminated powder blend could be determined through EDS analysis.

EDS methodology

Prior to EDS analysis, the contaminated powder blend for both feeds was weighed. This mass would later be used to determine the CP Ti powder fraction and the amount of contamination for both feeds. Only a small sample of the contaminated powder blend is required for analysis. For each test, three regions (spectra) on the sample were selected for elemental analysis in order to obtain an average. After analysis, the EDS software creates three tables (one for each spectrum), displaying the weight percentage and atomic percentage of each element in the contaminated powder blend. An example of the elements found in the contaminated powder blend for Ti-6Al-4V and CP Ti are shown in table 5.8 and 5.9 respectively.

Table 5.8: Example of EDS results for Ti-6Al-4V

Element	Weight%	Atomic%
Al K	1.76	3.21
Ti K	65.96	67.92
V K	1.74	1.68
Cr K	3.78	3.58
Fe K	25.54	22.56
Ni K	1.23	1.03

Table 5.9 : Example of EDS results for CP Ti.

Element	Weight%	Atomic%
Ti K	50.17	53.83
Cr K	6.14	6.06
Fe K	41.56	38.24
Ni K	2.13	1.87

CP Ti powder fraction

By using the average weight percentage of titanium in the sample and the mass of the corresponding contaminated powder blend, the mass of the titanium powder fraction was calculated for CP Ti. The titanium powder fraction, as a percentage of

the total feed mass, was then included on the product size distribution bar chart. Figure 5.10 below shows an example of the resulting product size distribution graph for CP Ti. Note that this graph now displays the total product yield recovered after milling. In addition, the 106 µm bar represents the actual powder yield, i.e. the magnetically separated powder recovered from the sieve separation process as well as the powder fraction of the contaminated powder blend (recovered from the filtration separation process) determined through EDS analysis.

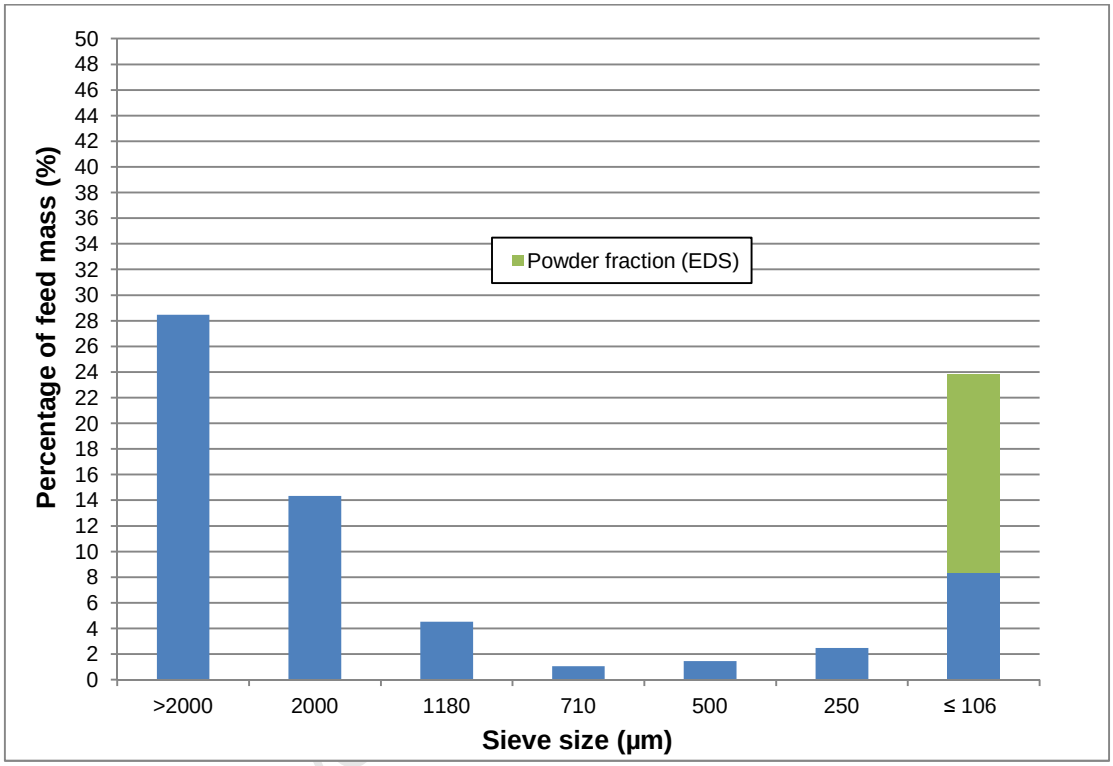

Figure 5.10: Shows the powder fraction results determined through EDS analysis for CP Ti.

Furthermore, since the Ti-6Al-4V powder fraction could not be determined through EDS analysis, the actual powder yield and therefore the total product yield could not be determined. Therefore the type of product size distribution bar chart in figure 5.10 could not be generated for the alloy.

CP Ti and Ti-6Al-4V contamination

In order to determine the optimum milling time for both feeds, the amount of contamination produced at each of the selected milling times were compared. By using the average weight percentage of all the contaminants in the EDS sample and the mass of the corresponding contaminated powder blend, the mass of the

contaminants was calculated for both CP Ti and Ti-6Al-4V. The amount of contamination, as a percentage of the total feed mass, was then determined for both feeds and presented in the form of a bar chart.

5.8 Unrecovered powder

As mentioned before, during milling, a certain percentage of the powder yield coats and forms an adherent layer on the stirrer, the grinding media as well as to the inner surfaces of the mill chamber. In order to determine this unrecovered powder yield, the total product yield (excluding contaminants) was subtracted from the initial feed amount. Note that the unrecovered powder yield could not be determined for Ti-6Al-4V because the total product yield could not be determined.

It is safe to assume that this unrecovered powder is less than 106 µm. The unrecovered powder yield for CP Ti, as a percentage of the total feed mass, was also added to the product size distribution bar chart. Figure 5.11 below shows an example of the resulting product size distribution graph. Note that the 106 µm bar now represents the expected powder yield which consists of the actual powder yield as well as the unrecovered powder yield. In the results section, all the product size distribution bar charts for CP Ti will be presented in this form.

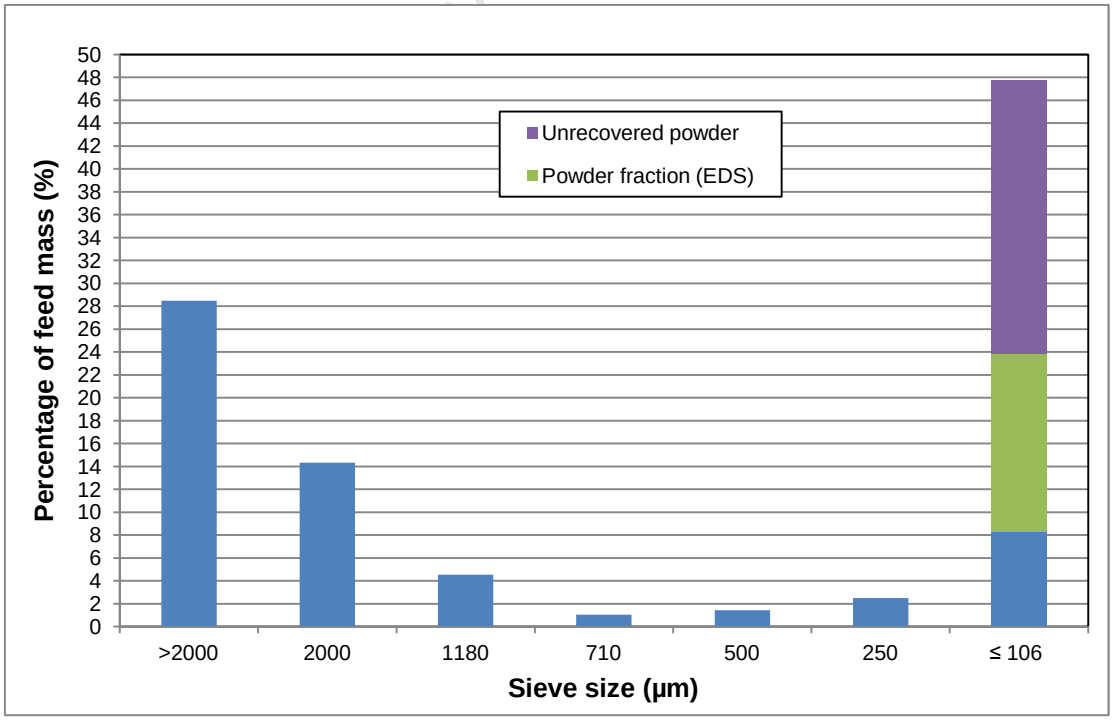

Figure 5.11: Shows the unrecovered powder yield added to the product size distribution bar chart.

6 RESULTS AND DISCUSSION

This chapter deals with the results and discussion of the experiments that were conducted on commercial pure titanium and Ti-6Al-4V. Initially the optimum stirrer design was investigated. Thereafter the effect of milling speed and milling time on the powder yield was investigated.

6.1 Optimizing stirrer design

As mentioned before, the stirrer assembly consist of a set of pin-collars. Each pin-collar consists of a pair of pins which are located 180° apart. The lengths of the pins as well as the number of pin-collars on the stirrer shaft are variable. As a result, the best combination of pin length and number of pin-collars has to be determined. This was achieved by investigating how each configuration affects the hydrogen absorption rate and resulting powder yield.

6.1.1 Effect of the pin length

The effect of the stirrer pin length on the hydrogen absorption rate was investigated. Initially, a stirrer design consisting of 5 pin-collars and therefore a total of 10 pins was used. The pin-collars were orientated at 90° to each other and spaced evenly along the stirrer, giving a three grinding media spacing between each successive pin. At first, a stirrer configuration consisting of 5 pin-collars with 30 mm long pins was tested and compared to one with shorter 26 mm long pins. The 30 mm pin length was chosen because it gave a two grinding media spacing between the stirrer pin tips and mill chamber wall, whereas the 26 mm pin length gave a three grinding media spacing. In order to determine the effect of the stirrer pin length, milling of CP Ti was conducted at a stirrer pin tip speed of 1.5 m/s for 2.5 hours for each stirrer configuration. The resulting variation in hydrogen pressure and temperature for the 30 mm and 26 mm pin length stirrers is illustrated in figures 6.1 and 6.2 respectively. Note that the corrected temperature is plotted on both graphs. By using figure 5.4 in section 5.4.1, the measured thermocouple temperature at each 10 minute interval was used to determine the corresponding corrected temperature for each pin length stirrer design.

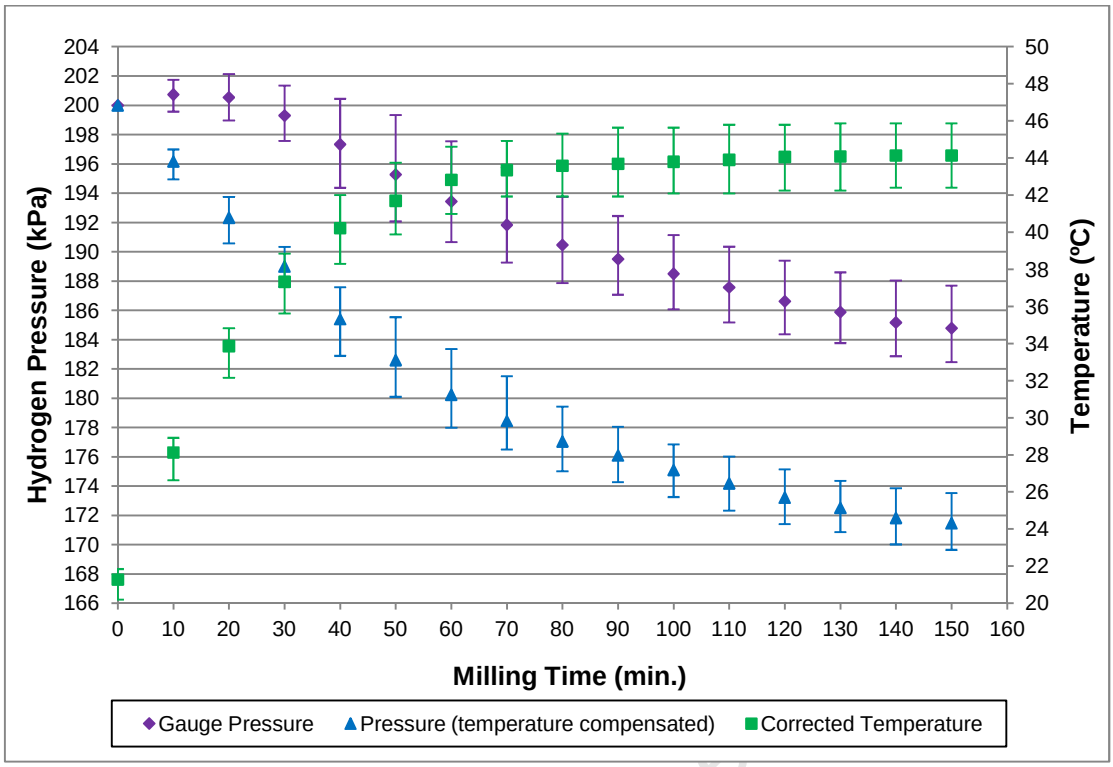

Figure 6.1: Variation in hydrogen pressure and temperature when using a 5 pin-collar stirrer configuration with 30 mm pins. Milling performed at 1.5 m/s for 2.5 hrs.

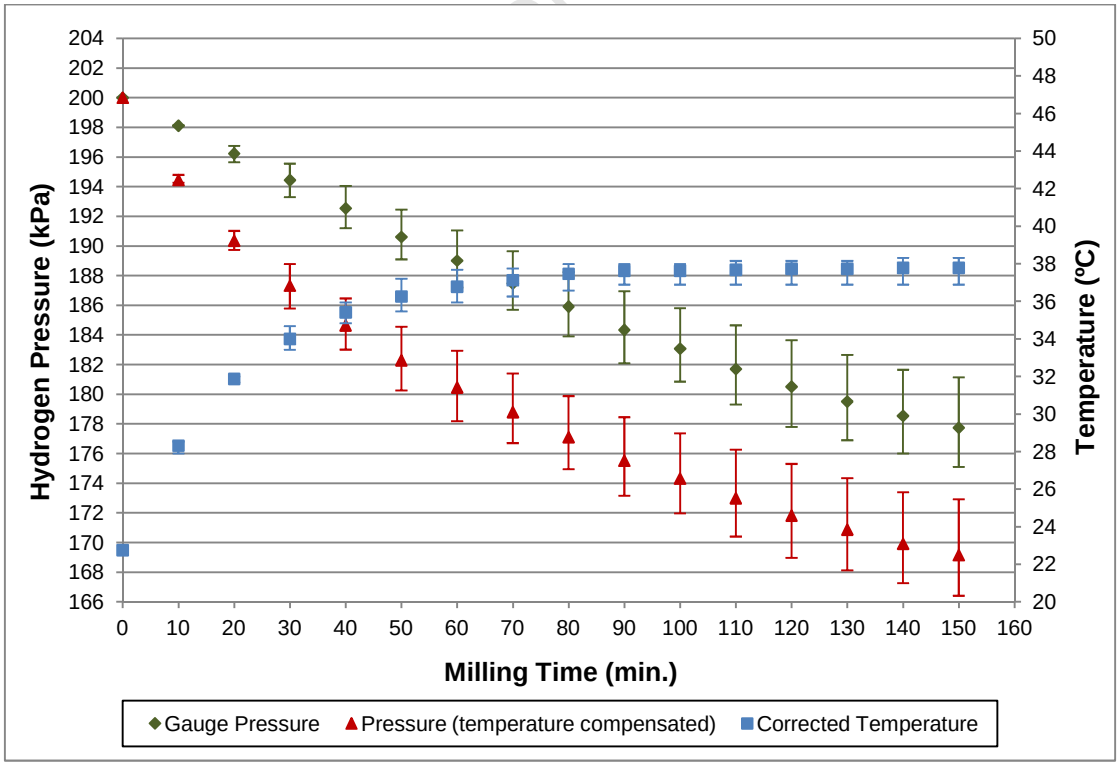

Figure 6.2: Variation in hydrogen pressure and temperature when using a 5 pin-collar stirrer configuration with 26 mm pins. Milling performed at 1.5 m/s for 2.5 hrs.

From figures 6.1 and 6.2 above, the general trend for both stirrer configurations is that the temperature in the mill chamber increases with increasing milling time. The temperature rise during milling is dependent on the kinetic energy of the grinding media. When the grinding media collide with one another, they lose a part of this energy to friction and therefore generate heat. Another contributing factor could be the heat generated from the exothermic reaction between hydrogen and titanium. Therefore, the overall rise in temperature is probably due to a combination of these factors. By comparing the two stirrer configurations, the 30 mm pin length stirrer generates more heat than the 26 mm pin length stirrer for a given milling time. This is expected since the 30 mm pin length stirrer agitates a large volume of grinding media, resulting in more grinding media collisions and therefore more frictional heating. However, for both stirrer configurations, the temperature only rises for the first 90 minutes; thereafter each stirrer reaches a maximum equilibrium temperature and remains at that temperature for the duration of the test. Since the cooling water flow rate remains constant throughout the test, the rise in temperature during the first 90 minutes of milling suggests that the amount of heat generated is much higher than what the cooling water can remove. On the other hand, it may be explained that after 90 minutes, less heat is generated from milling and therefore the cooling water flow rate is sufficient at maintaining a fixed temperature.

Figures 6.1 and 6.2 also demonstrate how the hydrogen pressure decreases with increasing milling time for each stirrer configuration. During milling, there are two factors that influence the hydrogen pressure i.e. the temperature rise and the rate of hydrogen absorption. As the temperature rises during milling, the hydrogen pressure is expected to rise as well. Alternatively, the hydrogen pressure will drop as more clean titanium surfaces are created to absorb hydrogen. Therefore, the recorded gauge pressure is actually the resultant pressure, showing the effect of both factors. However, in order to compare the hydrogen absorption rate by the feed for both pin length stirrers, only the drop in pressure associated with hydrogen absorption is required. Therefore, the temperature compensated pressure has to be determined for both pin length stirrers. In order to achieve this, equation 6.1 is used to calculate the temperature compensated pressure at a specific milling time, using the corresponding gauge pressure and corrected temperature at that same milling time. This temperature compensated pressure is calculated at each 10 minute interval and the resulting pressure data is included in figures 6.1 and 6.2 for the 30 mm and 26 mm pin length stirrers, respectively. As expected, the temperature compensated

pressure drops further than the recorded gauge pressure, at a given milling time, for both pin length stirrers.

$$\frac{P_{temperature,compensated,x}}{T_{ambient}} = \frac{P_{gauge,x}}{T_{corrected,x}} \quad (6.1)$$

Where: $P_{temperature,\ compensated,x}$ *- temperature compensated pressure at a milling time of x*

$T_{ambient}$ *- ambient temperature (remains constant)*

P_{gauge} *– recorded gauge pressure at a milling time of x*

$T_{corrected}$ *- corrected temperature at a milling time of x*

By comparing the temperature compensated pressure data for both pin length stirrers, it is clear from figure 6.3 that the hydrogen pressure data follows a similar trend. This suggests that the hydrogen absorption rate by the titanium feed is similar for both pin length stirrers.

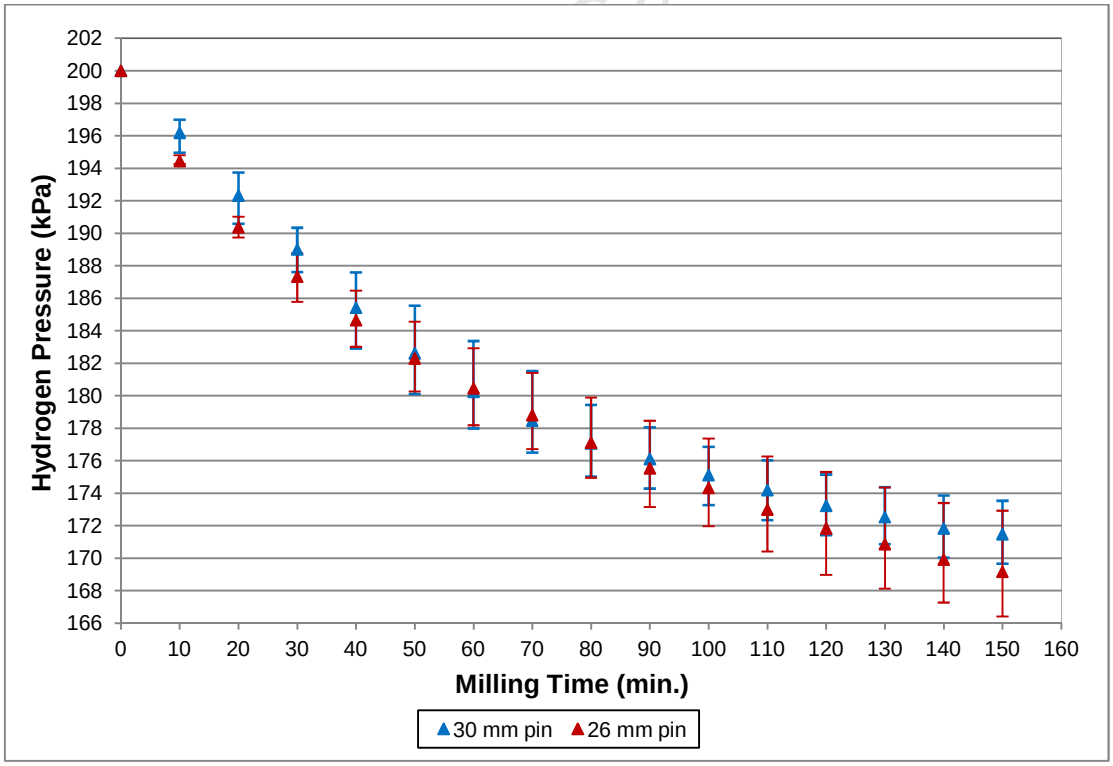

Figure 6.3: Effect of pin length on hydrogen pressure for 5 pin-collar stirrer configuration. Milling performed at 1.5 m/s for 2.5 hrs.

Since the hydrogen absorption rate is the same for both pin length stirrers, it is expected that the product size distribution would be similar. Figure 6.4 shows the product size distribution for the 26 mm and 30 mm pin length stirrer configuration. This graph includes the size distribution of the total product yield (excluding contaminants particles), as well as the unrecovered powder. Ideally, less of the product should be greater than 2000 µm as this indicates that more of the product has been ground to a finer size. By comparing the two pin length stirrers, the amount of product greater than 2000 µm is found to be less for the 26 mm pin length stirrer. It is also evident that the expected powder yield is higher for the 26 mm pin length stirrer. However, the error bars for the product yield between 2000 µm and 250 µm do not suggest an overwhelming difference between the 26 mm and 30 mm pin length stirrers.

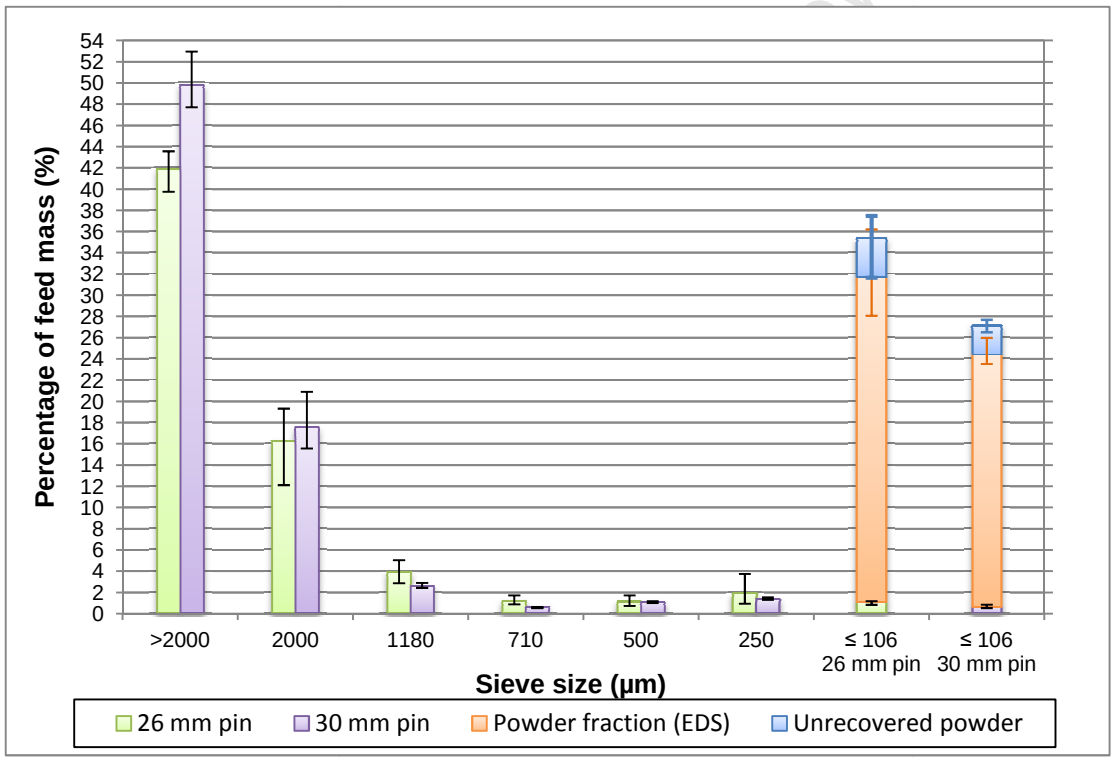

Figure 6.4: Effect of pin length on product size distribution for a 5 pin-collar stirrer configuration. Milling performed at 1.5 m/s for 2.5 hrs.

By analysing the powder results (i.e.106 µm sieve results) for both pin length stirrers, less than 1% of the feed mass is recovered as contaminant-free powder. In other words, this is the magnetically separated amount of powder that is recovered from the sieve separation process. Due to the presence of contaminants, the titanium powder fraction in the contaminated powder blend (i.e. powder recovered from the filtration separation process) is determined through EDS analysis as described in

section 5.7.2. From figure 6.4, the EDS powder fraction results clearly show that the majority of the titanium powder is found in the contaminated powder blend. More specifically, the EDS analysis results show that the titanium powder fraction is greater for the 26 mm pin length stirrer. Therefore the actual powder yield, which is the sum of the magnetically separated powder and powder fraction, is greater for the 26 mm pin length stirrer. Furthermore, figure 6.4 also shows the unrecovered amount of powder that adheres to the grinding media and mill. This is basically the difference between the expected and the actual powder yield. By comparing both pin length stirrers, more powder is unrecovered with the 30 mm pin length stirrer. The reason for this behaviour may lie in how the 30 mm pin length stirrer agitates a larger grinding volume. As a result, a larger surface area is coated with powder.

Overall, for a 5 pin-collar configuration, the results have shown that the hydrogen absorption rate by the titanium feed is similar for both the 26 mm and 30 mm pin length stirrer. Alternatively, the corresponding product size distribution graph shows that the expected powder yield is greater for the 26 mm pin length stirrer. In addition, the product yield with a size greater than 2000 µm is less for the 26 mm pin length stirrer. Although the difference in the product size distribution is not significant, the results suggest that the 26 mm pin length stirrer is as good as, if not better than, the 30 mm pin length stirrer.

6.1.2 Effect of the number of pins

For a fixed number of pins, the shorter pin length stirrer has been proven to perform slightly better in terms of producing more powder. However, the hydrogen absorption rate is similar for both pin length stirrers. Now it has to be determined whether a similar trend is observed when adding more pins and whether the number of pins on the stirrer influences the hydrogen absorption rate. In order to investigate this effect, an additional pin-collar is added to the stirrer. The stirrer now consists of 6 pin-collars and therefore a total of 12 pins. Once again, the pin-collars are orientated at 90° to each other and spaced evenly along the stirrer. Unlike the 5 pin-collar configuration, there is now two grinding media spacing between each successive pin along the stirrer, instead of three grinding media.

Firstly, it has to be established whether the pin length has a similar effect on the hydrogen absorption rate when using 6 pin-collars. Therefore a stirrer configuration consisting of 6 pin-collars with 30 mm long pins was tested and compared to one with

shorter 26 mm long pins. Each pin length stirrer configuration was tested under the exact same milling conditions as the corresponding pin length stirrers used for the 5 pin-collar configuration. The resulting variation in hydrogen pressure and temperature for the 30 mm and 26 mm pin length stirrer is shown figures 6.5 and 6.6 respectively. Similar to the 5 pin-collar configuration, the corrected temperature and the recorded gauge pressure is plotted on both graphs. In order to compare the rate of hydrogen absorption by the feed for both pin length stirrers, the temperature compensated pressure is plotted on both graphs as well.

Similar to the 5 pin-collar configuration, the 30 mm pin length stirrer with a 6 pin-collar configuration generates more heat for a given milling time because it agitates a larger grinding volume. Once again, for both pin length stirrers, figures 6.5 and 6.6 show that the temperature rises for the first 90 minutes and thereafter reaches a maximum equilibrium temperature. However, the equilibrium temperature for the 26 mm and 30 mm pin length stirrers are approximately 2.5℃ and 3.5℃ higher respectively, than that for the corresponding pin length stirrers used in the 5 pin-collar configuration. This proves that adding more pins increases the grinding media collisions, resulting in more frictional heating.

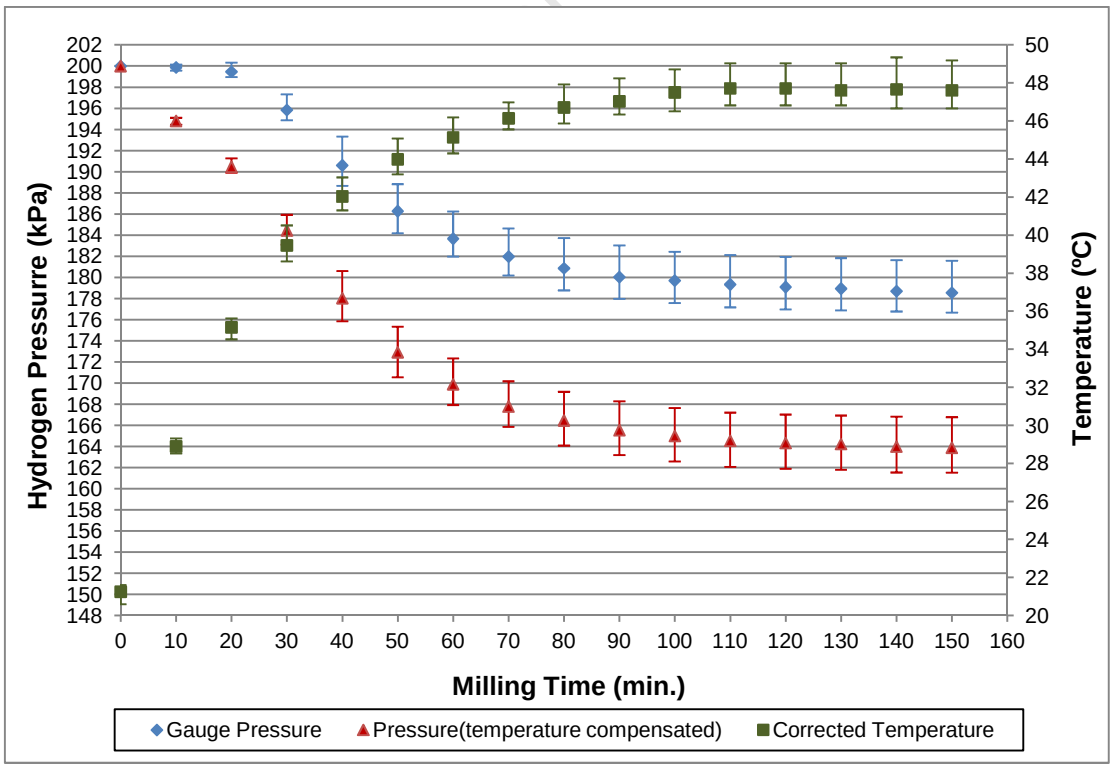

Figure 6.5: Variation in hydrogen pressure and temperature when using a 6 pin-collar stirrer configuration with 30 mm pins. Milling performed at 1.5 m/s for 2.5 hrs.

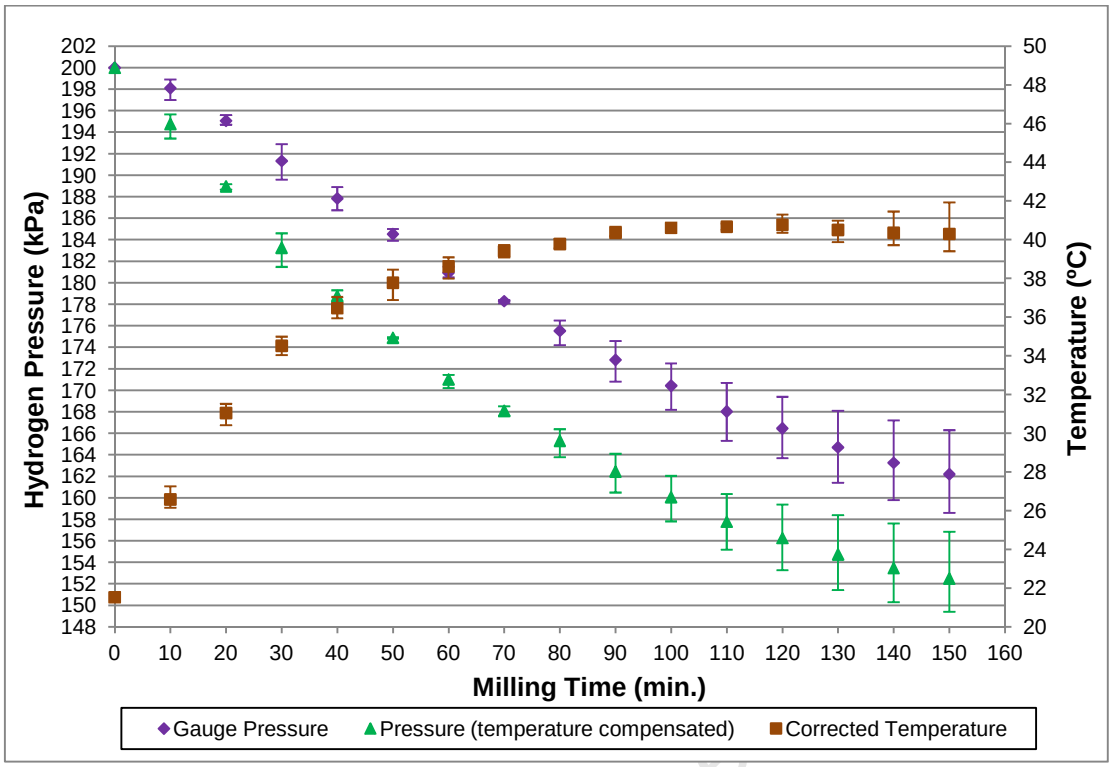

Figure 6.6: Variation in hydrogen pressure and temperature when using a 6 pin-collar stirrer configuration with 26 mm pins. Milling performed at 1.5 m/s for 2.5 hrs.

By using equation 6.1, the temperature compensated pressure was calculated at each 10 minute interval using the corresponding recorded gauge pressure and corrected temperature at the same interval. This was done for each pin length stirrer and is included in figures 6.5 and 6.6. Similar to the 5 pin-collar configuration, the temperature compensated pressure drops further than the gauge pressure, at given milling time, for both pin length stirrers. Figure 6.7 compares the temperature compensated pressure for both pin length stirrers.

For the 26 mm pin length stirrer, notice that the hydrogen pressure continues to drop throughout the test. This suggests that the titanium feed continues to absorb hydrogen throughout the test. However, unlike the 5 pin-collar configuration, the 30 mm pin length pressure data does not follow the exact same trend as the 26 mm. Instead, the hydrogen absorption rate for the 30 mm pin length stirrer is similar to the 26 mm pin length stirrer for the first 90 minutes only, implying that the feed only absorbs hydrogen during this period. Thereafter the pressure remains fixed for the duration of the test and may indicate that not enough clean titanium surfaces are created to absorb the hydrogen. It may also indicate that after the 90 minute period, the feed is saturated with hydrogen and can therefore not absorb any further

hydrogen. However, if this was the case, then the 26 mm pin length stirrer would have also reached saturation at a similar hydrogen pressure. Clearly, for the same amount of feed, the 26 mm pin length stirrer absorbs much more hydrogen after 90 minutes. Therefore, the reason for this behaviour may lie in how efficiently the 30 mm pin length stirrer facilitates feed breakage.

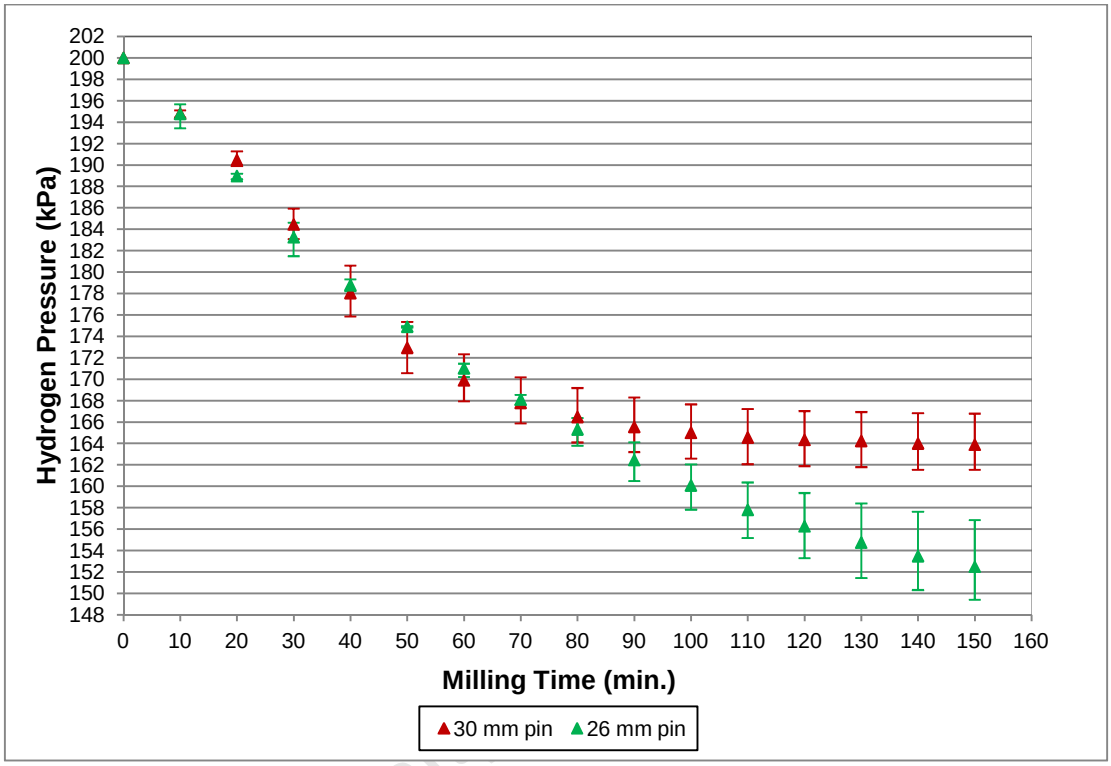

Figure 6.7: Effect of pin length on hydrogen pressure for 6 pin-collar stirrer configuration. Milling performed at 1.5 m/s for 2.5 hrs.

In order to investigate the stirrer efficiency, the product size distributions for both pin length stirrers are compared in figure 6.8. By analysing figure 6.8, the product yield with a size greater than 2000 µm is found to be greater for the 30 mm pin length stirrer. In other words, after milling for 2.5 hours, more of the initial coarse feed remains, implying that less breakage occurs compared to the 26 mm pin length stirrer. This would explain why the pressure remains fixed after 90 minutes, since not enough of the initial feed is broken down to expose clean titanium surfaces for hydrogen absorption. In addition, the product yield below 2000 µm is smaller for the 30 mm pin stirrer. Therefore, it may be explained that the 30 mm pin stirrer is less efficient at circulating the feed and facilitating feed breakage.

By analysing the 106 µm bar in figure 6.8 in more detail, the magnetically separated powder is found to be less than 1% of the feed mass for both pin length stirrers. As with the 5 pin-collar configuration, the EDS powder fraction results in figure 6.8 shows that significantly much more titanium powder is available in the contaminant powder blend. By comparing the actual powder yield (i.e. the sum of the powder fraction determined through EDS analysis and the magnetically separated powder) recovered for both pin length stirrers, the error bars show that both pin length stirrers produce a similar yield. Similarly, if the unrecovered powder is taken into account, the error bars overlap, implying that the expected powder yield is similar for both pin length stirrers.

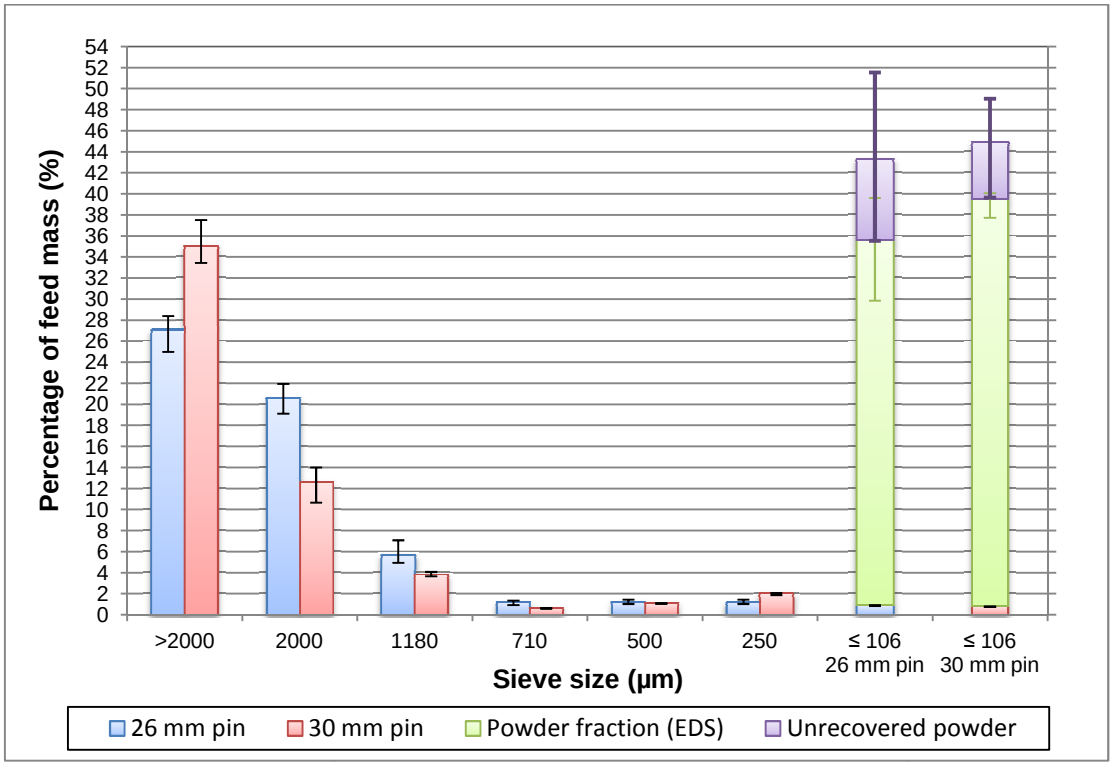

Figure 6.8: Effect of pin length on product size distribution for a 6 pin-collar stirrer configuration. Milling performed at 1.5 m/s for 2.5 hrs.

For the 6 pin-collar stirrer configuration, the results suggest that the 26 mm pin length stirrer is better than the 30 mm pin length stirrer in terms of exposing more clean titanium surfaces. As a result, more hydrogen is absorbed into the feed and the resulting product yield less than 2000 µm is greater for the 26 mm pin stirrer. However, the product yield between 1180 µm and 250 µm is similar for both pin length stirrers.

Since the 26 mm pin length stirrer is found to be slightly better than the 30 mm pin length stirrer, the relationship between the number of pins (or number of pin-collars) on the stirrer and the hydrogen absorption rate has to be determined for a 26 mm pin length stirrer. To investigate this effect, the temperature compensated pressure results for the 5 pin-collar stirrer configuration with 26 mm pins are compared to the 6 pin-collar configuration with the same pin length. Figure 6.9 illustrates the effect of the number of pins on the hydrogen absorption rate.

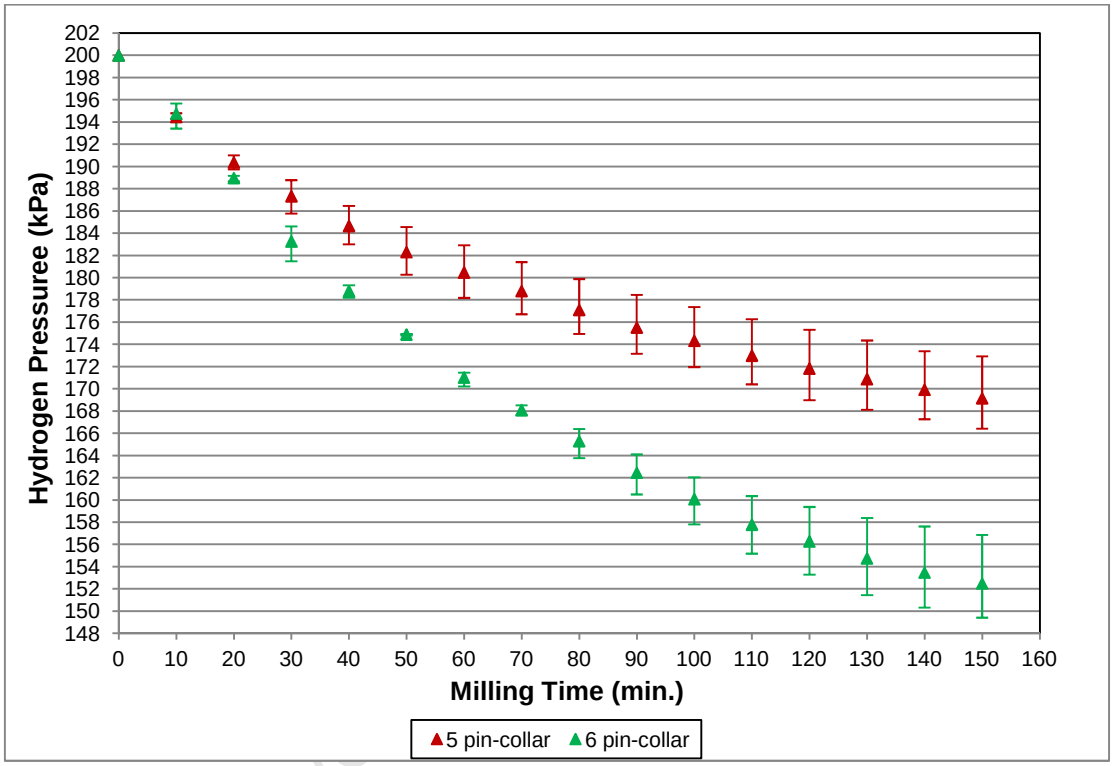

Figure 6.9 Effect of the number of pin-collars on hydrogen pressure when using 26 mm pins. Milling performed at 1.5 m/s for 2.5 hrs.

From figure 6.9, it is clear that the hydrogen pressure drops further for the 6 pin-collar configuration at a given milling time. In other words, the hydrogen absorption rate by the titanium feed is faster for the 6 pin-collar configuration. Furthermore, the hydrogen pressure drops by 15% with the 5 pin-collar configuration whereas the 6 pin-collar configuration results in a 24% drop at the end of the test. This suggests that, for a fixed 26 mm pin length, adding more pins results in more hydrogen absorption. This behaviour can be explained by the fact that adding more pins increases the active grinding volume. As a result, more of the initial feed is milled, creating more clean titanium surfaces to absorb hydrogen. Based on the amount of hydrogen absorbed, it is expected that a finer product size distribution and a higher

powder yield is produced when adding more pins. To verify this, the product size distributions for both configurations are compared in figure 6.10.

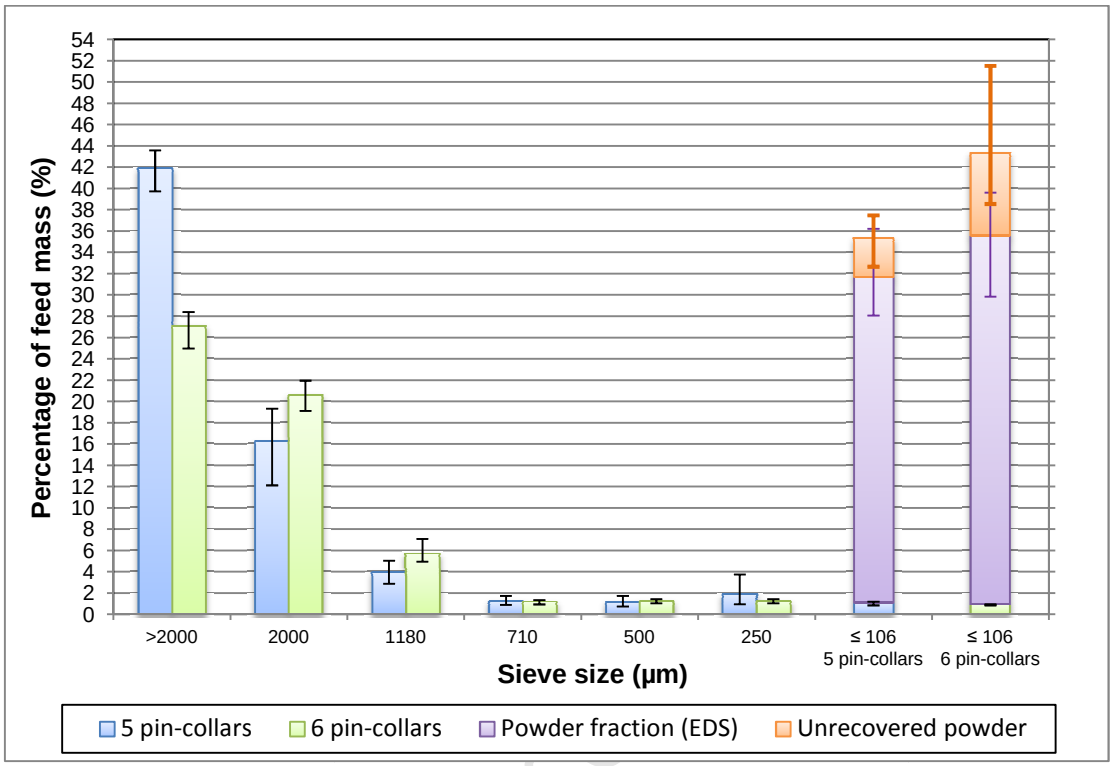

Figure 6.10: Effect of the number of pin-collars on the product size distribution when using 26 mm pins. Milling performed at 1.5 m/s for 2.5 hrs.

By analysing the 5 pin-collar product size distribution in figure 6.10, it is clear that the product yield greater than 2000 µm is larger than the corresponding expected powder yield. This suggests that less feed is milled with the 5 pin-collar configuration. Alternatively, with the 6 pin-collar configuration, the product yield greater than 2000 µm is less than the expected powder yield. In addition, the results show that the expected powder yield is much higher for the 6 pin-collar configuration. Consequently, the product size distribution can be seen as a further aid to prove the effectiveness of adding more pins.

Furthermore, as expected, the EDS powder fraction results show that most of the titanium powder is found in the contaminated powder blend. By comparing the powder fractions of both configurations, the error bars show that there is slightly more powder available with the 6 pin-collar configuration. As a result, the actual powder yield recovered after milling is found to be somewhat higher for the 6 pin-collar configuration. However, by comparing the unrecovered powder yield, significantly

more powder is unrecovered for the 6 pin-collar configuration. This might be due to the larger active grinding volume which is created when more pins are added. In other words, a larger surface area may be coated with powder when more pins are added, resulting in a lower powder yield.

In general, the pressure results in figure 6.9 have shown that the hydrogen absorption rate by the titanium feed is faster with the 6 pin-collar stirrer configuration. In addition, figure 6.10 shows that the expected powder yield is higher for the same configuration. Therefore, with a 26 mm pin length, the 6 pin-collar stirrer configuration performs better than the 5 pin-collar configuration. In other words, for a fixed three grinding media spacing between the pin tip and chamber wall, a two grinding media spacing between successive pins along the stirrer is better than three grinding media spacing. Consequently, this stirrer configuration will now be used to test the effect of the other milling conditions on the hydrogen absorption rate.

6.2 Effect of stirrer speed

The experiments to determine the effect of stirrer speed on the hydrogen absorption rate were initially performed on CP Ti in order to serve as a benchmark for Ti-6Al-4V. It is therefore assumed that Ti-6Al-4V will behave in a similar manner at each of the speeds tested on CP Ti.

6.2.1 CP Ti feed

The effect of the stirrer pin tip speed on the hydrogen absorption rate was investigated, using the 6 pin-collar stirrer design with 26 mm pins. In order to determine this, milling of CP Ti was conducted at four different stirrer pin tip speeds, i.e. 0.5 m/s, 1 m/s, 1.5 m/s and 2 m/s for a fixed milling time of 2.5 hours. Figures 6.11 to 6.14 show the relationship between the hydrogen pressure and corrected temperature for each stirrer pin tip speed. Both the recorded gauge and the temperature compensated pressure are included in each figure.

At the lowest stirrer pin tip speed, figure 6.11 shows that the temperature remains reasonably constant throughout the test. Due to the low stirrer speed, the resulting kinetic energy of the grinding media is also low and therefore minimum heat is generated at each grinding media collision. As a result, the cooling rate of the water is sufficient at maintaining a constant temperature throughout the test. In addition, since the temperature remains fairly constant at around room temperature,

temperature has minimum effect on the hydrogen pressure. Therefore the calculated temperature compensated pressure lies close to the recorded gauge pressure.

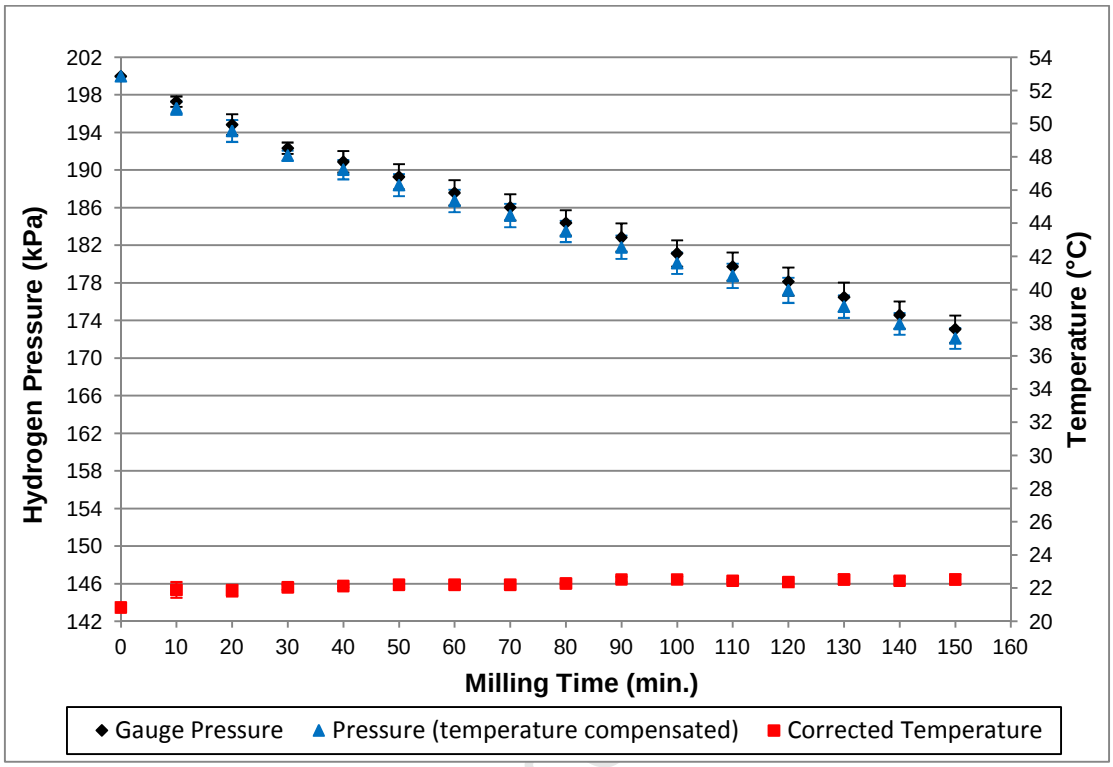

Figure 6.11: Variation in hydrogen pressure and temperature when milling CP Ti feed. Milling performed at 0.5 m/s for 2.5 hrs using the 6 pin-collar, 26 mm pin length stirrer.

Alternatively, at higher stirrer pin tip speeds above 0.5 m/s, the general trend is that the temperature rises steeply during the initial stage of milling and thereafter reaches a maximum equilibrium temperature. Figures 6.12 to 6.14 clearly show that the temperature is dependent on the stirrer pin tip speed. As the stirrer speed increases further for each test, more heat is generated at a given milling time. This behaviour is expected because the temperature rise during milling is dependent on the kinetic energy of the grinding media. In addition, the results also show that the time taken to reach the equilibrium temperature is dependent on the stirrer speed and therefore increases with increasing stirrer speed.

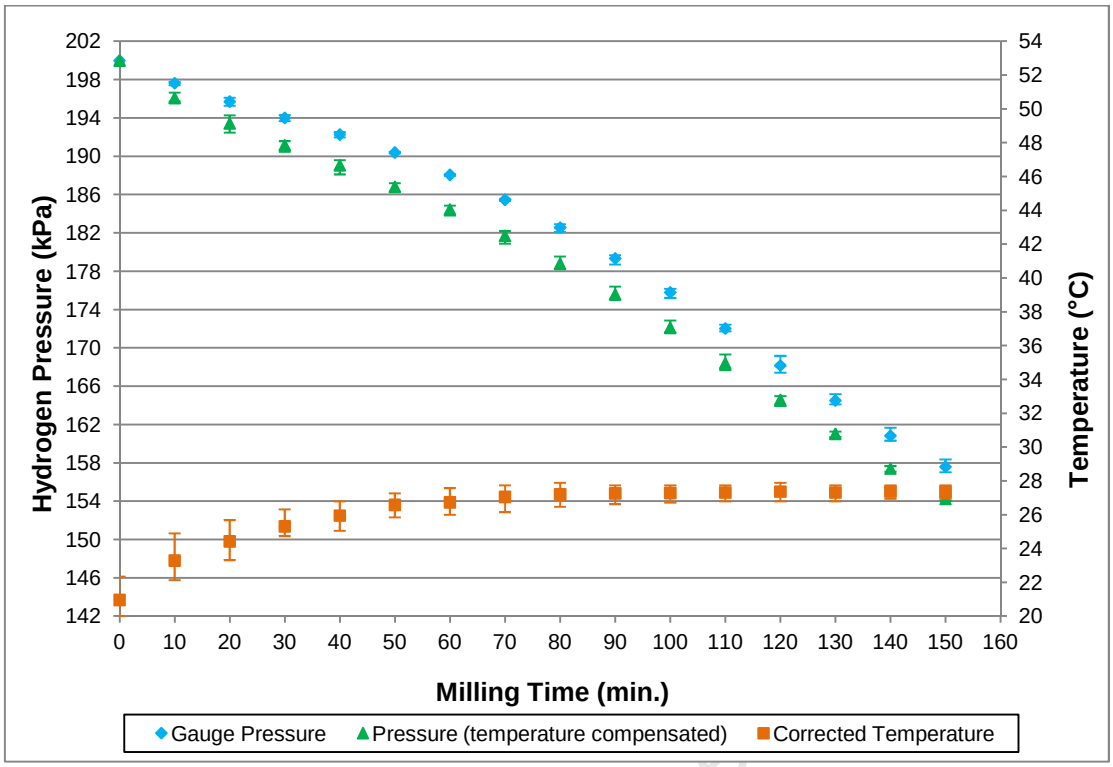

Figure 6.12: Variation in hydrogen pressure and temperature when milling CP Ti feed. Milling performed at 1 m/s for 2.5 hrs using the 6 pin-collar, 26 mm pin length stirrer.

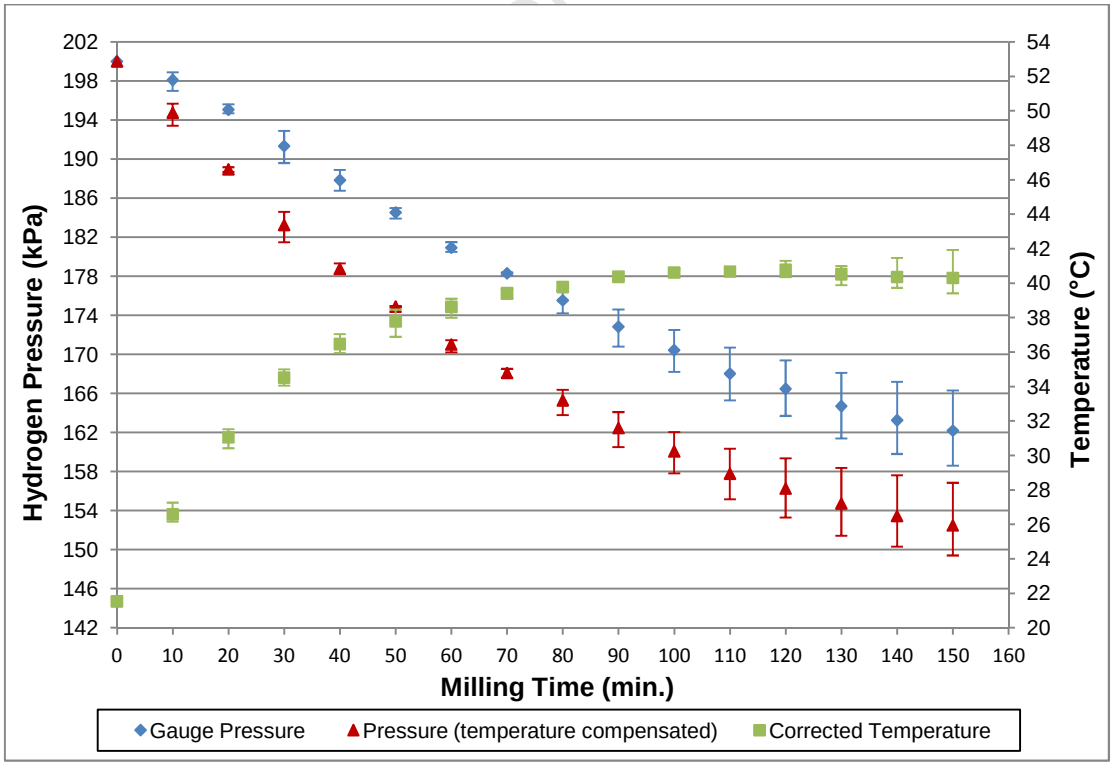

Figure 6.13: Variation in hydrogen pressure and temperature when milling CP Ti feed. Milling performed at 1.5 m/s for 2.5 hrs using the 6 pin-collar, 26 mm pin length stirrer.

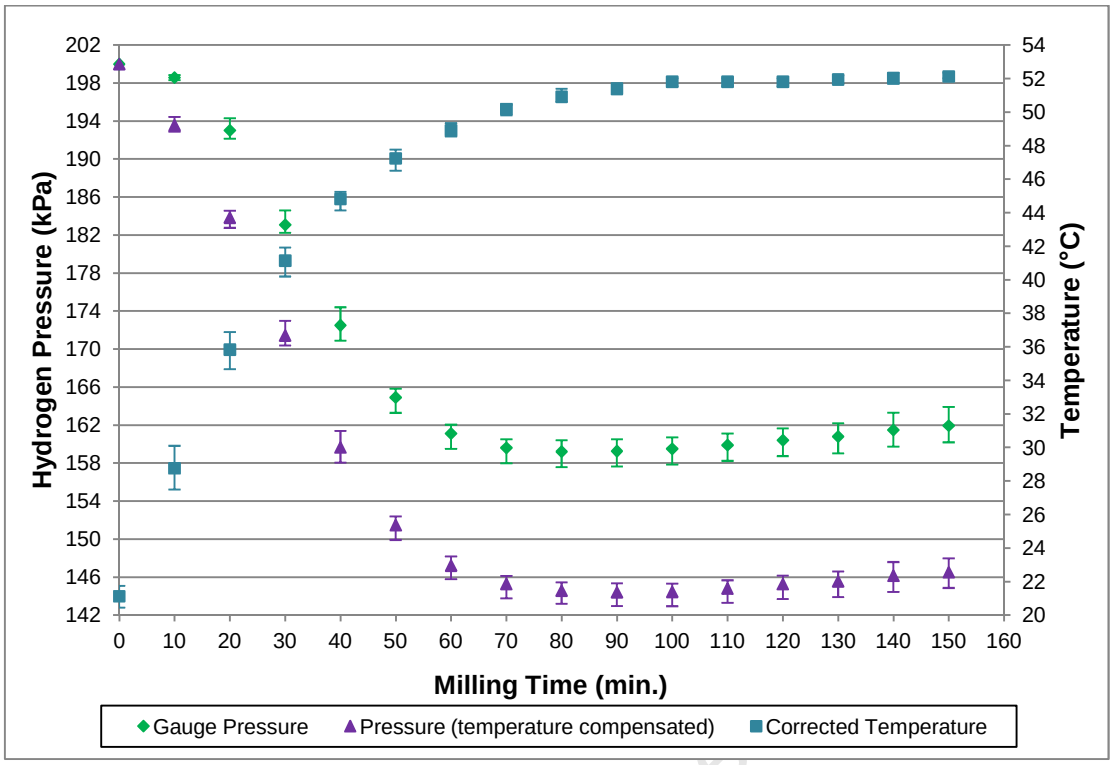

Figure 6.14: Variation in hydrogen pressure and temperature when milling CP Ti feed. Milling performed at 2 m/s for 2.5 hrs using the 6 pin-collar, 26 mm pin length stirrer.

Figure 6.15 below, compares the temperature compensated pressure data for each stirrer pin tip speed. Notice that the hydrogen pressure for the 0.5 m/s, 1 m/s and 1.5 m/s stirrer pin tip speeds follow a similar trend in that the pressure continues to decrease steadily for the duration of the test. However, for the 2 m/s test, the pressure drops rapidly for the first 60 minutes, and after 70 minutes the pressure remains constant with a slight increase in pressure after 90 minutes. This suggests that the hydrogen absorption rate into the titanium is much faster at a stirrer pin tip speed of 2 m/s, resulting in faster saturation and no further pressure drop after 70 minutes.

By comparing all the stirrer speeds for the first 60 minutes, the overall effect of the stirrer speed is that the hydrogen pressure drops further as the stirrer speed increases. Since the stress intensity of the grinding media is proportional to the square of the stirrer velocity, it is expected that the breakage rate increases with stirrer speed. As a result, the rate of creating new surfaces also increases with stirrer speed. This may explain the behaviour at each stirrer speed and why the hydrogen absorption rate is much higher at the fastest pin tip speed of 2 m/s.

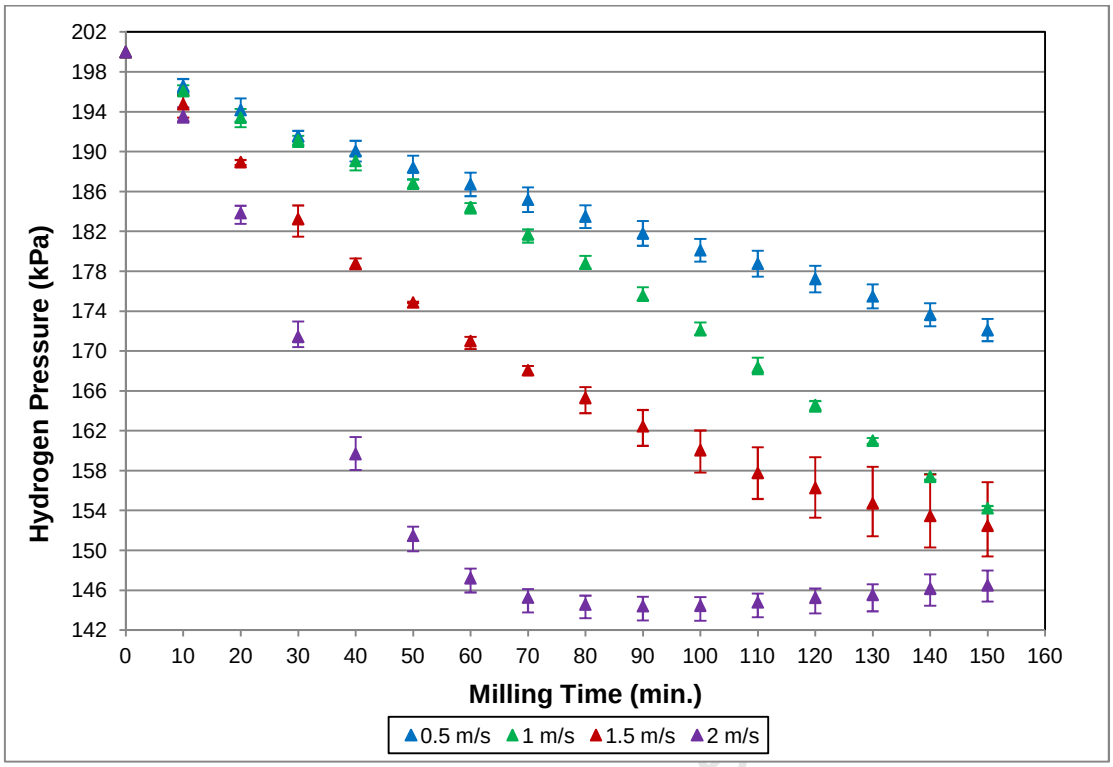

Figure 6.15: Effect of stirrer speed on hydrogen absorption when milling CP Ti feed for 2.5 hrs using the 6 pin-collar, 26 mm pin length stirrer.

It now has to be determined whether the stirrer speed has a similar effect on the product size distribution. Figure 6.16 below compares the product size distribution at each stirrer speed. At the lowest stirrer pin tip speed of 0.5 m/s, the results show that a large percentage of the product yield is at a coarse particle size between 2000 µm and 1180 µm. Relative to the expected powder yield, the product yield greater than 2000 µm is slightly higher. Note that the total product yield (excluding contaminants) recovered after milling at 0.5 m/s is nearly the same as the initial feed amount and therefore the unrecovered powder is negligible. Since the stress intensity and frequency of the grinding media collisions are much lower at low speed, this pattern is expected. Alternatively, at the fastest stirrer pin tip speed of 2 m/s, less of the product yield lies between 2000 µm and 1180 µm and the expected powder yield suggests that considerably much more of the feed is converted into powder. Consequently, the results suggest that the drive for powder production is much greater at higher stirrer speeds.

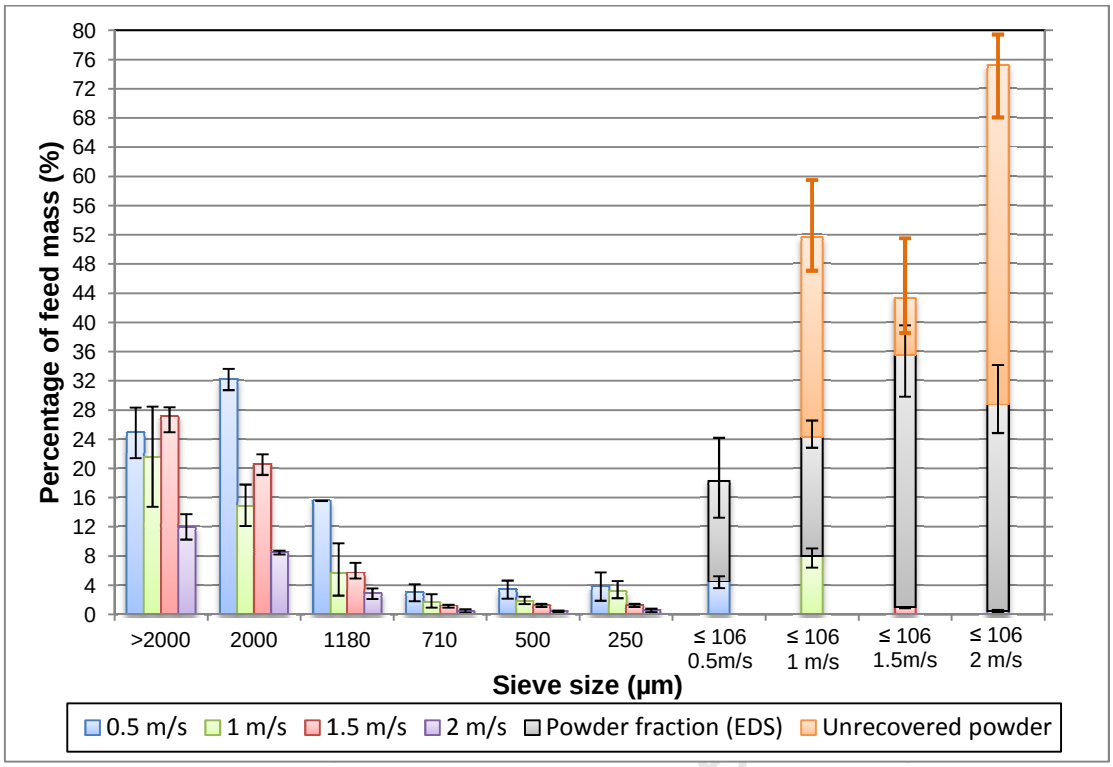

Figure 6.16: Effect of stirrer speed on product size distribution when milling CP Ti feed for 2.5 hrs using the 6 pin-collar, 26 mm pin length stirrer.

Figure 6.16 also shows that the product yield greater than 2000 µm is similar for the 0.5 m/s, 1 m/s and 1.5 m/s tests. Between 2000 µm and 1180 µm, the product yield for the 0.5 m/s test is found to be greater than both the 1 m/s and 1.5 m/s tests. However, between 710 µm and 250 µm, there is no significant difference between the product yields of these three speeds. When comparing the expected powder yield, it is clear that the 1 m/s and 1.5 m/s tests produce considerably more powder than the 0.5 m/s. Therefore, although the product yield greater than 2000 µm is similar for these three speeds, less of the product remains at a coarse size and more powder is produced as the speed increases in this range. However, note that the errors bars for the coarse product yield (between 2000 µm and 1180 µm) and expected powder yield suggest that there is no significant difference between the 1 m/s and 1.5 m/s results. Therefore, a difference in the product yield is only clear when comparing the 0.5 m/s results with either the 1 m/s or 1.5 m/s results.

Furthermore, intuitively, the unrecovered powder fraction of the expected powder yield is expected to increase with stirrer speed. Clearly this is the case when comparing the 0.5 m/s, 1 m/s and 2 m/s expected powder yield. However, when

comparing the 1 m/s and 1.5 m/s expected powder yield, this pattern is not observed. Instead, the powder fraction determined through EDS analysis increases.

Overall, in terms of the effect of stirrer speed, figure 6.15 and 6.16 above have clearly shown that the stirrer speed has a strong effect on the hydrogen absorption rate and therefore the product size distribution. By increasing the stirrer pin tip speed by 0.5 m/s, it was proven that the grinding intensity increases with stirrer speed. As a result, a faster stirrer speed facilitates faster hydrogen absorption and therefore produces a higher powder yield. For the range of speeds experimented on CP Ti, the optimum stirrer pin tip speed is found to be 2 m/s. This speed results in the fastest hydrogen absorption rate, allowing the CP Ti feed to reach saturation sooner than the other speeds. Consequently, it also produces the highest powder yield after 2.5 hours of milling, although much of the powder is unrecovered using the present methodology.

6.2.2 Comparison between Ti-6Al-4V and CP Ti feed

For the range of speeds tested on CP Ti, it is assumed that Ti-6Al-4V will also have the same optimum stirrer pin tip speed of 2 m/s. Now it has to be determined whether a similar behaviour in terms of hydrogen pressure and powder yield occurs when using Ti-6Al-4V feed. Therefore, Ti-6Al-4V was milled at a stirrer pin tip speed of 2 m/s for a milling time of 2.5 hours. Figure 6.17 shows the resulting variation in hydrogen pressure in terms of the recorded gauge and temperature compensated pressure. The corrected temperature is once again also plotted.

By comparing the temperature data of CP Ti in figure 6.14 with that of Ti-6Al-4V in figure 6.17, it is clear that the temperature data for both feeds follow a similar trend. Likewise, the temperature for the alloy also rises steeply during the initial stage of milling and thereafter reaches a maximum equilibrium temperature. However, the alloy generates more heat at a given time throughout the test. Since both feeds are tested at the same milling conditions, the effect of the heat generated by the kinetic energy of the grinding media would be the same. Therefore, the additional heat for the alloy has to be generated from the exothermic reaction between hydrogen and titanium. The fact that the alloy generates more heat may suggest that it is more reactive towards hydrogen than CP Ti.

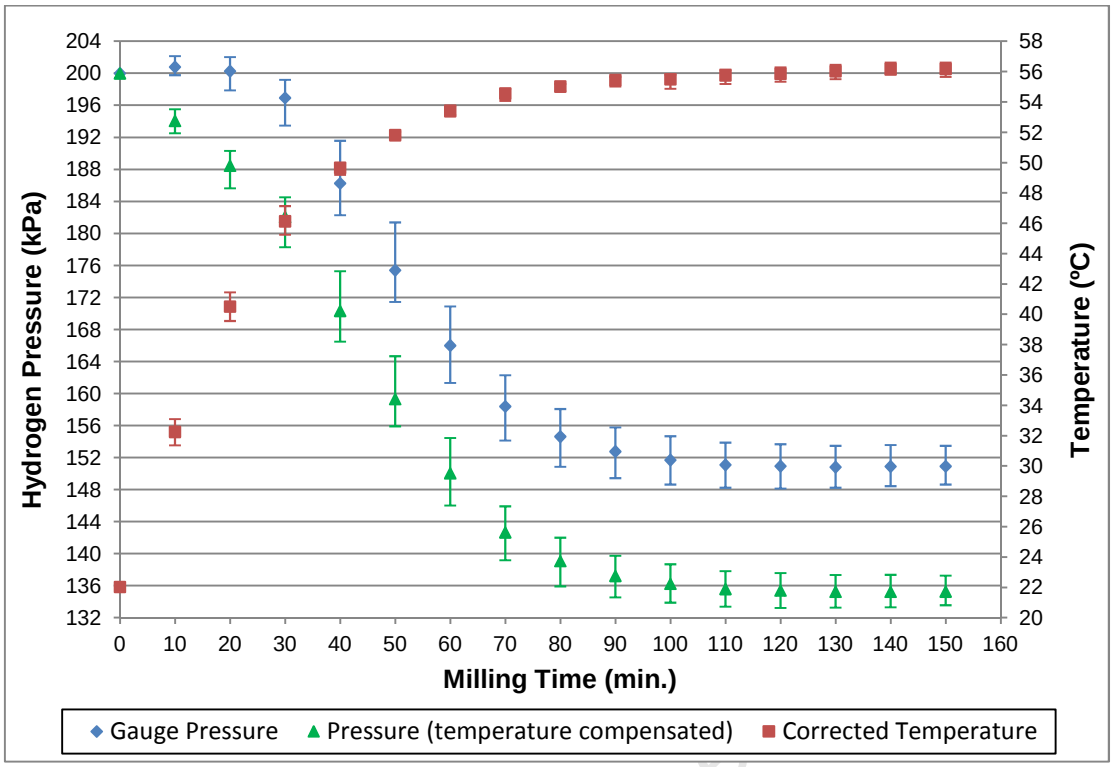

Figure 6.17: Variation in hydrogen pressure and temperature when milling Ti-6Al-4V. Milling performed at 2 m/s for 2.5 hrs using the 6 pin-collar, 26 mm pin length stirrer.

Figure 6.18 compares the temperature compensated pressure of both feeds, milled at the same stirrer speed and milling time. Notice that the Ti-6Al-4V pressure data follows a similar trend to that of CP Ti, in that there is a period of rapid hydrogen absorption until saturation is reached. However, the period of rapid hydrogen absorption is longer for the alloy and consequently, the time taken to reach saturation is also longer. By comparing the pressure data of each feed, the first 50 minutes of milling indicates that the alloy feed absorbs less hydrogen for a given milling time. Alternatively, after 70 minutes of milling, the alloy now absorbs more hydrogen for a further 30 minutes until saturation is reached. Therefore, overall, the alloy absorbs more hydrogen at the end of the 2.5 hour test. Since the density of the alloy (4.43 g/cm^3) is lower than that of CP Ti (4.51 g/cm^3), it has a greater surface area for a fixed mass and thus this may be the reason why the alloy absorbs more hydrogen.

A comparison of the product size distribution for both feeds is shown in figure 6.19. Note that the106 µm bar represents the expected powder yield for both feeds. This was calculated for both feeds by subtracting the total product yield greater than 250 µm from the initial feed mass. Clearly the difference in the hydrogen absorption rate for both feeds is reflected in the product size distribution. By comparing the

product size distribution, it is evident that the expected powder yield is higher for the alloy.

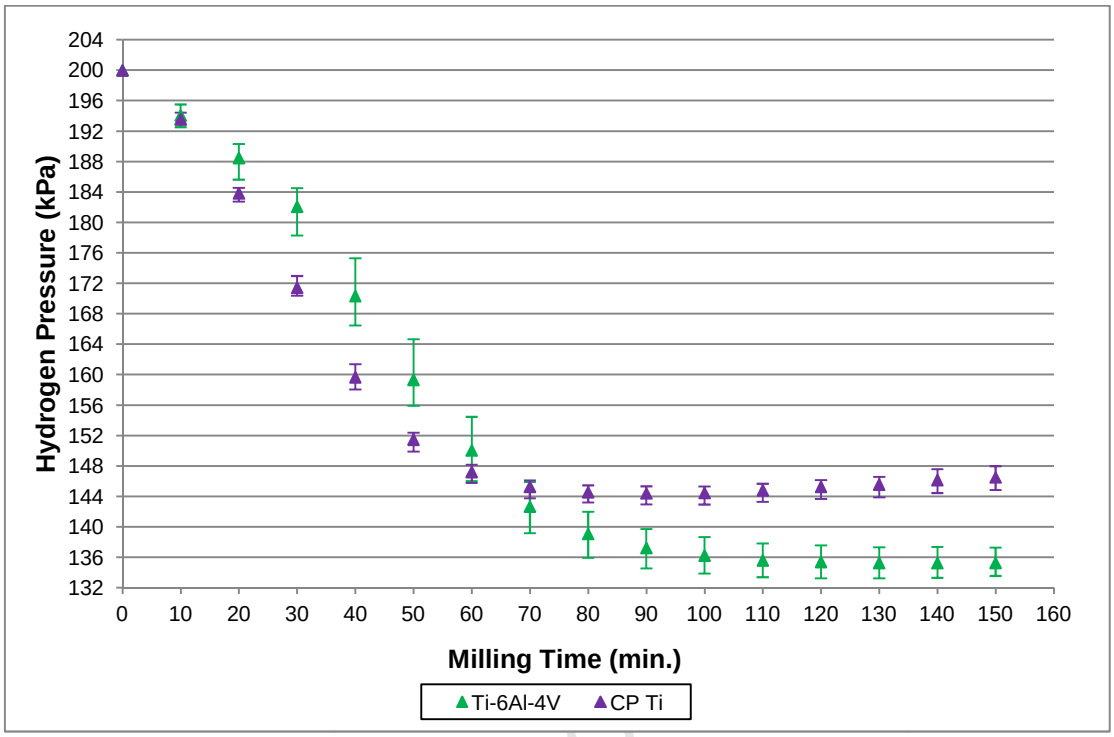

Figure 6.18: Comparison of the hydrogen pressure results for Ti-6Al-4V and CP Ti feed. Milling performed at 2 m/s for 2.5 hrs using the 6 pin-collar, 26 mm pin length stirrer.

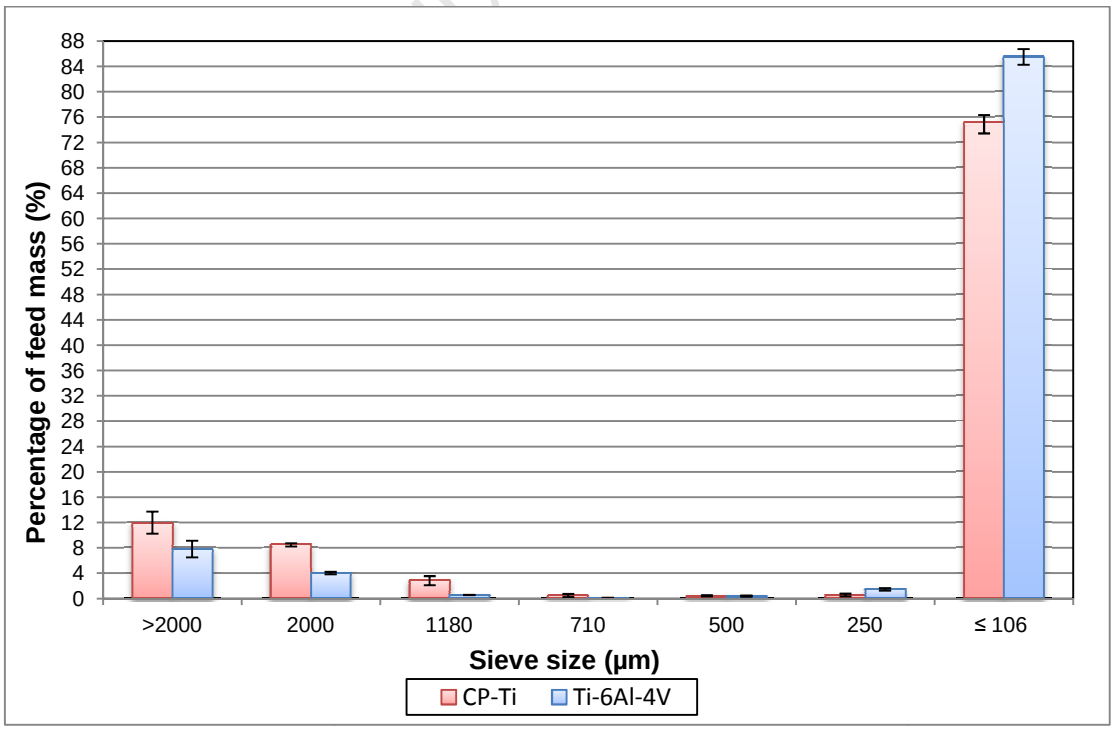

Figure 6.19: Comparison of the product size distribution for Ti-6Al-4V and CP Ti feed.

On the whole, it is clear that the stirrer pin tip speed of 2 m/s produces similar results for the alloy. In terms of the product size distribution, the majority of both feeds are converted into powder at this speed. However, by comparing figures 6.18 and 6.19, it is clear that the total amount of hydrogen absorbed has a stronger effect on the powder yield than the time taken to reach saturation. Therefore, even though the CP Ti feed reaches saturation sooner, the alloy absorbs more hydrogen overall and produces the most powder yield.

6.3 Effect of milling time

It has already been established that the optimum stirrer pin tip speed is 2 m/s. Now it has to be determined whether the corresponding milling time has any effect on the product size distribution and the powder yield. It also has to be determined whether an optimum milling time exists, which efficiently converts the titanium feed to powder without producing too much contamination. Once again, this effect will be tested on both titanium feeds.

6.3.1 CP Ti feed

By analysing the temperature compensated hydrogen pressure data for the 2 m/s stirrer pin tip speed, figure 6.14 in section 6.2.1 shows that there are three points of interest during the 2.5 hour test. Firstly, it would be interesting to know the product size distribution after the first 60 minutes of milling. This corresponds to a period of rapid hydrogen absorption, before saturation is reached. Secondly, the next point of interest would be after 90 minutes of milling, just before the pressure starts to rise. During the period between 70-90 minutes, the pressure remains constant, suggesting that the titanium is saturated with hydrogen. Therefore, the effect of this saturation period on the product size distribution is relevant. Finally, the product size distribution after 150 minutes of milling would also be useful, showing the effect of the slight pressure rise between 100-150 minutes. Since milling was already conducted for a milling time of 150 minutes (as shown in figure 6.14), further tests were only conducted at a stirrer pin tip speed of 2 m/s for a milling time of 60 minutes and 90 minutes.

Figure 6.20 compares the temperature compensated pressure for all three milling times, performed at a stirrer pin tip speed of 2 m/s. As expected, both the 60 minute and 90 minute tests follow the exact same trend as the 150 minute test. This is due to the fact that all the other milling conditions remain fixed at each milling time.

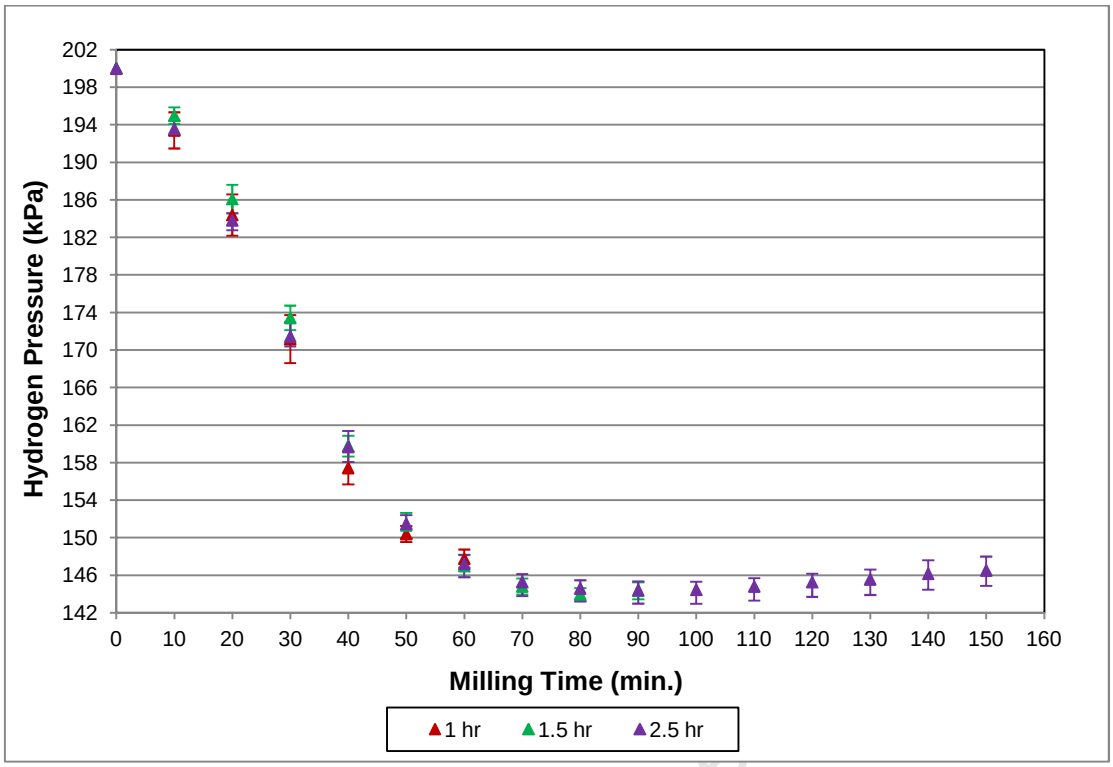

Figure 6.20: Effect of milling time on the hydrogen absorption rate of CP Ti. Milling performed at 2 m/s using the 6 pin-collar, 26 mm pin length stirrer.

The corresponding product size distribution for each milling time is shown in figure 6.21. For all three milling times, the expected powder yield is found to be significantly greater than the total product yield greater than 106 µm. By comparing the 1 hour and 1.5 hour product size distribution, the yield greater than 2000 µm is found to be lower for the 1.5 hour test. In addition, other differences are only found when comparing the 2000 µm product yield and expected powder yield. For the 1.5 hour test, the 2000 µm product yield is lower and the expected powder yield is significantly higher than the 1 hour test. By comparing the average expected powder yield, the 1.5 hour test shows that approximately 12% more powder is produced. As a result, it is clear that the saturation period between 70-90 minutes has a positive effect on the 1.5 hour product size distribution. On the other hand, compared to the 1.5 hour test, the 2.5 hour test has a similar product size distribution. This implies that the extra hour of milling after saturation has no further effect on the product size distribution. Therefore, milling for 2.5 hours is inefficient since a similar product size distribution or more importantly a similar expected powder yield can be achieved at a shorter milling time of 1.5 hours.

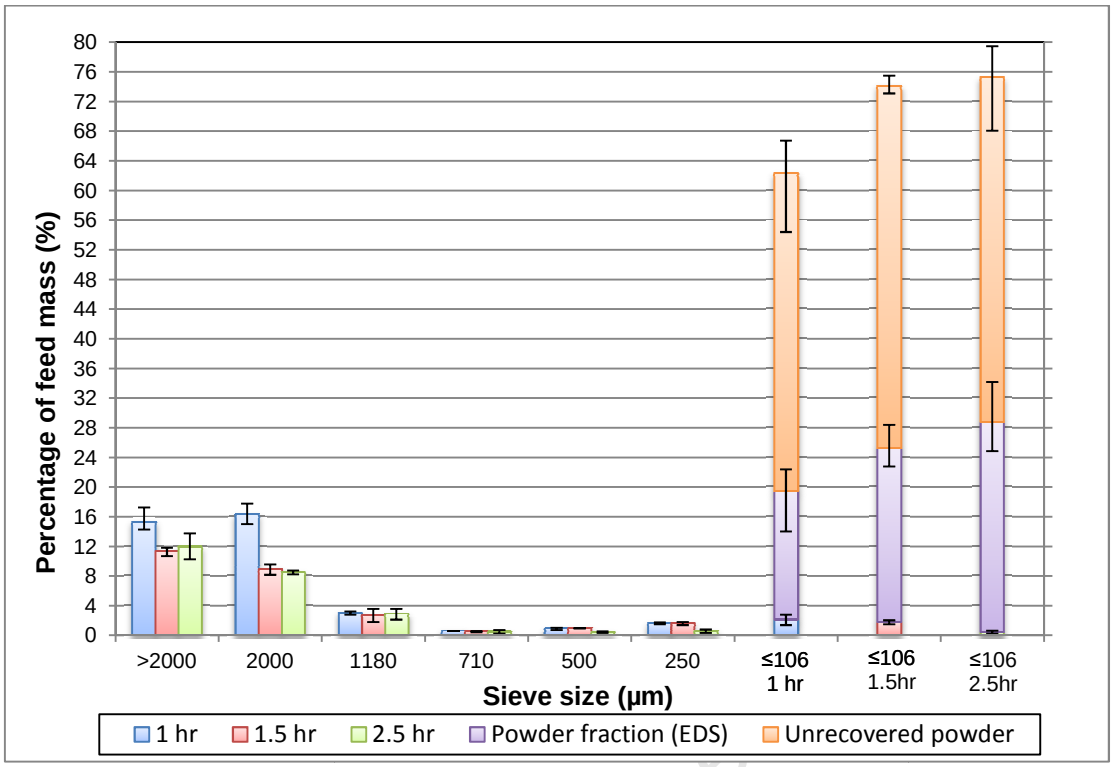

Figure 6.21: Effect of milling time on the product size distribution of CP Ti. Milling performed at 2 m/s using the 6 pin-collar, 26 mm pin length stirrer.

By analysing the expected powder yield in more detail, it is clear that the majority of the powder is unrecovered at each milling time. However, the error bars suggest that the unrecovered powder yield remains fairly the same for all three milling times. Consequently, the reason the expected powder yield increases, when comparing the 1 hour and 1.5 hour test, is due to the actual powder yield increasing. For these two milling times, figure 6.21 shows that the actual powder yield increases slightly with increasing milling time. Alternatively, the expected powder yield is similar for the 1.5 hour and 2.5 hour test because the corresponding actual powder yield is similar.

Furthermore, the amount of contamination in the contaminated powder blend produced after each milling time was determined through EDS analysis as explained in section 5.7.2. Since the contaminated powder blend passes through a 106 µm sieve, the contaminants are therefore also less than 106 µm. Figure 6.22 shows the amount of contamination produced, relative to the feed mass, at each milling time. By comparing the 1 hour and 1.5 hour results, the error bars do not suggest a significant difference between the amounts of contamination produced. This implies that the extra 30 minutes of milling has minimum effect on the amount of contamination produced. Alternatively, the amount of contamination produced after 2.5 hours of

milling is considerably higher than both the 1 hour and 1.5 hour test. This is clearly the result of excessive grinding that takes place after saturation is reached.

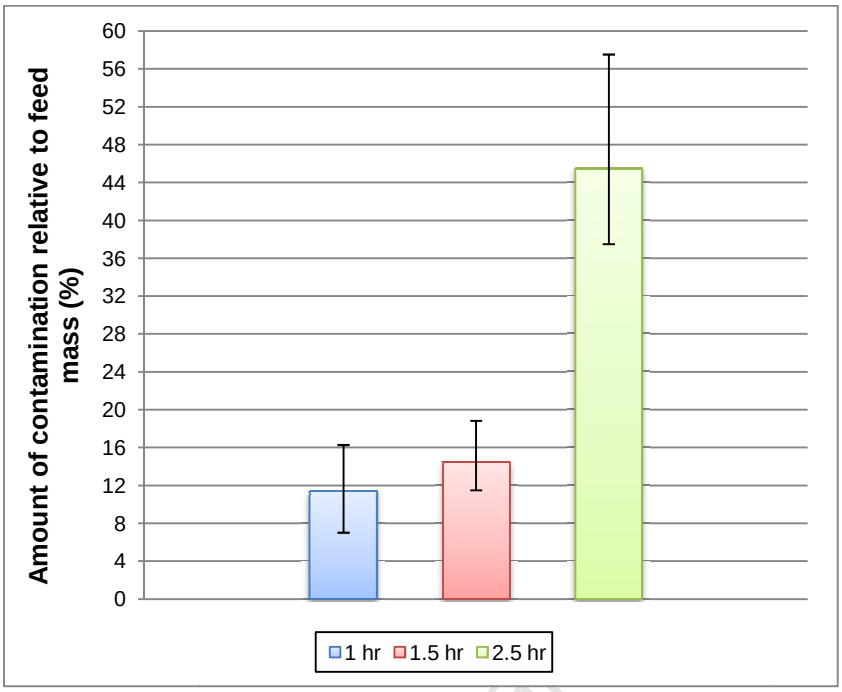

Figure 6.22: Amount of contamination produced at selected milling times for CP Ti.

Overall, the results show that the product size distribution is dependent on milling time, but only during the period between rapid hydrogen absorption and saturation. During this period, the expected powder yield is found to increase with milling time. In addition, minimum contamination is also produced during this period. However, after saturation, further milling has minimum effect on the product size distribution. The 2.5 hour test also shows that milling after saturation results in considerably much more contamination. As a result, milling for an extra hour after saturation is inefficient and only increases the wear rate of the mill. In terms of the optimum milling time, the 1.5 hour test is found to produce the best combination of minimum contamination and maximum powder production. Therefore for an optimum stirrer pin tip speed of 2 m/s, the corresponding optimum milling time is 1.5 hours when milling CP Ti.

6.3.2 Ti-6Al-4V feed

Similarly to CP Ti, figure 6.17 in section 6.2.2 shows that there are also three points of interest on the temperature compensated hydrogen pressure data for Ti-6Al-4V, when milling takes place at a stirrer pin tip speed of 2 m/s. The first point of interest would be after 90 minutes of milling as this corresponds to the end of the rapid

hydrogen absorption period, just before saturation. Secondly, the next point of interest would be after 120 minutes of milling. This will show the effect of the saturation period between 100 to120 minutes. Finally, the last point of interest would be after 150 minutes of milling, showing the effect of milling after saturation. Consequently, the corresponding product size distributions at these three milling times have to be analysed. Since milling was already conducted for a milling time of 150 minutes (as shown in figure 6.17), further tests were only conducted at a stirrer pin tip speed of 2 m/s for a milling time of 90 minutes and 120 minutes.

Figure 6.23 below compares the temperature compensated pressure data for all three milling times performed at a stirrer pin tip speed of 2 m/s. As expected, the hydrogen pressure for all three milling times follow the exact same trend. As mentioned before, this is due to the fact that all the other milling conditions remain fixed, while only the milling time is varied.

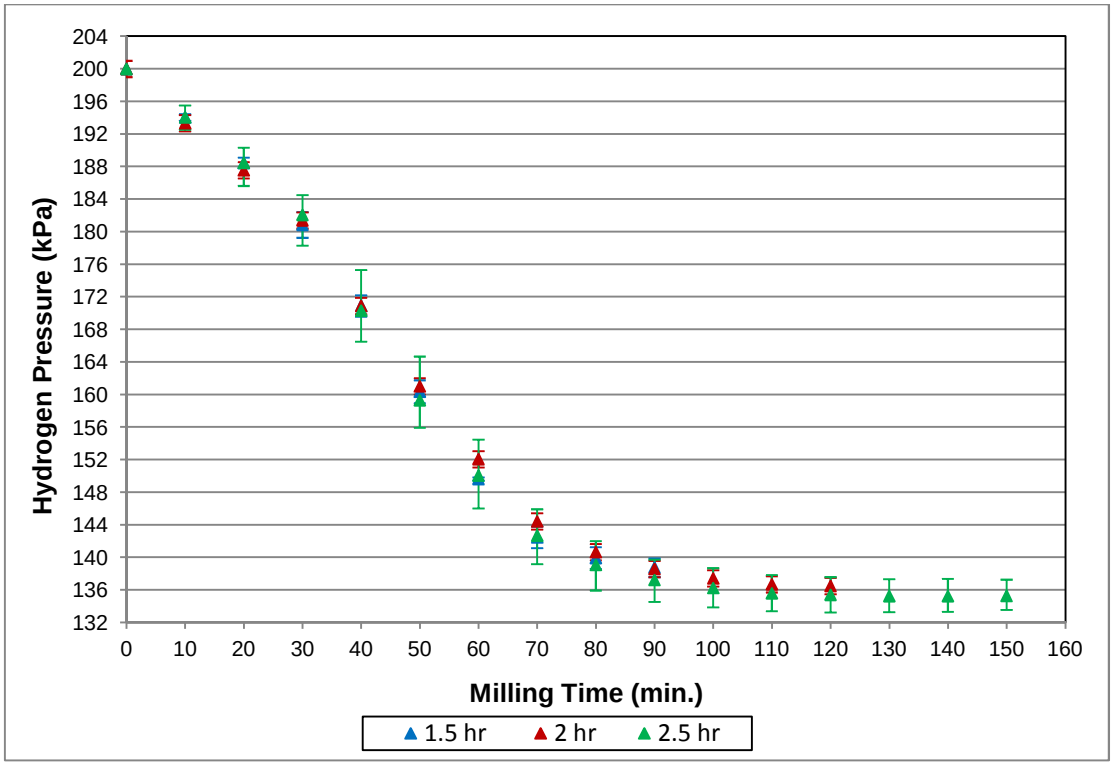

Figure 6.23: Effect of milling time on the hydrogen absorption rate of Ti-6Al-4V. Milling performed at 2 m/s using the 6 pin-collar, 26 mm pin length stirrer.

The product size distribution for each milling time is illustrated in figure 6.24. Clearly the 1.5 hour product size distribution shows the effect of the rapid hydrogen absorption period. As a result, the expected powder yield is significantly higher than

the product yield greater than 2000 µm. By comparing the 1.5 hour and 2 hour tests, the average product yield greater than 2000 µm is found to be approximately 8% lower for the 2 hour test. In addition, the average expected powder yield is approximately 9% higher for the 2 hour test. Since more of the initial feed is milled, the saturation period between 100-120 minutes proves to have a positive effect on the 2 hour product size distribution. Alternatively, by comparing the 2 hour and 2.5 hour tests, the product size distribution is found to be similar for both milling times. The error bars for the expected powder yield also show no distinct difference between the two milling times. Therefore, milling for a further 30 minutes after saturation shows no significant improvement in terms of a higher expected powder yield.

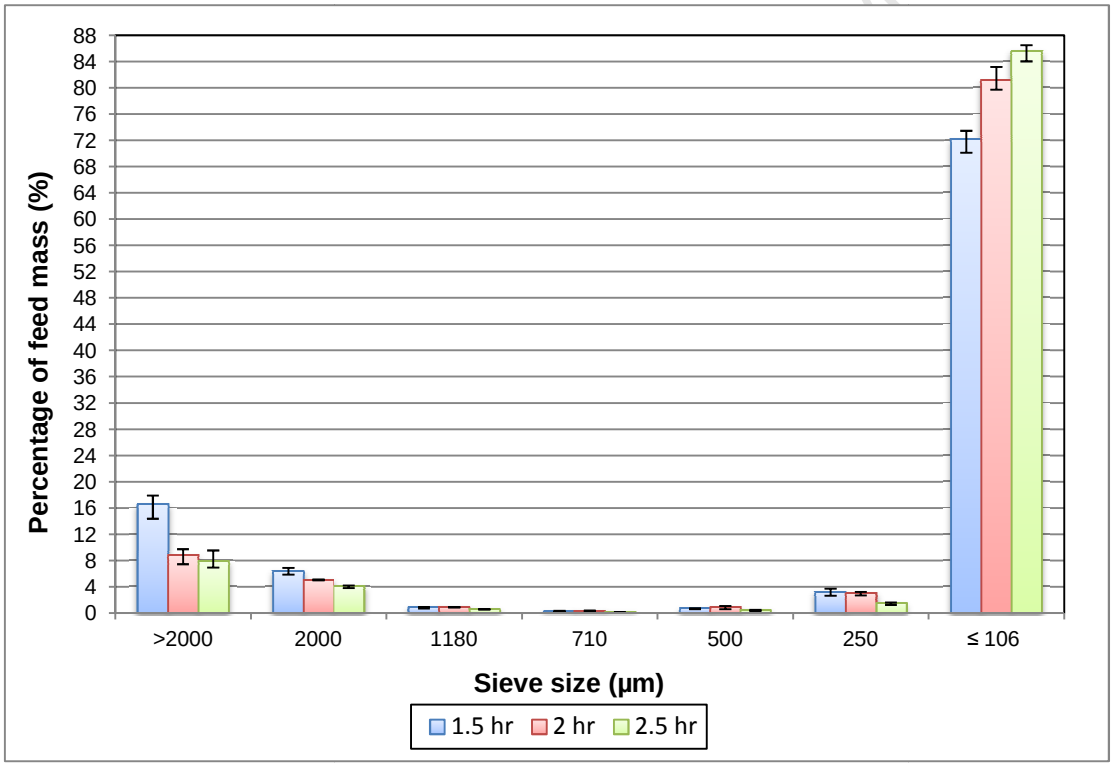

Figure 6.24 : Effect of milling time on the product size distribution of Ti-6Al-4V. Milling performed at 2 m/s using the 6 pin-collar, 26 mm pin length stirrer.

Furthermore, the amount of contamination produced after each milling time was also determine through EDS for Ti-6Al-4V Figure 6.25 illustrates the total amount of contamination produced, relative to the feed mass, after each test. By comparing the 1.5 hour and 2 hour results, the 2 hour test produces more contamination. In addition, milling for a further 30 minutes shows that the 2.5 hour test produces

slightly more contamination than the 2 hour test. As expected, the results show that the level of contamination increases with milling time.

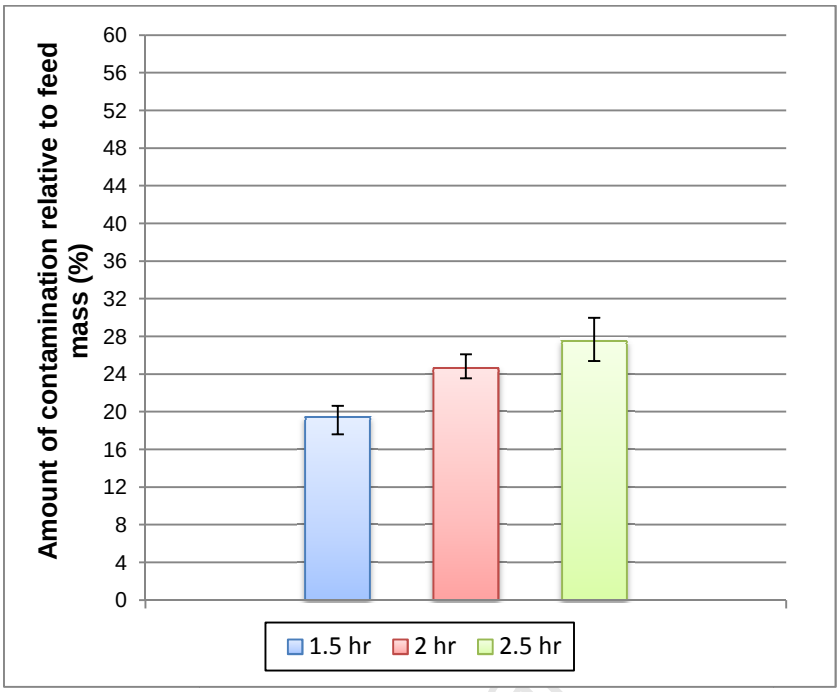

Figure 6.25: Amount of contamination produced at selected milling times for Ti-6Al-4V.

On the whole, the alloy results also show that the product size distribution is dependent on milling time. Similarly to CP Ti, the expected powder yield is the highest after saturation is reached. However, the 2.5 hour results show that milling for a further 30 minutes after saturation has no significant impact on the product size distribution. Therefore the optimum milling time has to lie between 1.5 and 2 hours. By comparing the 1.5 hour and 2 hour tests, the expected powder yield is higher for the 2 hour test. Alternatively, the 1.5 hour test produces the least amount of contamination. Since the difference in the amount of contamination is approximately only 5%, the 2 hour test is found to produce the best combination of minimum contamination and maximum powder production. Therefore for an optimum stirrer pin tip speed of 2 m/s, the corresponding optimum milling time is 2 hours when milling Ti-6Al-4V.

6.4 Summary of Results

6.4.1 Optimising stirrer design

Initially, the effect of the stirrer pin length on the hydrogen absorption rate and the powder yield was investigated. For a fixed number of pin-collars (i.e. number of pins), a stirrer with 26 mm long pins was compared to one with 30 mm long pins. This was done for a 5 pin-collar configuration as well as a 6 pin-collar configuration. Thereafter, the relationship between the number of pins on the stirrer and the hydrogen absorption rate was investigated.

For the 5 pin-collar configuration, the temperature compensated hydrogen pressure for both pin length stirrers are found to follow a similar trend. This suggests that the hydrogen absorption rate into the titanium feed is similar for both pin length stirrers. Alternatively, when comparing the product size distribution for both pin length stirrers, the expected powder yield is found to be higher for the 26 mm pin length stirrer. In addition, the 26 mm pin length stirrer produces less product yield with a size greater than 2000 µm. Therefore, for the 5 pin-collar configuration, the 26 mm pin length stirrer is found to perform slightly better than the 30 mm pin length stirrer.

For the 6 pin-collar configuration, the temperature compensated hydrogen pressure for both pin length stirrers are found to follow a similar trend for only the first 90 minutes of milling. Thereafter, the hydrogen pressure for the 26 mm pin length stirrer continues to drop for the duration of the test whereas the hydrogen pressure for the 30 mm pin length stirrer remains fixed. From the product size distribution chart, the product yield with a size greater than 2000 µm is found to be greater for the 30 mm pin length stirrer. As a result, it can be explained that the hydrogen pressure remains fixed after 90 minutes because not enough of the initial coarse feed is milled to expose clean titanium surfaces for hydrogen absorption. Therefore, it can further be explained that the 30 mm pin length stirrer is less efficient at circulating the feed and facilitating feed breakage. Furthermore, in terms of the expected powder yield, the error bars for both pin length stirrers are found to overlap and therefore suggested that there was no significant difference between the powder yields. Nevertheless, the total product yield less than 2000 µm is still higher for the 26 mm pin length stirrer. Therefore, for the 6 pin-collar configuration, the 26 mm pin length stirrer also performs slightly better than the 30 mm pin length stirrer in terms of exposing more clean titanium surfaces.

Overall, both the 5 and 6 pin-collar configuration with 26 mm long pins were found to perform better than the corresponding pin-collar configuration with 30 mm long pins. In order to investigate whether the number of pins on the stirrer influences the hydrogen absorption rate, the temperature compensated pressure results for the 5 and 6 pin-collar stirrer configuration with 26 mm long pins were compared. The hydrogen absorption rate into the titanium feed was found to be much faster for the 6 pin-collar configuration. This behaviour can be explained by the fact that adding more pins increases the active grinding volume. As a result, more of the initial feed is milled, creating more clean titanium surfaces to absorb hydrogen. In terms of the product size distribution, the product yield with a size greater than 2000 µm was found to be lower for the 6 pin-collar configuration. In addition, the expected powder yield was found to much higher for the 6 pin-collar configuration.

Therefore, from the pin lengths and number of pins used in this project, the optimum stirrer design consists of 6 pin-collars (i.e. 12 pins) and 26 mm long pins. Under fixed milling conditions, this configuration results in the fastest hydrogen absorption rate and therefore produces the highest expected powder yield. Consequently, this stirrer configuration was used to test the effect of the other milling conditions on the hydrogen absorption rate.

6.4.2 Effect of stirrer speed

In order to investigate the effect of the stirrer speed on the hydrogen absorption rate and powder yield, four stirrer pin tip speeds were investigated. Initially CP Ti was milled at each of these speeds for a fixed milling time. A pin tip velocity of 0.5 m/s, 1 m/s, 1.5 m/s and 2 m/s was selected for investigation. By comparing the temperature compensated pressure data for all four speeds, the pressure drops further as the stirrer speed increases at a given milling time. More importantly, the fastest stirrer pin tip speed of 2 m/s is found to facilitate a faster hydrogen absorption rate. As a result, for the 2 m/s test, the pressure drops rapidly for the first 60 minutes and after 70 minutes the pressure remains constant suggesting that the feed is saturated with hydrogen. Since the stress intensity of the grinding media is proportional to the square of the stirrer velocity, the breakage rate of the feed is expected to increase with stirrer speed. As a result, the rate of creating clean titanium surfaces for hydrogen absorption also increases with stirrer speed. This may therefore explain why the hydrogen absorption rate is much higher at the fastest stirrer pin tip speed of 2 m/s.

By analysing the 0.5 m/s product size distribution, a large percentage of the product yield is found to lie between 2000 µm and 1180 µm. In addition, the product yield greater than 2000 µm is found to be higher than the expected powder yield. Since the stress intensity and frequency of the grinding media collisions are much lower at low speed, this pattern is expected. On the other hand, for the other stirrer speeds, the expected powder yields are found to be considerably higher than the corresponding product yields with a size greater than 2000 µm. More specifically, the trend in the results show that the expected powder yield increases with stirrer speed. Since a faster stirrer speed facilitates faster hydrogen absorption, this behaviour is expected. Overall, the stirrer pin tip speed of 2 m/s is found to produce the highest expected powder yield, although much of the powder yield is unrecovered.

For the range of speeds tested on CP Ti, the optimum stirrer pin tip speed is found to be 2 m/s. Since it is assumed that the Ti-6Al-4V feed will follow a similar trend and therefore have the same optimum stirrer pin tip speed as CP Ti, milling of Ti-6Al-4V was only performed at this optimum stirrer pin tip speed. The resulting hydrogen absorption rate and the product size distribution of both feeds were then compared for the same milling time. By comparing the temperature compensated pressure data for CP Ti and Ti-6Al-4V, the alloy is found to absorb more hydrogen over a longer period of time before saturation is reached. As a result, the rapid hydrogen absorption period and therefore the time taken to reach saturation is longer than CP Ti. Furthermore, by comparing the product size distribution for both feeds, the majority of both feed are converted to powder. However, since the alloy absorbs more hydrogen, the expected powder yield is found to be higher for the alloy.

6.4.3 Effect of milling time

The effect of milling time on the product size distribution and powder yield of both feeds was investigated at the optimum stirrer pin tip speed of 2 m/s. It had to be determined whether a corresponding optimum milling time exists, which efficiently converts the titanium feed to powder without producing too much contamination. By examining the temperature compensated pressure data for each feed, three milling times were selected for investigation. The milling times that were selected corresponded to the time taken for rapid hydrogen absorption, the time taken for saturation and the time after saturation is reached. For each feed, the corresponding product size distribution at each milling time was then compared to one another.

For CP Ti, the product size distribution at milling times of 1 hour, 1.5 hour and 2.5 hour were selected for analysis. By comparing the 1 hour rapid hydrogen absorption period with the 1.5 hour saturation period, the product yield greater than 2000 µm is found to be lower for the 1.5 hour test. In addition, the expected powder yield is much higher for the 1.5 hour test. On the other hand, by comparing the 1.5 hour test with the 2.5 hour post saturation period, no significant difference is found in the product size distribution. Therefore, further milling after saturation is inefficient since a similar product size distribution or more importantly a similar expected powder yield can be achieved at a shorter milling time of 1.5 hours. Furthermore, by comparing the amount of contamination produced at each milling time, the 1 and 1.5 hour test produced similar amounts of contamination. However, the 2.5 hour test produced considerably much more contamination than the 1 and 1.5 hour test. This is clearly the result of excessive milling that takes place after saturation is reached. Overall, a 1.5 hour milling time, which corresponds to the time taken to reach saturation, is found to produce the best combination of minimum contamination and maximum powder production. Therefore for an optimum stirrer pin tip speed of 2 m/s, the corresponding optimum milling time is 1.5 hours when milling CP Ti.

For Ti-6Al-4V, the product size distribution at milling times of 1.5 hour, 2 hour and 2.5 hour were selected for analysis. When comparing the 1.5 hour rapid hydrogen absorption period with the 2 hour saturation period, the product yield greater than 2000 µm is found to be lower for the 2 hour test. In addition, the expected powder yield is much higher for the 2 hour test. Alternatively, by comparing the 2 hour test with the 2.5 hour post saturation period, a similar product size distribution is produced for both tests. Therefore, similarly to CP Ti, the expected powder yield is higher for the saturation period than the rapid hydrogen absorption period. In addition, further milling after saturation is found to be inefficient. In terms of the amount of contamination produced at each milling time, the level of contamination is found to increase with milling time, although not as considerably as the CP Ti contamination. Overall, the 2 hour milling time, which corresponds to the time taken to reach saturation, is found to produce the best combination of minimum contamination and maximum powder production. Therefore for an optimum stirrer pin tip speed of 2 m/s, the corresponding optimum milling time is 2 hours when milling Ti-6Al-4V.

7 CONCLUSIONS

A laboratory scale stirred ball mill capable of hydrogenating titanium scrap and producing titanium hydride powder at room temperature and low hydrogen pressure has successfully been designed and built. The stirred mill was successful used to convert both commercially pure titanium and Ti-6Al-4V machine turnings into titanium hydride powder with a particle size less than 106 µm. For a fixed ball charge and feed mass, the stirrer design, stirrer speed and milling time are found to strongly influence the hydrogen absorption rate and resulting powder yield. The optimum milling parameters are discussed further below:

i. Stirrer Design

In terms of finding the optimum stirrer design, the results have shown that both the pin length and the number of pin-collars (i.e. number of pins) influence the hydrogen absorption rate and therefore the powder yield. For the range of pin lengths and number of pin-collars used in this project, the trend is that more powder is produced as the pin length decreases and the number of pins along the stirrer increases. In other words, more powder is produced as the grinding media spacing between the pin tip and mill chamber wall increases and the grinding media spacing between successive pins along the stirrer decreases. The optimum stirrer design therefore consisted of 6 pin-collars (12 pins) with a pin length equal to 26 mm.

ii. Stirrer Speed

Since the stress intensity and frequency of the grinding media increase with stirrer speed, the breakage rate and therefore the rate of exposing more clean titanium surfaces increases with speed. Consequently, for the range of stirrer speeds used in this project, a faster stirrer speed is found to facilitate faster hydrogen absorption and therefore produce a higher powder yield. Overall, the fastest stirrer pin tip speed of 2 m/s is found to be the optimum speed. Compared to the other stirrer speeds, this speed results in the fastest hydrogen absorption rate and allows both feeds to reach saturation. It therefore produces the highest powder yield for both feeds, after a fixed milling time.

iii. Milling Time

For both feeds, the powder yield produced at the milling time taken for saturation is found to be higher than that produced at the milling time for rapid hydrogen absorption. However, for both feeds, further milling after saturation is found to be inefficient because a similar powder yield is produced at saturation. In addition, the wear rate of the mill and therefore the level of contamination increases after saturation. Therefore, the optimum milling time which produces the most powder yield and least amount of contamination corresponds to the time taken for the feed to reach saturation. For the CP Ti feed, the optimum milling time at an optimum stirrer pin tip speed of 2 m/s, is found to be 1.5 hours. Alternatively, for Ti-6Al-4V, the optimum milling time for the same optimum stirrer pin tip speed is found to be 2 hours.

8 FUTURE WORK

The following recommendations are made in anticipation that further investigation will be made into improving the titanium powder yield and reducing the level of contamination.

- The mill chamber needs to be upgraded to include more wear resistant materials because it is found to be the main source of contamination. Possibly, a wear resistant lining can be installed into the existing mill chamber.

- The resulting powder yield produced by maintaining the pressure of the hydrogen at approximately 200 kPa throughout the milling process should be investigated.

- The optimum stirrer design in this project has a three grinding media spacing between the pin tip and mill chamber wall as well as a two grinding media spacing between successive pins along the stirrer. Therefore, the effect of reducing the grinding media spacing between successive pins along the stirrer by adding an extra set of pins should be investigated. In addition, the effect of increasing the grinding media spacing between the pin tip and mill chamber wall by using shorter pins should be investigated.

- The effect of using a disc stirrer design on the powder yield should be determined. The diameter of the disc should be chosen such the grinding media spacing between the disc and the mill chamber wall is the same as that used for the optimum pin tip in this project.

- The powder yield produced by increasing the ball charge and / or feed mass should be investigated.

9 REFERENCES

[1] E. Tal-Gutelmacher and D. Eliezer, “The hydrogen embrittlement of titanium-based alloys,” *JOM*, vol. 57, no. 9, pp. 46-49, Sep. 2005.

[2] S. J. Gerdemann, “Titanium Process Technologies,” *Advanced Materials & Processes*, vol. 159, no. 7, pp. 41-43, Jul. 2001.

[3] V. Moxson, O. N. Senkov, and F. H. Froes, “Innovations in titanium powder processing,” *JOM*, vol. 52, no. 5, pp. 24-26, May 2000.

[4] M. Mitkov and D. Božić, “Hydride-dehydride conversion of solid Ti6Al4V to powder form,” *Materials Characterization*, vol. 37, no. 2–3, pp. 53-60, Sep. 1996.

[5] H. R. Z. Sandim, B. V. Morante, and P. A. Suzuki, “Kinetics of thermal decomposition of titanium hydride powder using in situ high-temperature X-ray diffraction (HTXRD),” *Materials Research*, vol. 8, no. 3, pp. 293-297, Sep. 2005.

[6] D. A. Small, G. R. MacKay, and R. A. Dunlap, “Hydriding reactions in ball-milled titanium,” *Journal of Alloys and Compounds*, vol. 284, no. 1–2, pp. 312-315, Mar. 1999.

[7] H. Zhang and E. H. Kisi, “Formation of titanium hydride at room temperature by ball milling,” *J. Phys.: Condens. Matter*, vol. 9, no. 11, p. L185-L190, Mar. 1997.

[8] Y. Chen and J. S. Williams, “Formation of metal hydrides by mechanical alloying,” *Journal of Alloys and Compounds*, vol. 217, no. 2, pp. 181-184, Feb. 1995.

[9] M. J. Donachie, “Introduction,” in *Titanium: A technical guide*, ASM International, 1988, pp. 9-19.

[10] M. Peters, J. Hemptenmacher, J. Kumpfert, and C. Leyens, “Structure and Properties of Titanium and Titanium Alloys,” in *Titanium and Titanium Alloys: Fundamentals and Applications*, WILEY-VCH, 2003, pp. 1-36.

[11] H. Sibum, “Titanium and Titanium Alloys - From Raw Material to Semi-finished Products,” in *Titanium and Titanium Alloys: Fundamentals and Applications*, WILEY-VCH, 2003, pp. 231-244.

[12] “Titanium Advances at AeroMat 2008,” *Advanced Materials & Processes*, vol. 166, no. 6, pp. 25-26, Jun. 2008.

[13] M. J. Donachie, “Understanding Ti’s Metallurgy,” in *Titanium: A technical guide*, ASM International, 1988, pp. 21-36.

[14] F. H. Froes, “The production of low-cost titanium powders,” *JOM*, vol. 50, pp. 41-43, Sep. 1998.

[15] M. J. Donachie, “Wrought Alloying Processing,” in *Titanium: A technical guide*, ASM International, 1988, pp. 37-56.

[16] A. J. Fenn, G. Cooley, D. Fray, and L. Smith, “Exploiting the FFC Cambridge Process,” *Advanced Materials & Processes*, vol. 162, no. 2, pp. 51-53, Feb. 2004.

[17] S. J. Oosthuizen, “In search of low cost titanium: the Fray Farthing Chen (FFC) Cambridge process,” *The Journal of The Southern African Institute of Mining and Metallurgy*, vol. 111, pp. 199-202, Mar. 2011.

[18] R. W. Schutz and D. E. Thomas, “Corrosion of titanium and titanium alloys,” in *ASM Handbook: Corrosion*, vol. 13, ASM International, 1987, pp. 669-706.

[19] E. W. Collings, *Materials properties handbook: titanium alloys*. ASM International, 1994.

[20] D Eliezer, N Eliaz, O.N Senkov, and F.H Froes, “Positive effects of hydrogen in metals,” *Materials Science and Engineering: A*, vol. 280, no. 1, pp. 220-224, Mar. 2000.

[21] I. A. Mwamba and L. H. Chown, “The use of titanium hydride in blending and mechanical alloying of Ti-Al alloys,” *The Journal of The Southern African Institute of Mining and Metallurgy*, vol. 111, pp. 159-165, Mar. 2011.

[22] W. Lee, J. Jang, S. Ko, and S. Park, “Manufacturing method for titanium hydride powders,” World Intellectual Property Organisation, Patent number WO 2008/030029 A1.

[23] Z.-H. Cheng, G. R. MacKay, D. A. Small, and R. A. Dunlap, “Phase development in titanium by mechanical alloying under hydrogen atmosphere,” *J. Phys. D: Appl. Phys.*, vol. 32, no. 15, pp. 1934-1937, Aug. 1999.

[24] J.-L. Bobet, C. Even, and J.-M. Quenisset, “On the production of ultra-fine titanium hydride powder at room temperature,” *Journal of Alloys and Compounds*, vol. 348, no. 1–2, pp. 247-251, Jan. 2003.

[25] R. A. Dunlap, D. A. Small, and G. R. MacKay, “Hydriding reactions induced by ball milling in group IV and V transition metals,” *Journal of Material Science Letters*, pp. 881– 883, 1999.

[26] R. Hogg and H. Cho, “Grinding,” in *Encyclopaedia of Materials: Science and Technology (Second Edition)*, Oxford: Elsevier, 2001, pp. 3652-3658.

[27] ASM Committee on Milling, “Milling of Brittle and Ductile Materials,” in *ASM Handbook: Powder Metal Technologies and Applications*, vol. 7, ASM International, 1998, pp. 56-70.

[28] M. Gao and E. Forssberg, “Prediction of product size distributions for a stirred ball mill,” *Powder Technology*, vol. 84, no. 2, pp. 101-106, Aug. 1995.

[29] A. Jankovic, “Media stress intensity analysis for vertical stirred mills,” *Minerals Engineering*, vol. 14, no. 10, pp. 1177-1186, Oct. 2001.

[30] R. Schilling, “Attritor grinding mills and new developments,” Akron, Ohio, Apr-2000.

[31] C. Suryanarayana, "Mechanical alloying and milling," *Progress in Materials Science*, vol. 46, no. 1–2, pp. 1-184, Jan. 2001.

[32] A. J. Lynch and C. A. Rowland, *The history of grinding*. SME, 2005.

[33] P. Baláž, "High-Energy Milling," in *Mechanochemistry in Nanoscience and Minerals Engineering*, Berlin, Heidelberg: Springer Berlin Heidelberg, pp. 103-132.

[34] A. Kwade, "Wet comminution in stirred media mills -- research and its practical application," *Powder Technology*, vol. 105, no. 1–3, pp. 14-20, Nov. 1999.

[35] T. Partyka and D. Yan, "Fine grinding in a horizontal ball mill," *Minerals Engineering*, vol. 20, pp. 320-326, Apr. 2007.

[36] F. Shi, R. Morrison, A. Cervellin, F. Burns, and F. Musa, "Comparison of energy efficiency between ball mills and stirred mills in coarse grinding," *Minerals Engineering*, vol. 22, no. 7–8, pp. 673-680.

[37] A. Jankovic, "Variables affecting the fine grinding of minerals using stirred mills," *Minerals Engineering*, vol. 16, no. 4, pp. 337-345, Apr. 2003.

[38] "Grinding Balls, Media | Union Process®, Inc." [Online]. Available: http://www.unionprocess.com/grinding.html. [Accessed: 08-Mar-2010].

[39] G. A. Graves and T. Boehm, "Mill media considerations for high energy mills," *Minerals Engineering*, vol. 20, no. 4, pp. 342-347, Apr. 2007.

[40] L. Blecher, A. Kwade, and J. Schwedes, "Motion and stress intensity of grinding beads in a stirred media mill. Part 1: Energy density distribution and motion of single grinding beads," *Powder Technology*, vol. 86, no. 1, pp. 59-68, Jan. 1996.

[41] A. Kwade, L. Blecher, and J. Schwedes, "Motion and stress intensity of grinding beads in a stirred media mill. Part 2: Stress intensity and its effect on comminution," *Powder Technology*, vol. 86, no. 1, pp. 69-76, Jan. 1996.

[42] A. Kwade and J. Schwedes, "Breaking characteristics of different materials and their effect on stress intensity and stress number in stirred media mills," *Powder Technology*, vol. 122, no. 2–3, pp. 109-121, Jan. 2002.

[43] A. Kwade, "Determination of the most important grinding mechanism in stirred media mills by calculating stress intensity and stress number," *Powder Technology*, vol. 105, no. 1–3, pp. 382-388, Nov. 1999.

[44] "Online Materials Information Resource - MatWeb." [Online]. Available: http://www.matweb.com/index.aspx. [Accessed: 15-Feb-2010].

[45] *Categorization and conformity assessment criteria for all pressure equipment,* SANS 347, 2010

[46] "Stainless Steel Balls, Inox Steel Ball, AISI 304, 316, 302, 304L, 316L." [Online]. Available: http://www.steelmedia.com/stainless-steel-balls.htm. [Accessed: 09-Mar-2010].

[47] "316 and 316L Stainless Steel Balls - TRD Specialties." [Online]. Available: http://www.trdspecialties.com/316-stainless-steel-balls.asp. [Accessed: 09-Mar-2010].

10 APPENDIX

10.1 Mill Chamber Calculations

10.1.1 Calculating the minimum wall thickness

In order to calculate the minimum wall thickness of the mill chamber to safely hold 200 kPa, the following formula was used:

$$P_{all} \times s.f = \frac{\sigma_y}{2R_2^2}\left(R_2^2 - R_1^2\right)$$

Where: P_{all} - allowable working pressure = 0.2 MPa

s.f - safety factor

σ_y - yield strength of mild steel ≈ 200 MPa

R_1 - inner radius of the mill chamber = 60 mm

R_2 - outer radius of the mill chamber

For a safety factor of 4, R_2 can be calculated as follows:

$$R_2 = \sqrt{\frac{\sigma_y R_1^2}{\sigma_y - 2P_{all} x s.f}}$$

$$R_2 = \sqrt{\frac{200x(60)^2}{200 - 2(0.2)x4}}$$

$$R_2 = 60.24mm$$

The minimum wall thickness min_t can be calculated as follows:

$$min_t = R_2 - R_1$$

$$min_t = 60.24 - 60$$

$$min_t = 0.24mm$$

10.1.2 Maximum shear stress yield criterion

For a pressurised cylinder, the maximum shear stress yield criterion is normally used for ductile materials. According to this yield criterion failure of the mill chamber can be avoided by ensuring that the maximum shear stress in the chamber wall is less than (or equal to) the maximum shear stress at yield in a tension-test specimen of the same material.

Since the maximum shear stress is half the greatest difference between two principal stresses, the criterion becomes:

$$\tau_{max} \leq \tau^{test}$$

$$\frac{1}{2}(\sigma_1 - \sigma_3) \leq \frac{1}{2}\sigma_y \quad ; \qquad \sigma_1 > \sigma_3$$

In the case of a cylinder, the maximum shear stress is at the inside radius and is given by the following equation:

$$\tau_{max} = \frac{\sigma_H - \sigma_R}{2} \quad ; \quad \text{where } \sigma_H > \sigma_R$$

Where: τ_{max} *- maximum shear stress*

σ_{H-}*hoop stress*

σ_R *- radial stress*

The maximum hoop stress which occurs at the inside radius, R_1 was calculated by using the following formula:

$$(\sigma_H)_{max} = P_{all}\left(\frac{R_2^2 + R_1^2}{R_2^2 - R_1^2}\right)$$

Where: P_{all} *- allowable working pressure = 0.2 MPa*

R_1 *- inner radius of the mill chamber = 60 mm*

R_2 *- outer radius of the mill chamber = 66*

For a 6 mm wall thickness, the maximum hoop stress can be calculated as follows:

$$(\sigma_H)_{\max} = 0.2\left(\frac{66^2 + 60^2}{66^2 - 60^2}\right)$$

$$(\sigma_H)_{\max} = 2.1 MPa$$

The maximum radial stress (σ_r) is simply equal to the internal pressure of - 0.2 MPa (compressive)

In order to prevent cylinder failure: $\tau_{max} = \frac{\sigma_H - \sigma_R}{2} \leq \frac{\sigma_y}{2}$

$$\therefore \sigma_H - \sigma_R \leq \sigma_y$$

Where: σ_y - yield strength of mild steel ≈ 200 MPa

By substituting the hoop and radial stress into the above condition, the left side of the condition becomes:

$$\begin{aligned} &\sigma_H - \sigma_R \\ &= 2.1 - (-0.2) \\ &= 2.3 MPa \end{aligned}$$

Since this difference is significantly lower than the yield strength of mild steel, the above condition to prevent failure is satisfied. Therefore the dimensions of the mill chamber are acceptable.

10.2 Operating Procedure

Formal instructions for the start-up and shutdown of the hydrogen pressurised stirred ball mill.

10.3 Machine Drawings

Complete set of machine drawings for the stirred ball mill components

Assembly	Part	Material
Mill Chamber Assembly		
	Mill Chamber	**Mild Steel**
	Hub Flange	**Mild Steel**
	Feed Inlet/Outlet Neck Flange	**Mild Steel**
	Feed Inlet/Outlet Plug	**Mild Steel**
	Gas Inlet/Outlet Neck Flange	**Mild Steel**
Stirrer Assembly		
	Stirrer Shaft	**Stainless Steel AISI 304**
	Pin-Collar	**M300**
	26mm Pins	**Stainless Steel AISI 304**
	30mm Pins	**Stainless Steel AISI 304**
	Spacer Collars	**M300**
Hub Support Stand		
	Hub Support Stand Base	**Mild Steel**
	Hub Support Stand	**Mild Steel**
	Hub Support Stand Bush	**Phosphor Bronze**
Mil Chamber Support Stand		
	Mil Chamber Support Stand Base	**Mild Steel**
	Mil Chamber Support Stand	**Mild Steel**
	Mil Chamber Support Stand Bush	**Phosphor Bronze**
Pipeline		
	Centring Ring	**Brass**
	Clamping Collar	**Acetal**
	Pressure Gauge Adapter	**Aluminium**
	Gas Manifold Fitting	**Aluminium**

Originated by:	Reviewed by:	Approved by:
C.Chhiba	K Balchin Pr Eng	Professor R.D. Knutsen
Date:	Date:	Date:

PURPOSE

The purpose of this procedure is to ensure that the Hydrogen Pressure Mill is operated safely and correctly without injury to personnel or damage to plant property.

SCOPE

This procedure covers the operation of the Hydrogen Pressure Mill at the Centre for Materials Engineering Laboratory in the Menzies Building (Level 2) on Upper Campus.

GENERAL

Only personnel who have been assessed as competent operators and are fully conversant with this procedure are permitted to operate the Hydrogen Pressure Mill.

Under no circumstances is the Hydrogen Pressure Mill to be operated when unattended.

ANNEXURES

Appendix A - Training Register

OPERATING PROCEDURE

1. Preliminary Safety Checks

1.1 Ensure that there is a fire extinguisher at hand.

1.2 Ensure that all taps on the gas cylinders are closed.

1.3 Ensure that the gas regulator taps are closed.

1.4 Ensure that only the correct gas cylinders are installed.

1.5 Ensure that all gas fittings and cylinders are secured tightly

1.6 Ensure that there are no leaks from any of the cylinder valves, the hose connections to the gas cylinders and the mill chamber. Spray soapy water on possible leak points, bubbles reveal leaks.

1.7 Ensure that there are no vacuum leaks on the mill assembly. Evacuate the mill chamber and close the Speedi-valve. Monitor the pressure gauge on the mill.

1.8 Ensure that the power switches are initially off.

1.9 Ensure that the fume cupboard is switched on and that it remains operational throughout the duration of the experiment.

Originated by:	Reviewed by:	Approved by:
C.Chhiba	K Balchin Pr Eng	Professor R.D. Knutsen
Date:	Date:	Date:

2. Feed and Grinding Media Insertion into Mill

2.1 In order to open the feed inlet, ensure that the mill pressure gauge reads atmospheric pressure (0 kPa). If not, open the vent valve to fume cupboard (turn valve anticlockwise).

2.2 Open the feed inlet and insert the feed together with grinding media.

2.3 Close the feed inlet afterwards (turn clockwise).

2.4 Close the vent valve (turn clockwise).

3. Obtaining Vacuum and Purging with Argon

3.1 Make sure that all valves and taps are closed.

3.2 Isolate vacuum pumping system from mill by closing the Speedi-valve.

3.3 Ensure that the Argon gas cylinder is connected to the Argon valve.

3.4 Open Argon gas bottle tap.

3.5 Open regulator valve (turn clockwise) on Argon gas cylinder until the regulator pressure gauge reads 200 kPa.

3.6 Switch on vacuum backing pump (rotary pump).Wait for pump to warm up

3.7 Open the vacuum isolation valve and hydrogen gas inlet valve (1^{st} cycle only).

3.8 Monitor vacuum gauge (Pirani) – when vacuum is better than $1x10^{-1}$ mbar, close the vacuum isolation valve and hydrogen gas inlet valve (1^{st} cycle only).

3.9 Open Argon gas inlet valve (turn anticlockwise) on mill to permit gas flow into mill until the mill pressure gauge reads 200 kPa.

3.10 Close Argon gas inlet valve (turn clockwise) on mill.

3.11 Repeat steps 3.7 to 3.10 and move on to following step

3.12 Close regulator valve (turn anticlockwise) and bottle tap on Argon gas cylinder.

Originated by:	Reviewed by:	Approved by:
C.Chhiba	K Balchin Pr Eng	Professor R.D. Knutsen
Date:	Date:	Date:

4. Introducing Hydrogen Gas

4.1. Make sure that all valves and taps are closed.

4.2. Ensure that the Hydrogen gas cylinder is connected to the Hydrogen valve.

4.3. Open Hydrogen gas bottle tap.

4.4. Open regulator valve (turn clockwise) on Hydrogen gas cylinder until the regulator pressure gauge reads 200 kPa.

4.5. Open the vacuum isolation valve.

4.6. Monitor vacuum gauge (Pirani) – when vacuum is better than $1x10^{-1}$ mbar, close the vacuum isolation valve.

4.7. Open Hydrogen gas inlet valve (turn anticlockwise) on mill to permit gas flow into mill until the pressure gauge on mill reads 200 kPa.

4.8. Close Hydrogen gas inlet valve (turn clockwise) on mill.

4.9. Switch off backing pump (rotary pump).

4.10. Close the regulator valve (turn anticlockwise) and bottle tap on the Hydrogen gas cylinder.

5. Operating the Mill

5.1 After the steps above have been followed successfully, milling of the feed sample can take place.

5.2 Switch on the 3-phase plug at the wall.

5.3 Open the water tap to supply water for the cooling coils. Make sure the outlet pipe is in the drain. Check that the water is flowing out into drain

5.4 Clear the preset counter and input the required number of cycles. Together with the rotational speed of the motor, the number of cycles can be used to determine the grinding time.

5.5 Switch on the motor and adjust to the desired rotational speed (rpm).

5.6 The pressure within the mill should be monitored and maintained at 200 kPa throughout the milling process. (Optional)

5.7 If the pressure drops below 200 kPa, repeat steps 4.3, 4.4, 4.7 & 4.8 (section 4 above) until milling is complete.(Optional)

5.8 After milling process, switch off motor and 3-phase plug at wall.

5.9 Close the water tap

5.10 Close the regulator valve and bottle tap on the Hydrogen gas cylinder

Originated by:	Reviewed by:	Approved by:
C.Chhiba	K Balchin Pr Eng	Professor R.D. Knutsen
Date:	Date:	Date:

6. Venting the Mill

6.1. Slowly open the vent valve (turn anticlockwise) to allow residual gas mixture in the mill to flow into the fume cupboard.

6.2. Open Hydrogen gas inlet valve (turn anticlockwise) on the mill to relieve the pressure in the hose lines.

6.3. As soon as the Hydrogen regulator pressure gauge reads 0 kPa, close the gas inlet valve (turn clockwise) on the mill.

6.4. Close the vent valve (turn clockwise) after the mill pressure gauge reads 0 kPa.

7. Flushing the mill

7.1. Open Argon gas bottle and regulator valve (turn clockwise) until the regulator pressure gauge reads 200kPa

7.2. Flush the mill with Argon by opening the Argon gas inlet valve (turn anticlockwise) until the mill pressure gauge reads 200 kPa

7.3. Close the regulator valve and bottle tap on the Argon gas cylinder

7.4. Slowly open the vent valve (turn anticlockwise) to allow Argon gas to flow from the mill and argon hose line into the fume cupboard

7.5. As soon as the Argon regulator pressure gauge reads 0 kPa, close the gas inlet valve (turn clockwise) on the mill

7.6 Close the vent valve (turn clockwise) after the mill pressure gauge reads 0 kPa.

8 Product removal

8.1 Ensure that the mill has been vented and flushed (see section 6 & 7 above).

8.2 Open the feed inlet (turn anticlockwise)

8.3 Loosen the grub screws at the cradle supports to allow the mill to rotate.

8.4 Rotate the mill 180° in order to empty the feed and grinding media contents.

TIDY UP WORK SPACE AFTER USE AND ENSURE THAT ALL ELECTRICAL PLUGS ARE SWITCHED OFF

Originated by:	Reviewed by:	Approved by:
C.Chhiba	K Balchin Pr Eng	Professor R.D. Knutsen
Date:	Date:	Date:

TRAINING REGISTER

Description of Training:	Instruction on the correct and safe operation of the Hydrogen Pressure Mill in the Centre for Materials Engineering Laboratory.

Name of Trainee	Date of Training	Name of Instructor	Signature of Trainee

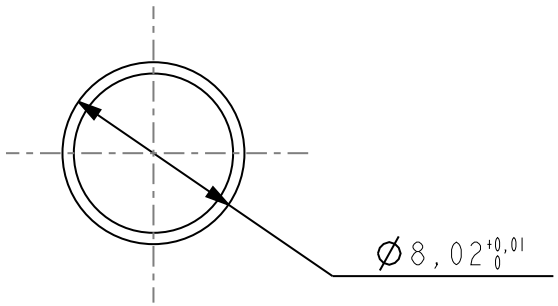

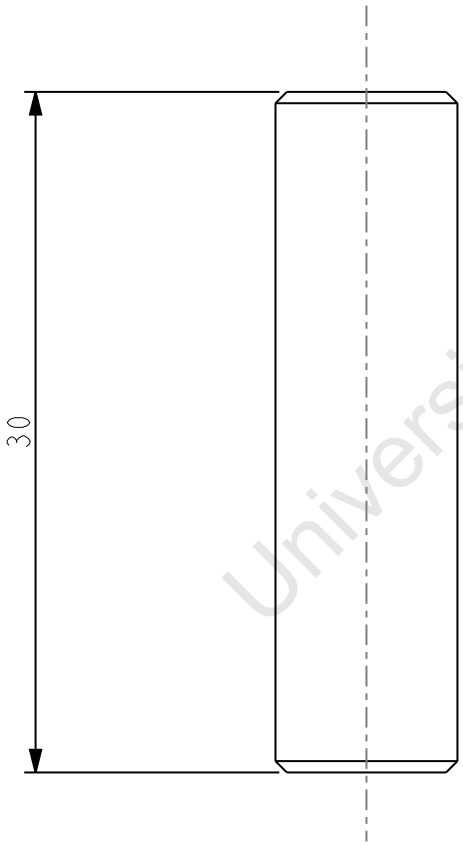

All Chamfers 0.5 x 45°

	SST 304	12	
Item	Material	Qty	Remarks

University of Cape Town
Department of Mechanical Engineering

Title: 26mm Pins

Dimensions in mm Tolerance U.O.S. 0.1	Scale 3,000	Date March 2011	Sheet	of
	Drawn By Chetan Chhiba		Drawing Number	

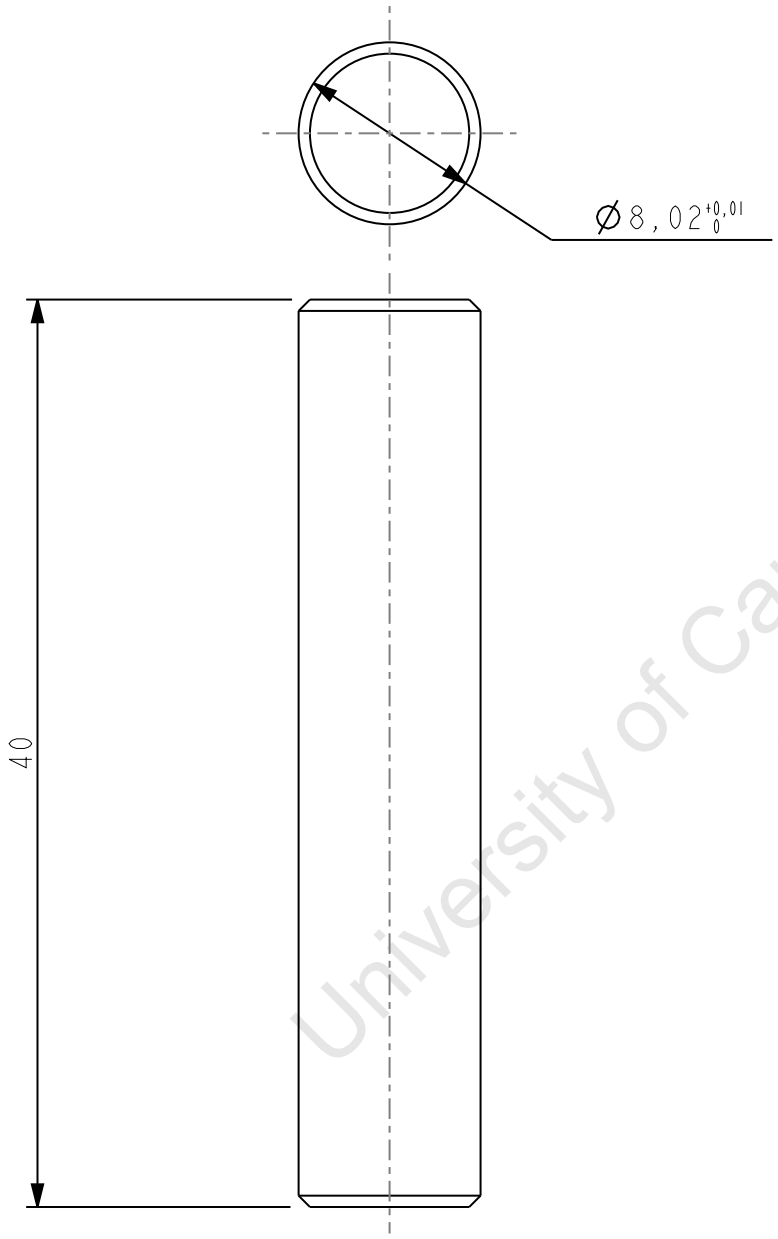

All Chamfers 0.5 x 45°

	SST 304	12	
Item	Material	Qty	Remarks

University of Cape Town
Department of Mechanical Engineering

Title: 30mm Pins

Dimensions in mm Tolerance U.O.S.	Scale	Date	Sheet	of
0.1	3,000	March 2010		
	Drawn By: Chetan Chhiba		Drawing Number	

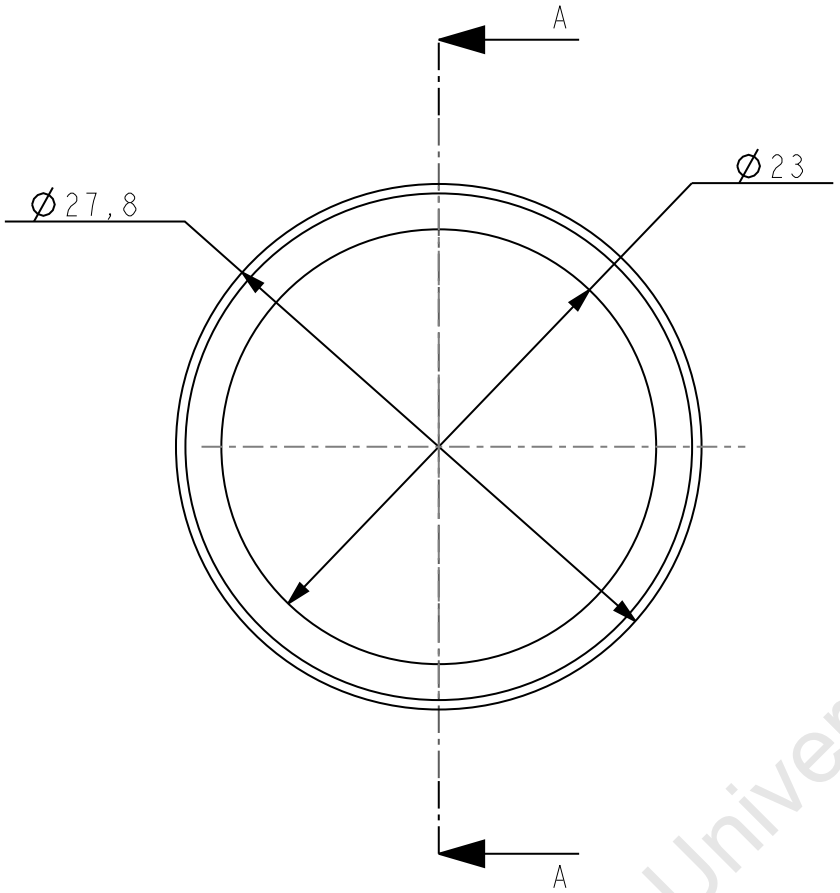

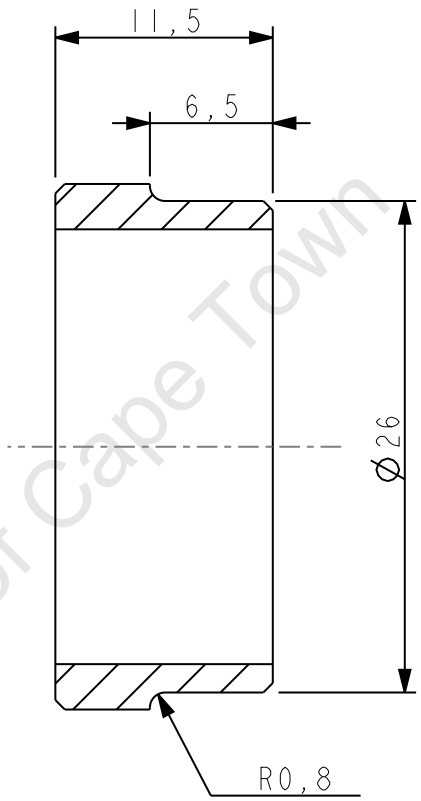

SECTION A-A

All unspecified chamfers 45° x 0.5

	BRASS	6	
Item	Material	Qty	Remarks

University of Cape Town
Department of Mechanical Engineering

Title
Centering Ring

Dimensions in mm Tolerance U.O.S.	Scale 2,500	Date March 2010	Sheet	of
	Drawn By Chetan Chhiba		Drawing Number	
0.1				

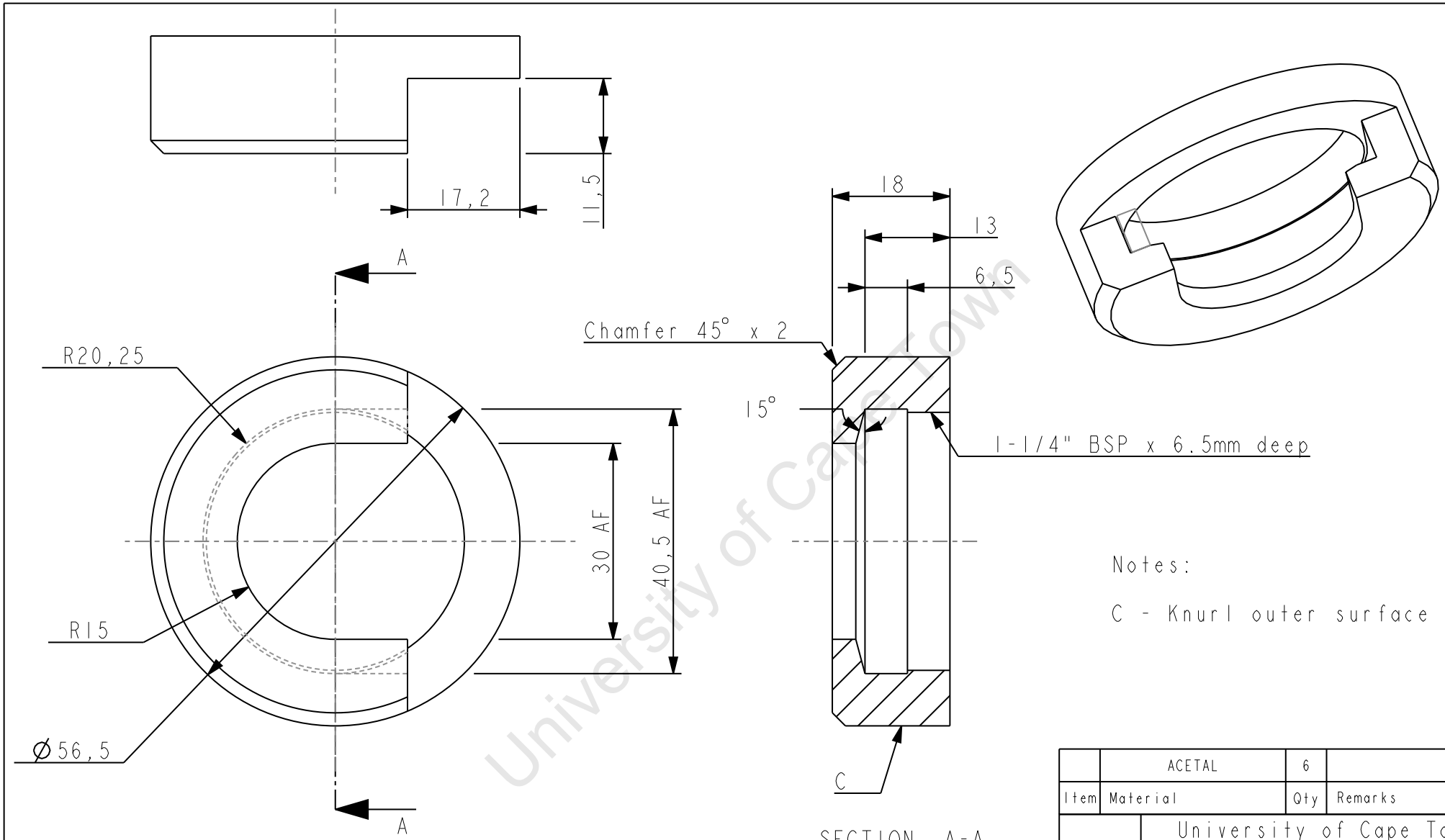

Notes:

C - Knurl outer surface

	ACETAL	6	
Item	Material	Qty	Remarks

University of Cape Town
Department of Mechanical Engineering

Title: Pipe Fitting Clamp

Dimensions in mm Tolerance U.O.S.	Scale 1,200	Date March 2010	Sheet / of
0.1	Drawn By Chetan Chhiba		Drawing Number

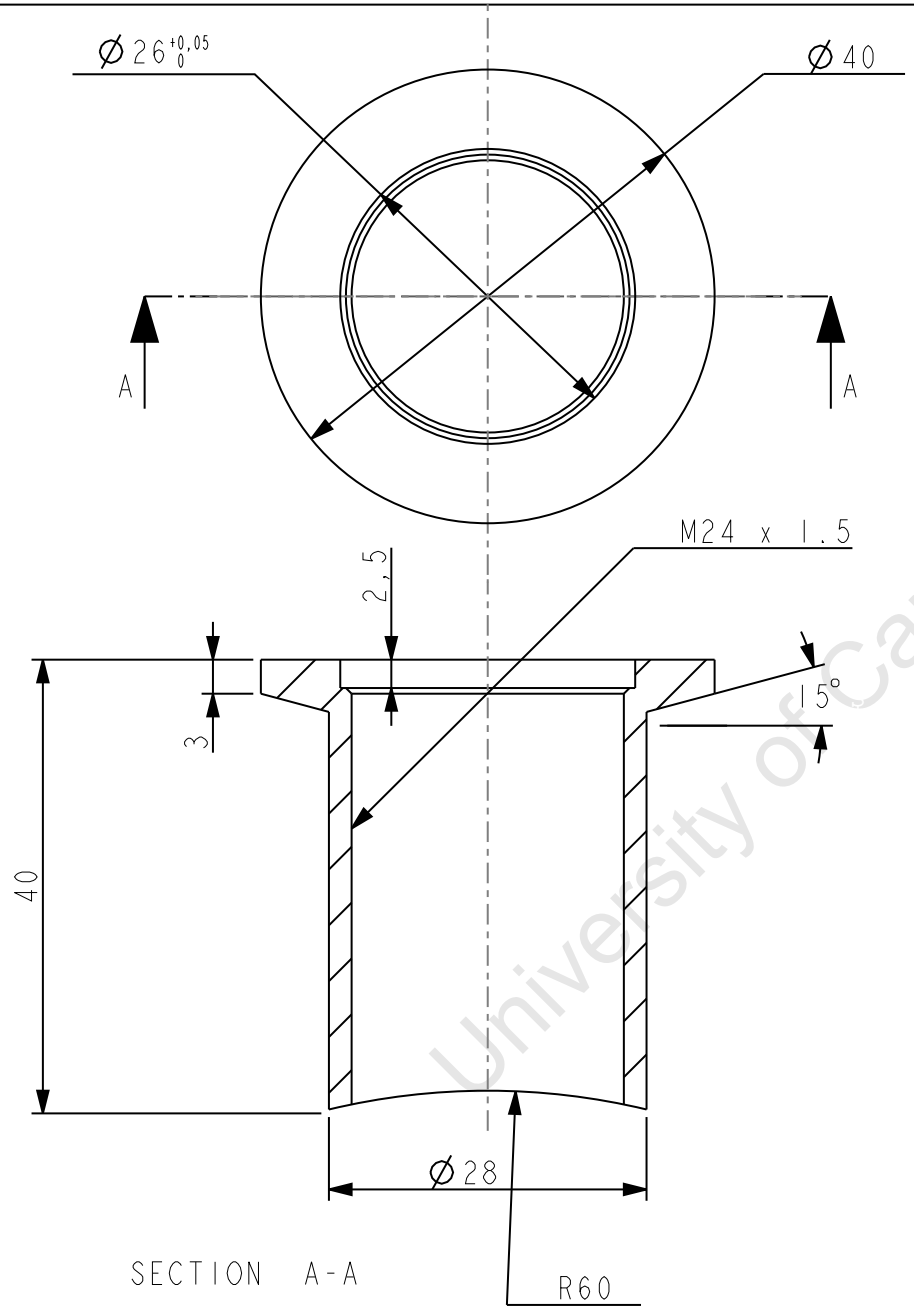

SECTION A-A

All Chamfers 0.5 x 45°

	STEEL_LC	1	
Item	Material	Qty	Remarks

University of Cape Town
Department of Mechanical Engineering

Title: Feed Inlet/Outlet Flange

Dimensions in mm Tolerance U.O.S.	Scale	Date	Sheet	of
0.1	1,500	March 2010		
	Drawn By: Chetan Chhiba		Drawing Number	

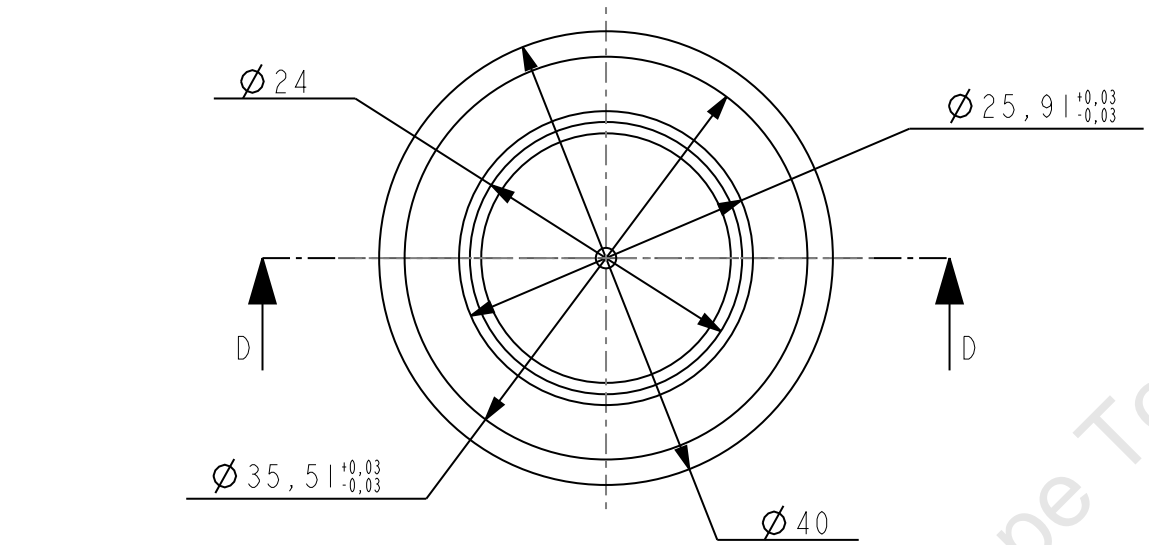

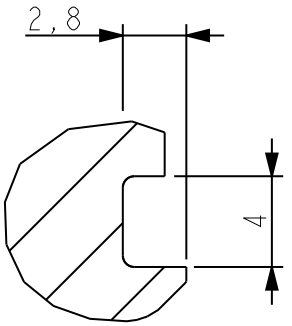

DETAIL A
ENLARG.VIEW

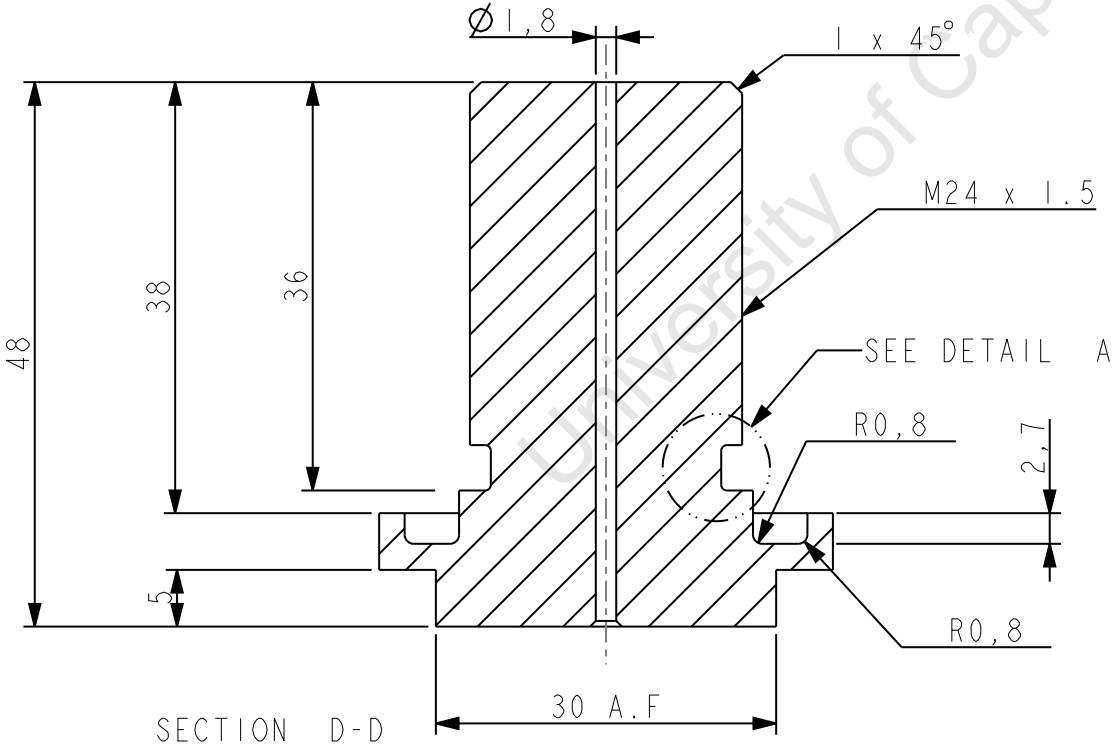

SECTION D-D

All unspecified chamfers 0.5 x 45°
All unspecified fillet radii 0.5

	STEEL_LC	1	
Item	Material	Qty	Remarks

University of Cape Town
Department of Mechanical Engineering

Title
Feed Inlet/Outlet Plug

Dimensions in mm Tolerance U.O.S.	Scale	Date	Sheet	of
0.1	1,000	March 2010		
	Drawn By: Chetan Chhiba		Drawing Number	

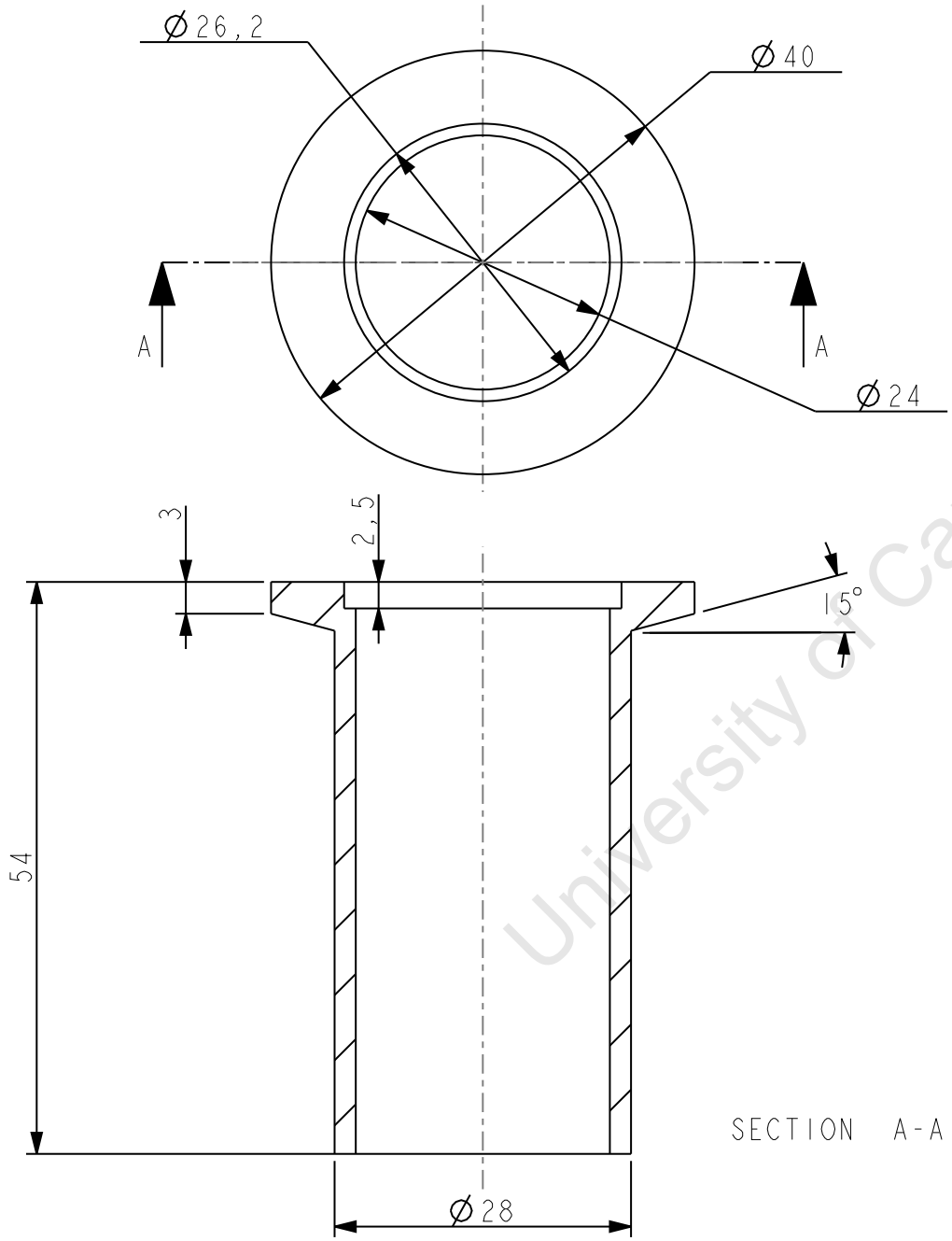

SECTION A-A

	STEEL_LC	1	
Item	Material	Qty	Remarks

University of Cape Town
Department of Mechanical Engineering

Title
Gas Inlet/Outlet Flange

Dimensions in mm Tolerance U.O.S.	Scale 1,500	Date March 2010	Sheet	of
	Drawn By Chetan Chhiba		Drawing Number	
0.1				

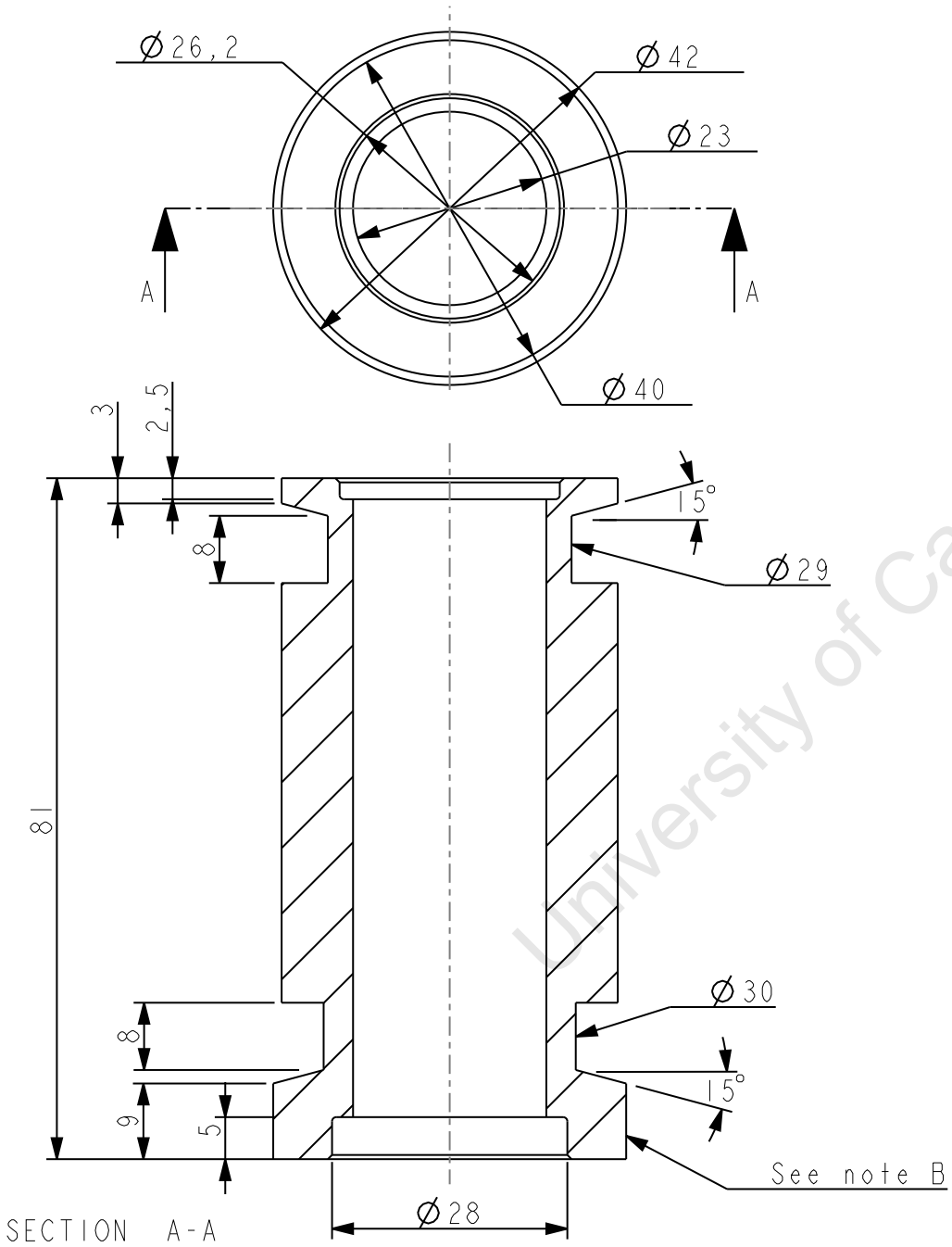

Notes:

B 1-1/4" BSP thread, 9mm long

All unspecified chamfers 45° x 0.5

All unspecified fillet radii 0.5mm

	ALUMINIUM	1	
Item	Material	Qty	Remarks

University of Cape Town
Department of Mechanical Engineering

Title
Gas Manifold Fitting

Dimensions in mm Tolerance U.O.S.	Scale	Date	Sheet	of
	1,200	March 2010		
	Drawn By		Drawing Number	
0.1	Chetan Chhiba			

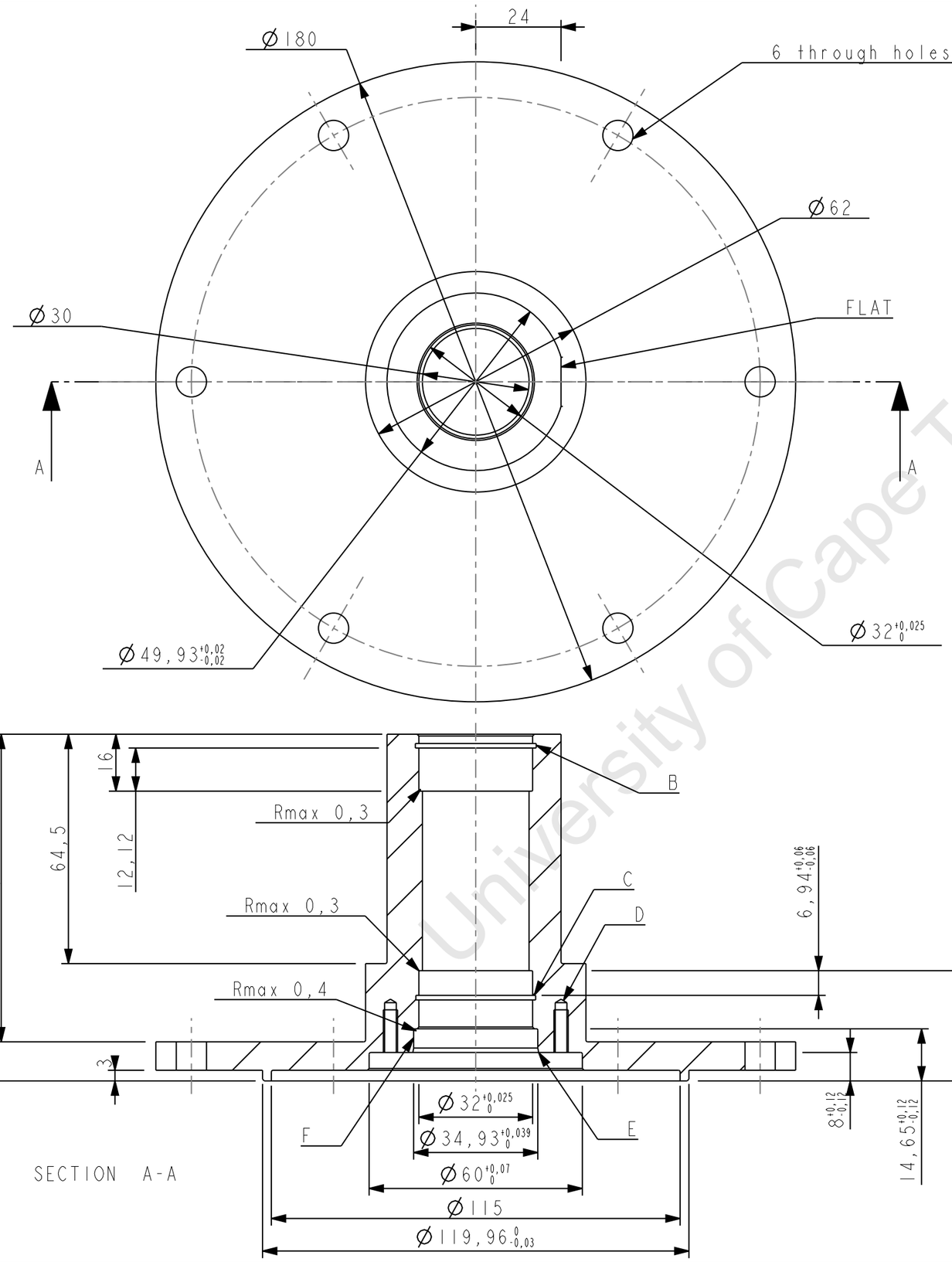

SECTION A-A

NOTES:

B , C - Flat Bottom Groove
Ø $33.7^{+0.25}_{0}$
width 1.28±0.02

D - 4 threaded holes M4 x 0.7
spaced at 90° apart on Ø42 PCD
Ø3.3 drill 14mm deep
tap 12mm deep

E - Chamfer 1.25 x 10° to the vertical

F - Surface roughness $\frac{1,6}{6,3}$

All unspecified radii 0.5mm

All unspecified chamfers 0.5 x 45°

Item	Name	Qty	Material	Remarks
1		1	STEEL_LOW_CARBON	

University of Cape Town
Department of Mechanical Engineering

Title: Hub Flange

Dimensions in mm Tolerance U.O.S.	Scale	Date	Sheet	of
0.1	0,750	March 2010		
	Drawn By: Chetan Chhiba		Drawing Number	

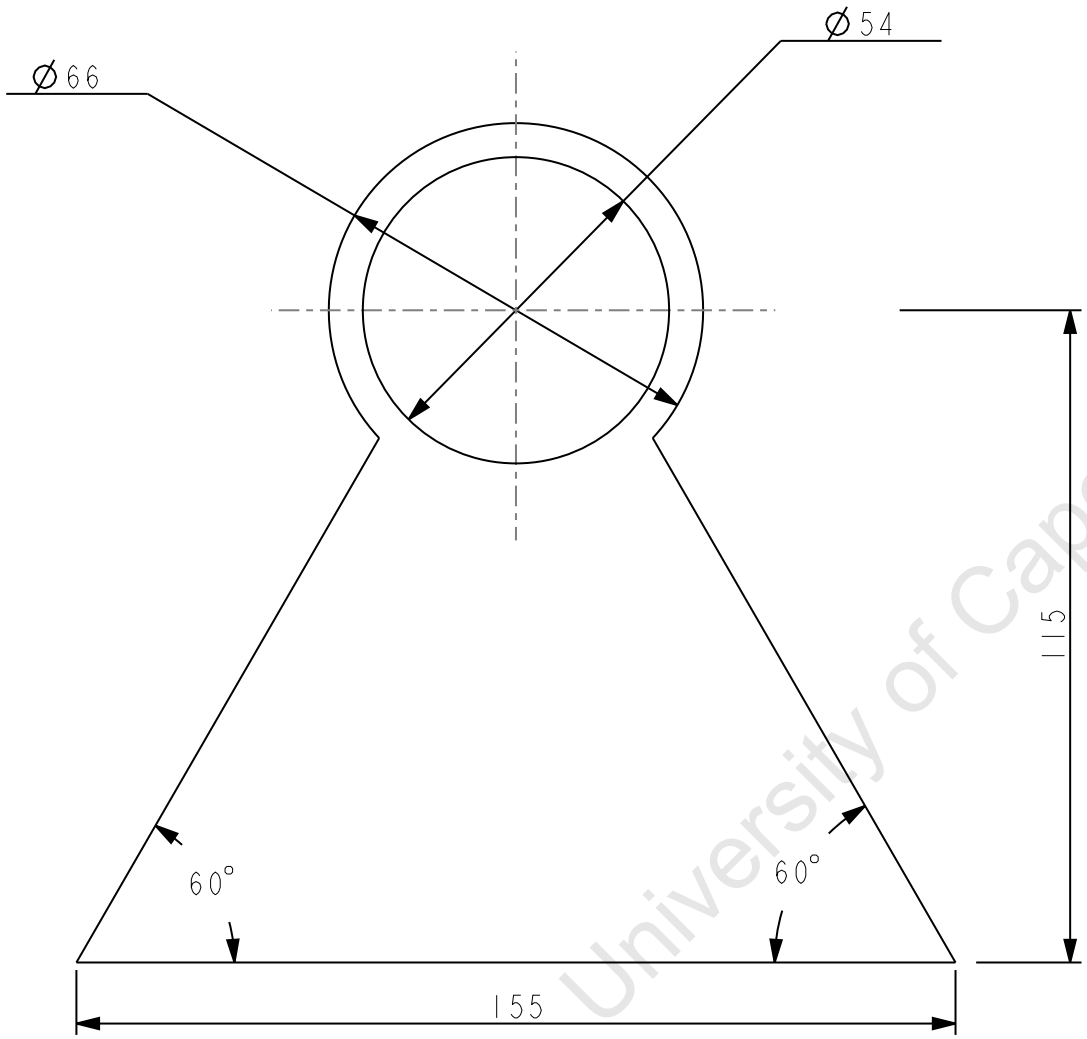

Plate thickness 10 mm

	STEEL_LC	1	
Item	Material	Qty	Remarks

University of Cape Town
Department of Mechanical Engineering

Title
Hub Support Stand

Dimensions in mm Tolerance U.O.S.	Scale	Date	Sheet	of
	0,750	March 2010		
	Drawn By		Drawing Number	
0.1	Chetan Chhiba			

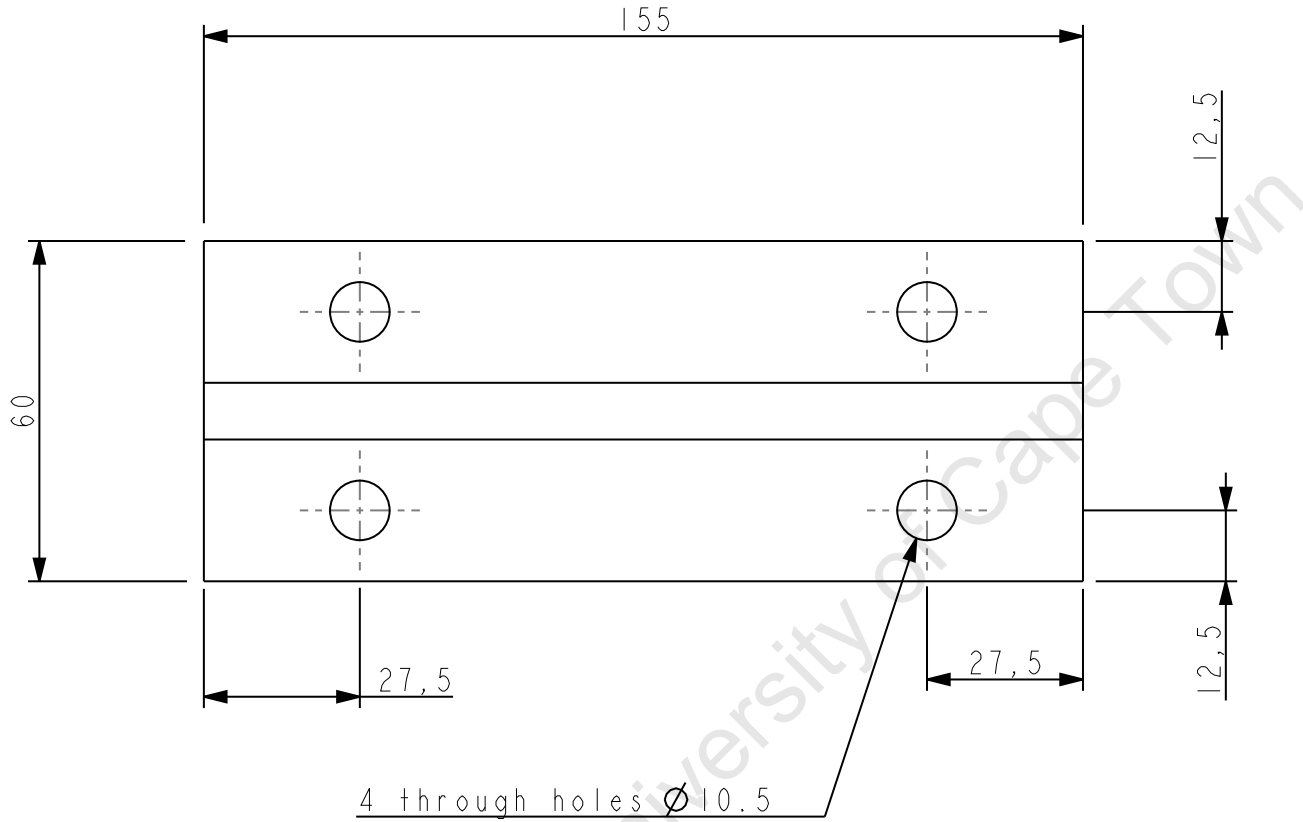

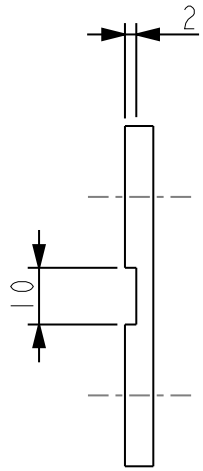

Plate thickness 5mm

	STEEL_LC	1	
Item	Material	Qty	Remarks

University of Cape Town
Department of Mechanical Engineering

Title
Hub Support Stand Base

Dimensions in mm Tolerance U.O.S.	Scale 0,750	Date March 2010	Sheet	of
	Drawn By Chetan Chhiba		Drawing Number	
0.1				

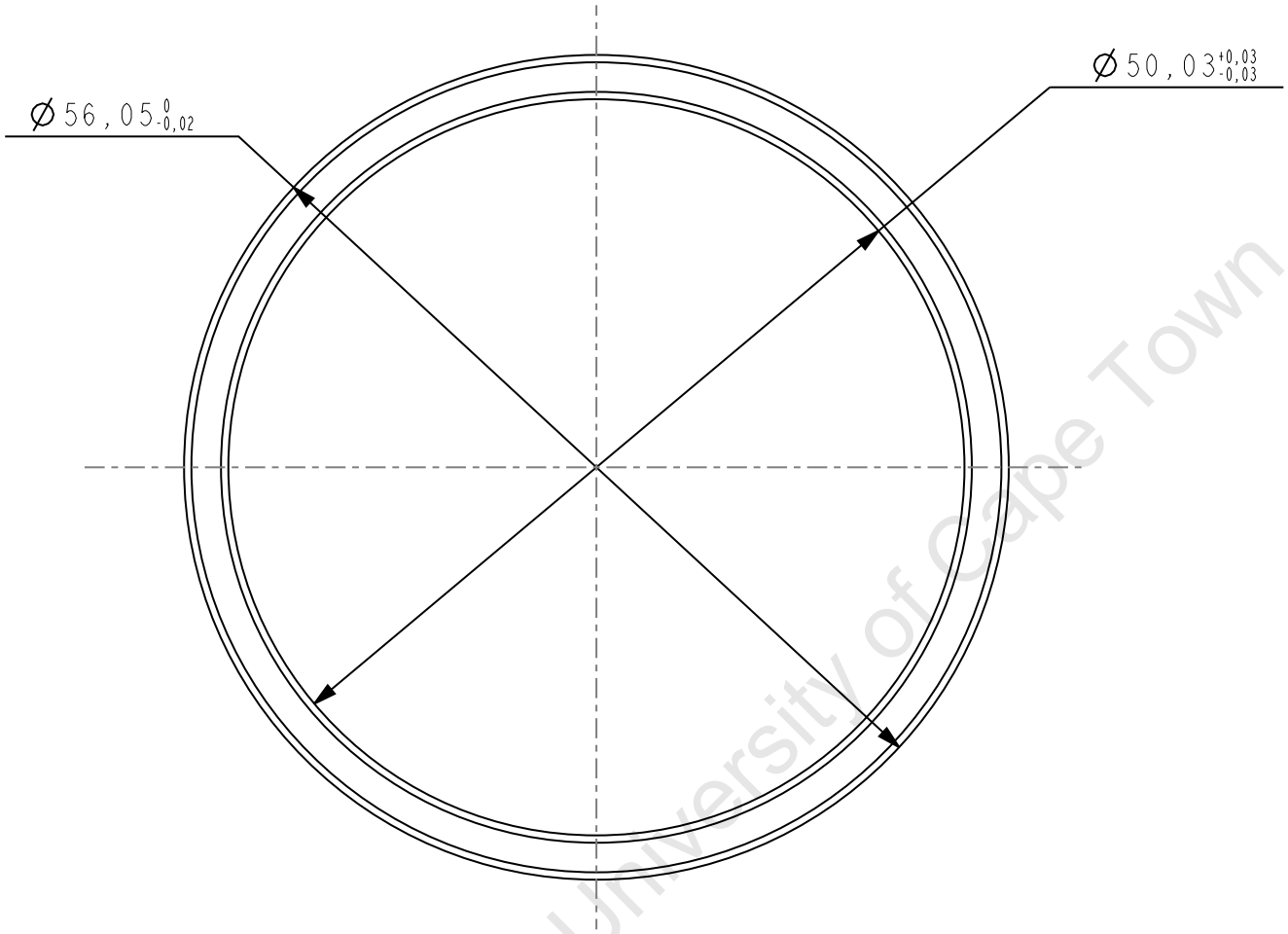

Collar thickness 10 mm

All Chamfers 0.5 x 45°

	PHOSPHUR BRONZE	1	
Item	Material	Qty	Remarks

University of Cape Town
Department of Mechanical Engineering

Title
Hub Support Stand Bush

Dimensions in mm Tolerance U.O.S.	Scale	Date	Sheet	of
	2,000	March 2010		
	Drawn By		Drawing Number	
0.1	Chetan Chhiba			

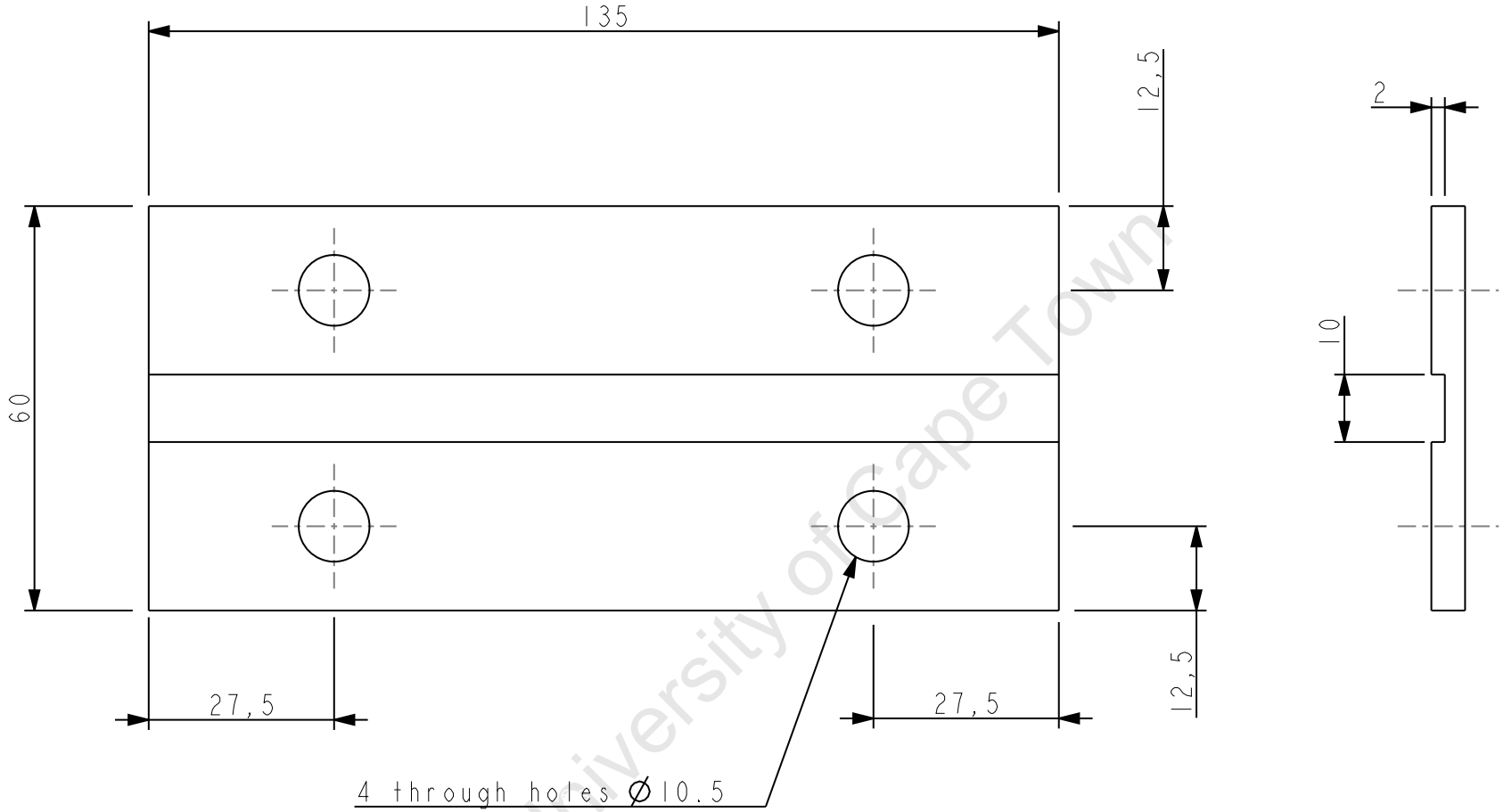

Plate thickness 5mm

	STEEL_LC	1	
Item	Material	Qty	Remarks

University of Cape Town
Department of Mechanical Engineering

Title
Mill Chamber Support Stand Base

Dimensions in mm Tolerance U.O.S.	Scale 1,000	Date March 2010	Sheet	of
	Drawn By Chetan Chhiba		Drawing Number	
0.1				

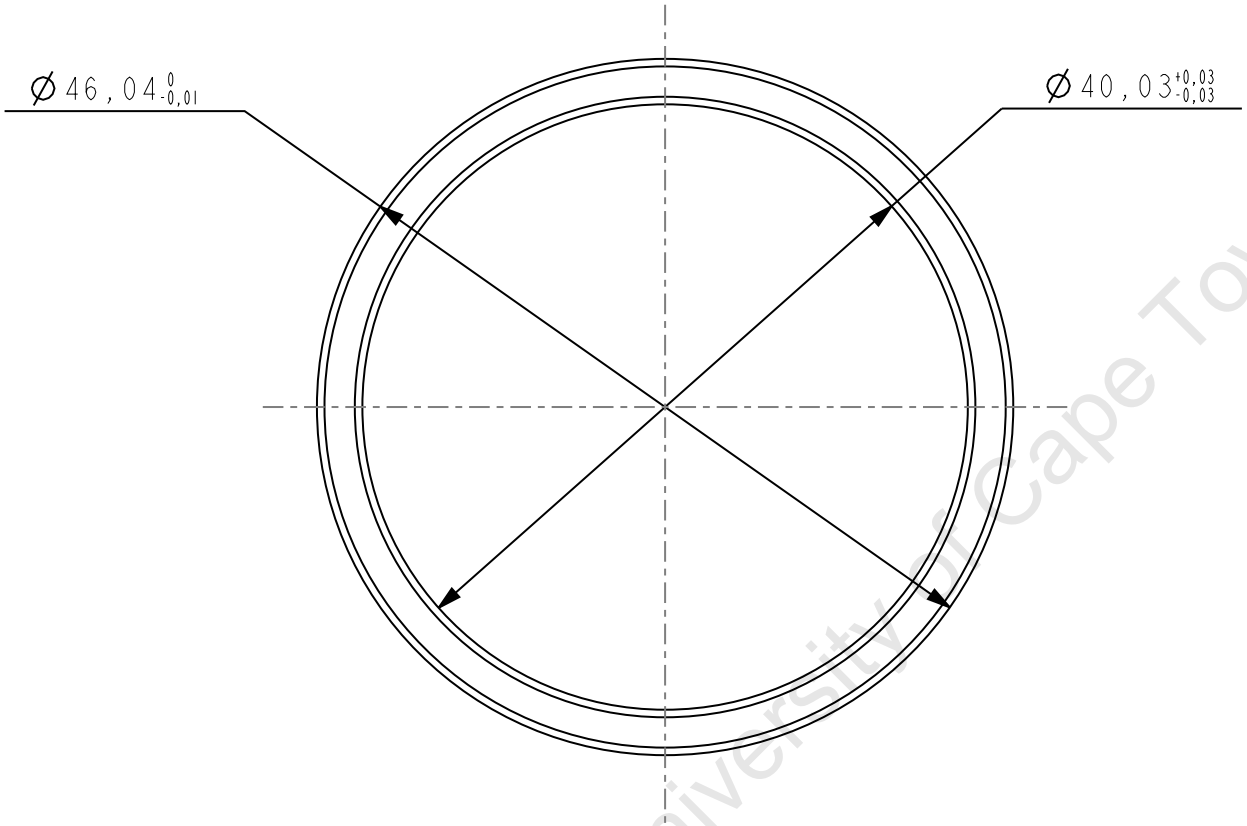

Collar thickness 10mm

All Chamfers 0.5 x 45°

	PHOSPHUR BRONZE	1	
Item	Material	Qty	Remarks

University of Cape Town
Department of Mechanical Engineering

Title
Mill Chamber Support Stand Bush

Dimensions in mm Tolerance U.O.S.	Scale	Date	Sheet	of
	2,000	March 2010		
	Drawn By		Drawing Number	
0.1	Chetan Chhiba			

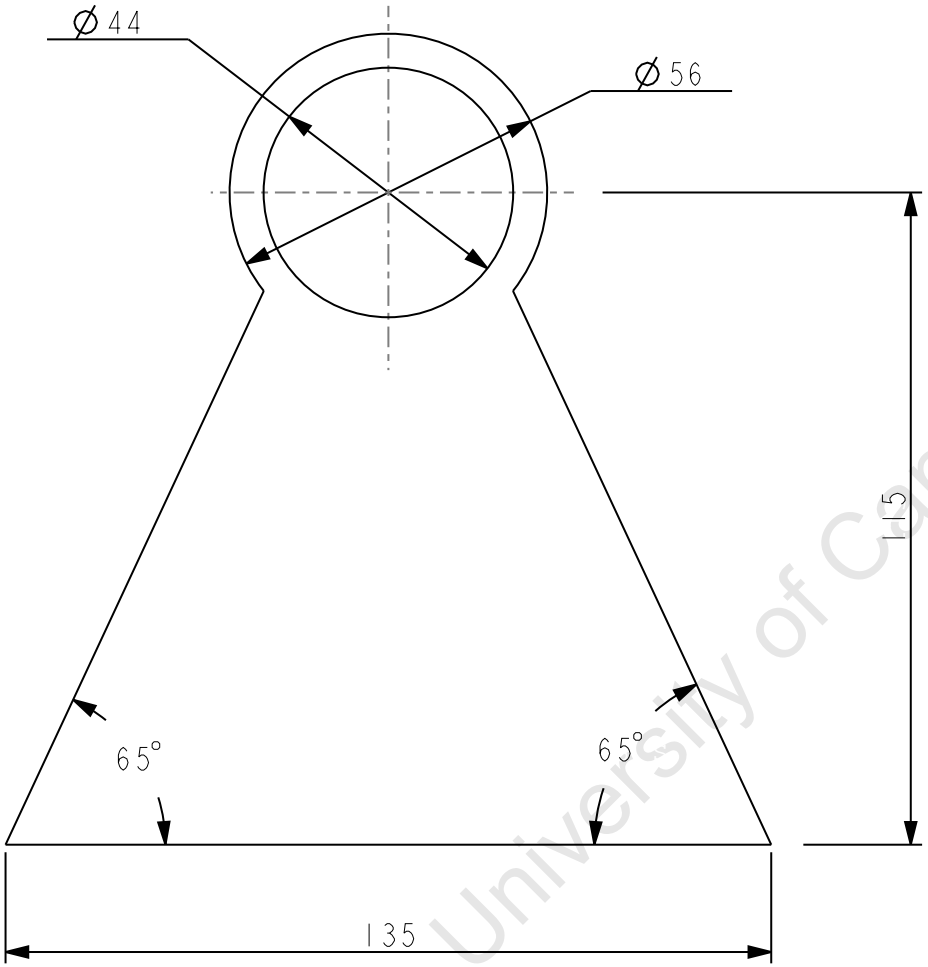

Plate thickness 10 mm

	STEEL_LC	1	
Item	Material	Qty	Remarks

University of Cape Town
Department of Mechanical Engineering

Title
Mill Chamber Support Stand

Dimensions in mm Tolerance U.O.S.	Scale	Date	Sheet	of
	0,750	March 2010		
	Drawn By		Drawing Number	
0.1	Chetan Chhiba			

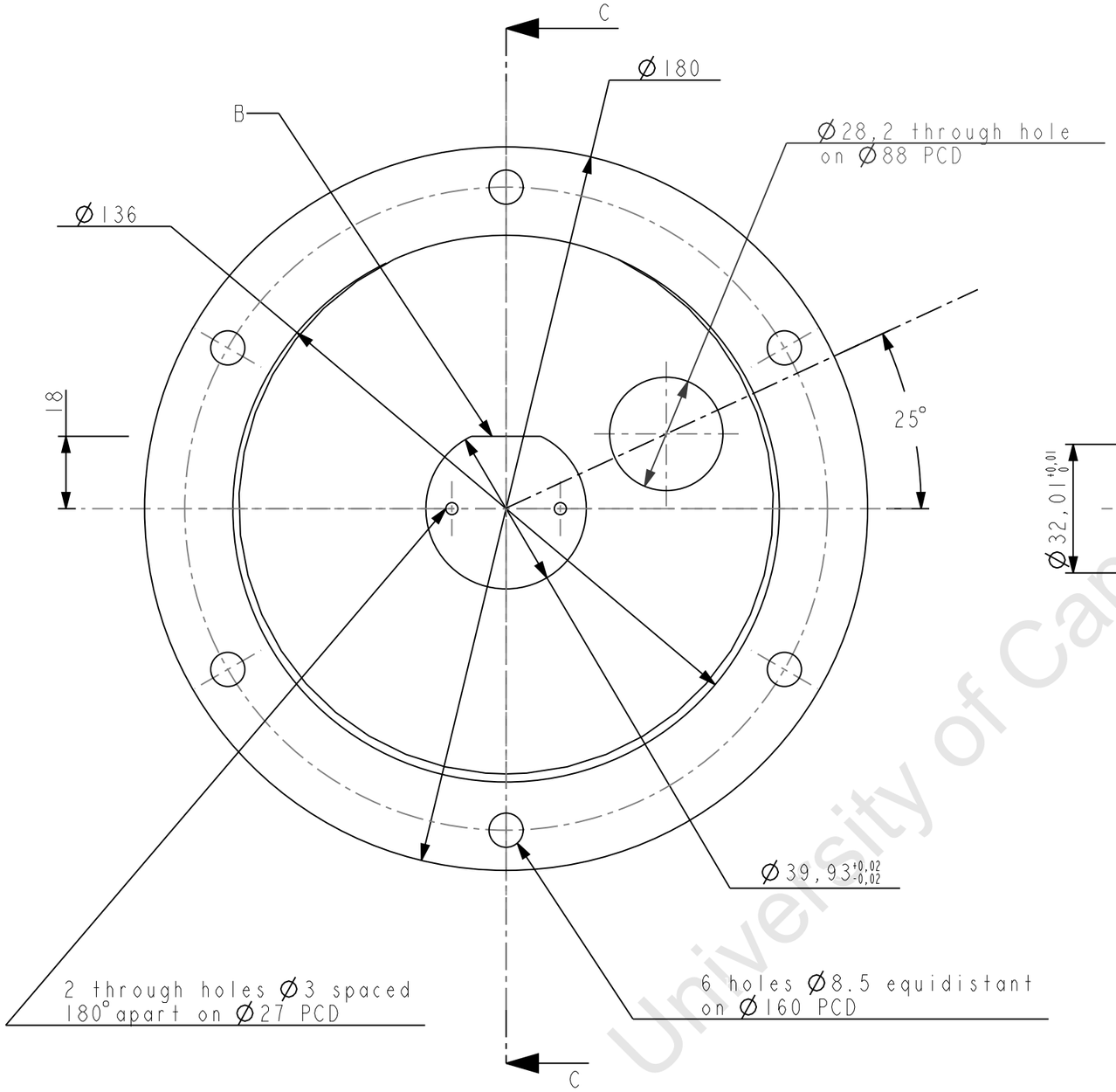

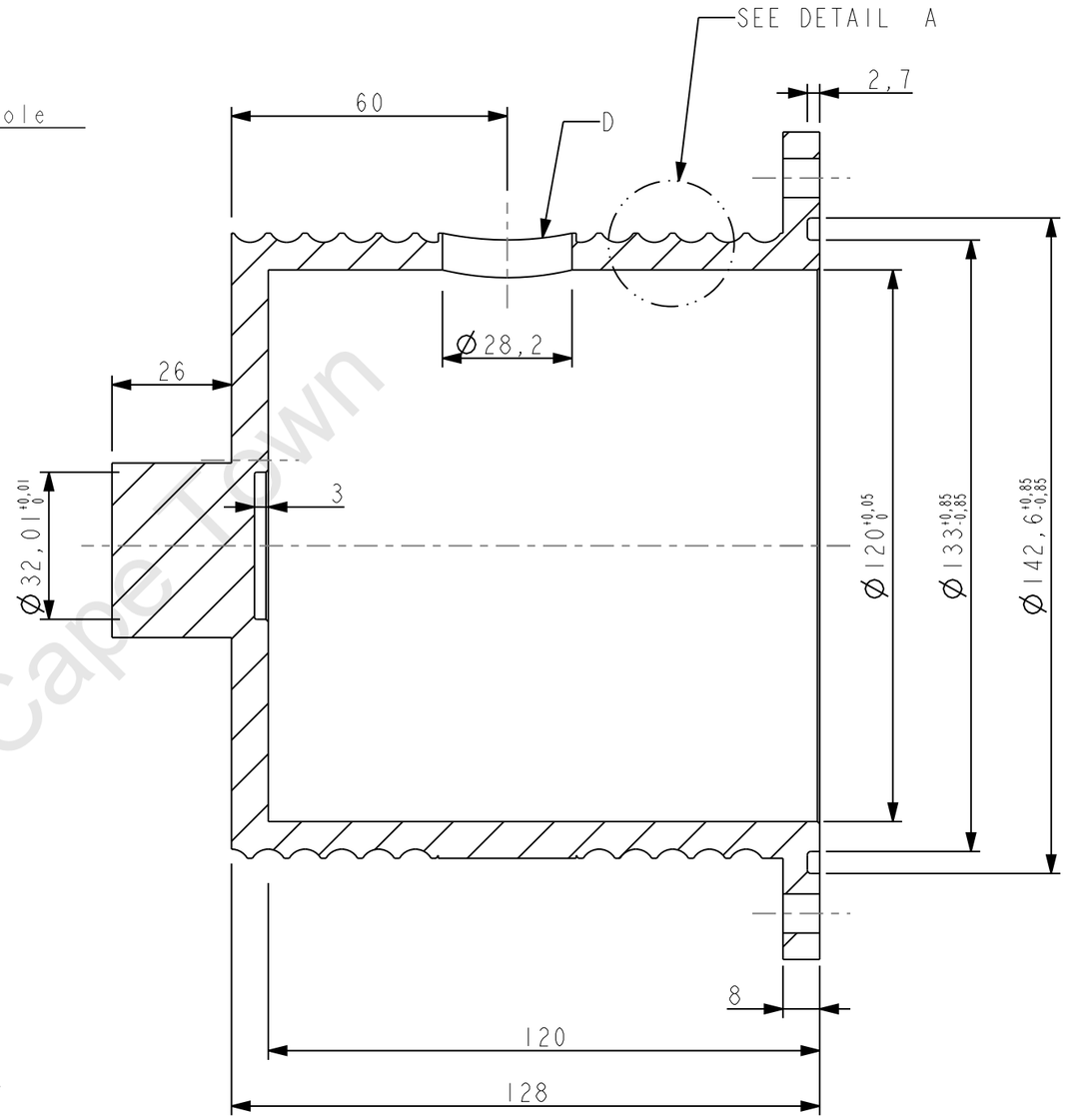

SECTION C-C

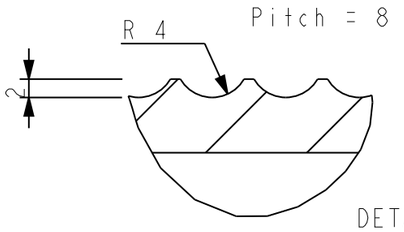

DETAIL A
ENLARG. VIEW

NOTES:

B,D - ENSURE THAT HOLE D IS ⊥ TO FLAT ON B

ALL CHAMFERS 0.5 x 45°

Item	Name	Qty	Material	Remarks
1		1	STEEL_LOW_CARBON	

University of Cape Town
Department of Mechanical Engineering

Title: Mill Chamber

Dimensions in mm Tolerance U.O.S.	Scale	Date	Sheet	of
0.1	0,750	March 2010		
	Drawn By: Chetan Chhiba		Drawing Number	

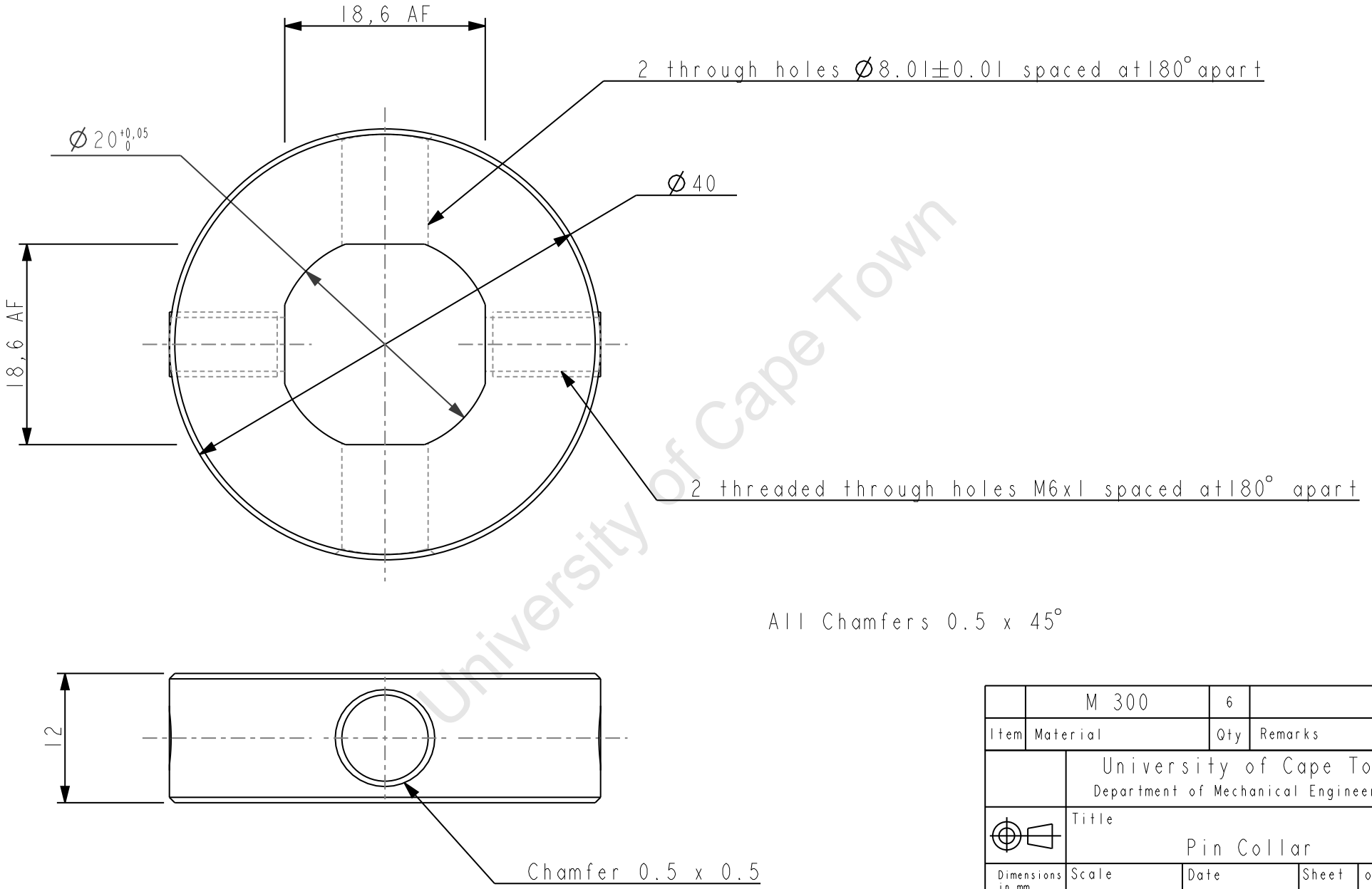

	M 300	6	
Item	Material	Qty	Remarks

University of Cape Town
Department of Mechanical Engineering

Title: Pin Collar

Dimensions in mm Tolerance U.O.S.	Scale	Date	Sheet	of
0.1	2,000	March 2010		
	Drawn By: Chetan Chhiba		Drawing Number	

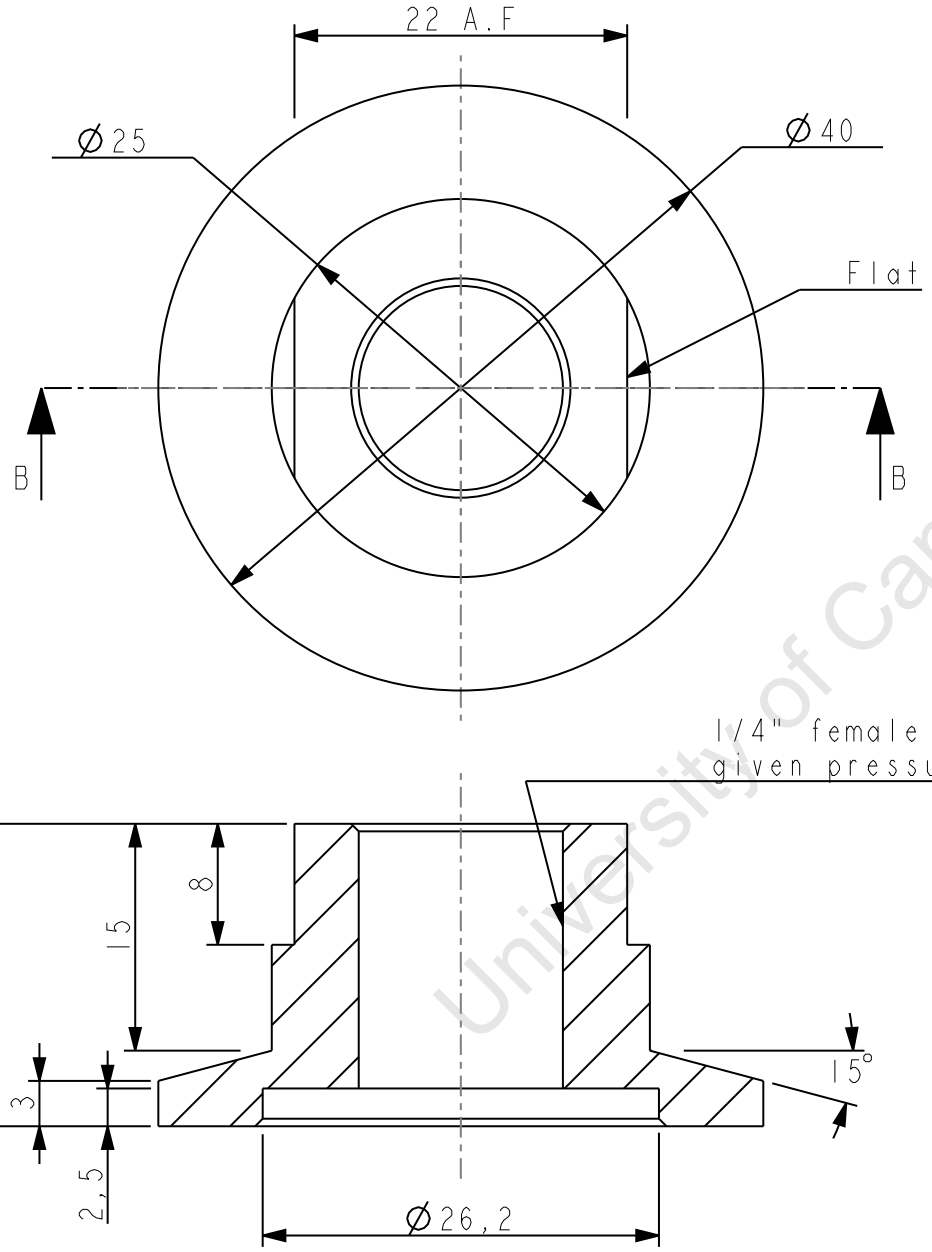

SECTION B-B

All Chamfers 45° x 0.5

	ALUMINIUM	1	
Item	Material	Qty	Remarks

University of Cape Town
Department of Mechanical Engineering

Title
Pressure Gauge Adapter

Dimensions in mm Tolerance U.O.S.	Scale	Date	Sheet	of
	2,000	March 2010		
	Drawn By		Drawing Number	
0.1	Chetan Chhiba			

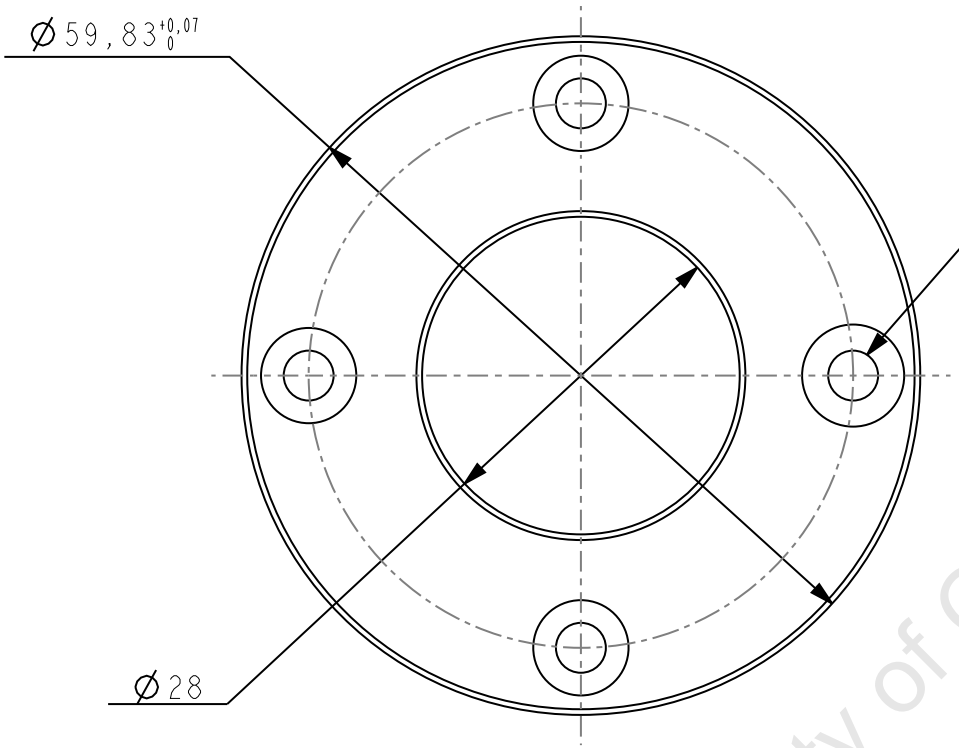

All Chamfers 0.5 x 45°

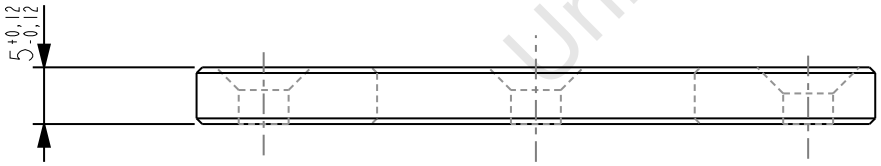

	STEEL_LC	1	
Item	Material	Qty	Remarks

University of Cape Town
Department of Mechanical Engineering

Title: Shaft Seal Cover

Dimensions in mm Tolerance U.O.S.	Scale	Date	Sheet	of
	1,500	March 2010		
	Drawn By		Drawing Number	
0.1	Chetan Chhiba			

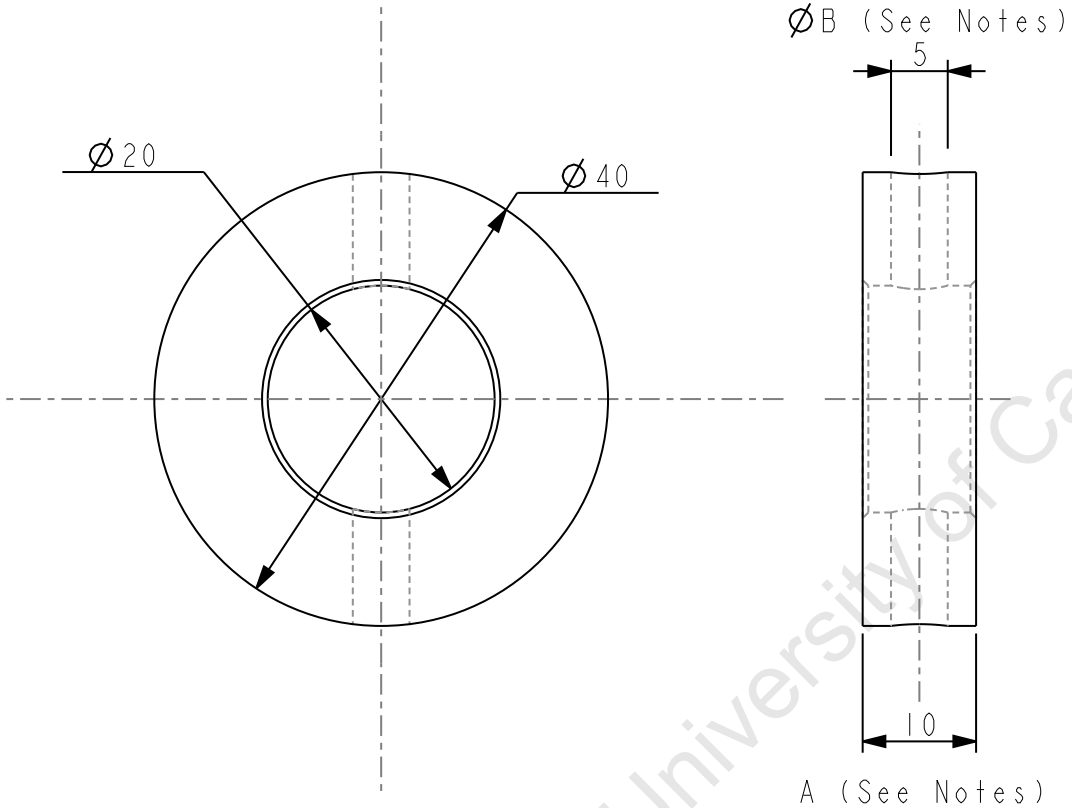

Notes

5 collars, 6mm thick (A) with Ø2.5 hole (B)
2 collars, 8mm thick (A) with Ø3.3 hole (B)
4 collars, 9mm thick (A) with Ø4.2 hole (B)
2 collars, 11mm thick (A) with Ø5 hole (B)

All Chamfers 0.5 x 45°

	M 300	13	
Item	Material	Qty	Remarks

University of Cape Town
Department of Mechanical Engineering

Title: Spacer and End Collars

Dimensions in mm Tolerance U.O.S.	Scale	Date	Sheet	of
0.1	1,500	March 2010		
	Drawn By: Chetan Chhiba		Drawing Number	

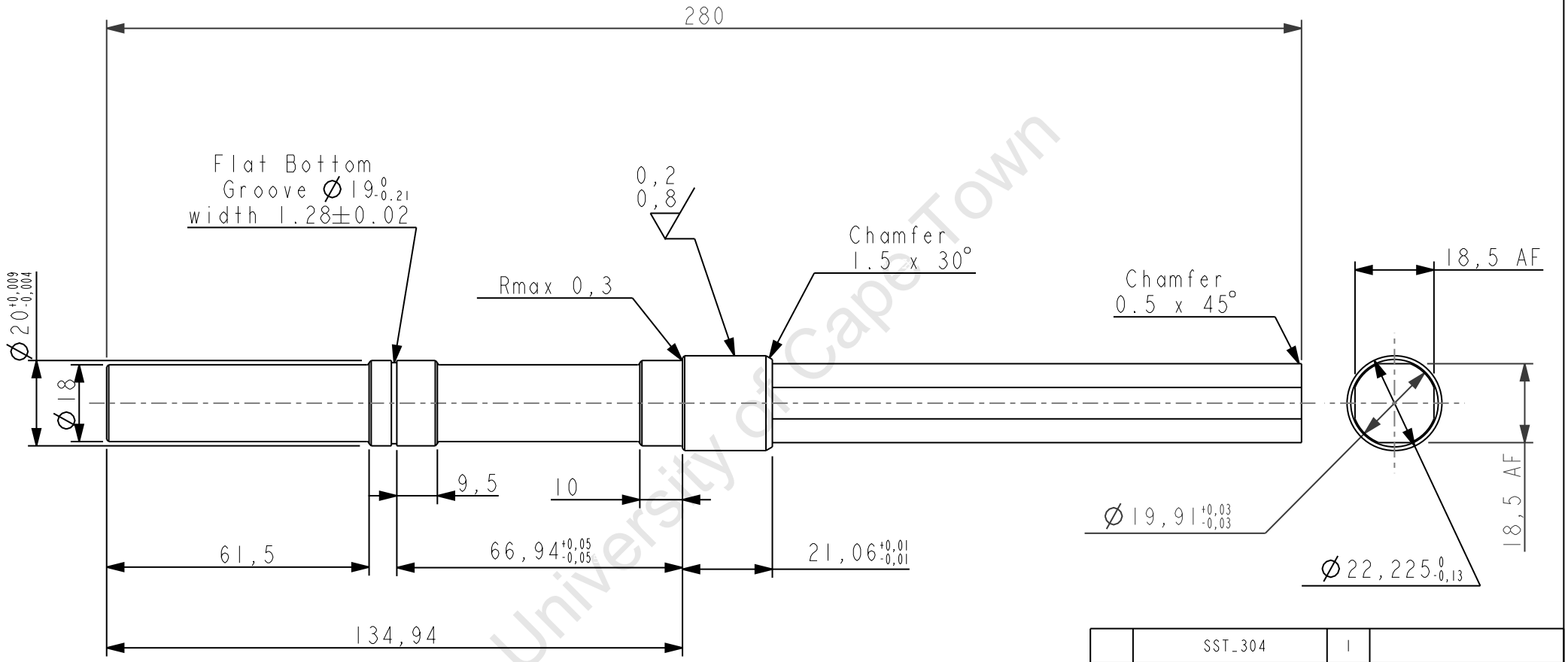

All unspecified chamfers 0.5 x 45°
All unspecified radii 0.5

	SST_304	1	
Item	Material	Qty	Remarks

University of Cape Town
Department of Mechanical Engineering

Title: Stirrer Shaft

Dimensions in mm Tolerance U.O.S.	Scale	Date	Sheet	of
0.1	0,750	March 2010		
	Drawn By: Chetan Chhiba		Drawing Number	